

Use of Non-linearity as a Characteristic in the Selection of Filtering Algorithms in Kinematic Positioning

A thesis accepted by the Faculty of Aerospace Engineering and Geodesy of the University of Stuttgart in partial fulfillment of the requirements for the degree of Doctor of Engineering Sciences (Dr.-Ing.)

by

M. Sc. Trung Dung Pham

Born in Quang Ninh - Vietnam

Main referee : Prof. Dr.-Ing. habil. Dr. h.c. Volker Schwieger

Co-referee : Prof. Dr.-Ing. Uwe Sörgel

Date of defence : 28.05.2020

Institute of Engineering Geodesy (IIGS)

University of Stuttgart

2020

Contents

Abstract	5
Zusammenfassung	6
1. Introduction	8
1.1 Motivation	8
1.2 Objectives	9
1.3 Thesis outline	10
2. Background of Non-linear Models and Measures of Non-linearity	11
2.1 Linear and Non-linear Models	11
2.1.1 Linear Model	11
2.1.2 Non-linear Model	11
2.1.3 Linearization of a Non-linear Model	13
2.1.4 Unscented transform	15
2.1.5 Monte Carlo simulation	16
2.2 Theory of Measures of Non-linearity	18
2.2.1 Coefficient of Determination	18
2.2.2 Multivariate Association	20
2.2.3 Non-linearity Measures Based on Deviation from Linear Function	23
2.3 Procedure of Measures of Non-linearity	25
2.4 Empirical non-linearity	27
3. Filtering Algorithms for Positioning	29
3.1 Non-linear Filtering Algorithms	29
3.1.1 Kalman filter	29
3.1.2 Linearized Kalman filter	31
3.1.3 Extended Kalman filter	33
3.1.4 Unscented Kalman filter	34
3.1.5 Particle filter	36
3.2 Computational complexity	40
3.3 Non-linear System and Observation Models	41
3.3.1 Non-linear System Models	41
3.3.2 Non-linear Observation Models	46
4. Accuracy and Computational Time of Kinematic Positioning	50
4.1 Kinematic Position Accuracy	50

4.1.1 Introduction of Scenarios	51
4.1.2 Impact of Measurement Uncertainty on Position Accuracy	52
4.1.3 Impact of Observation Geometry on Position Accuracy	54
4.1.4 Impact of Number of Measurements on Position Accuracy	56
4.2 Computational complexity	58
4.3 Summary	59
5. Choice of Filtering Algorithms using Non-linear Characteristic	60
5.1 Measures of Non-linearity	60
5.1.1 Non-linearity of the system model	61
5.1.2 Non-linearity of the observation model	63
5.2 Relationship between Non-linearity and Position Accuracy	67
5.2.1 Variation of measurement uncertainty	67
5.2.2 Variation of observation geometry	69
5.2.3 Variations of both measurement uncertainty and observation geometry	70
5.2.4 Summary	73
5.3 Evaluation of the non-linear characteristic for the selection of algorithms	74
5.3.1 Procedure of the selection of algorithms	74
5.3.2 Numerical examples	75
5.3.3 Assessments of the non-linear characteristic in choice of algorithms	80
5.4 Summary	82
6. Conclusions	83
References	85
Appendix A1: Accuracy of measurements of bearing and range radars	89
Appendix A2: Influence of the number of measurements on position accuracy	90
Appendix A3: Optimal number of MC runs for determining non-linearity	91
Appendix A4: Non-linearity of the system model with varying the data rate, velocity, and orientation change	92
Appendix A5: Determination of the coefficients of fitting function and their GOFs for different measurement uncertainties	93
Appendix A6: Determination of the coefficients of fitting function and their GOFs for different observation geometries	96
Appendix A7: Hypothesis test for the quadratic coefficient b_2	99
Acknowledgements	100
Curriculum Vita	101

Abstract

Selection of an optimal filtering algorithm for kinematic positioning systems constitutes one of the most extensively studied applications in the surveyor engineering community. The ability of a filtering algorithm is often assessed through its performance. The performance of a filtering algorithm is frequently evaluated in terms of accuracy and computational time. According to the accuracy parameter, it is often determined by a comparison between true trajectory and the estimated one from an algorithm. However, the true trajectory is commonly unknown in real-life situations, and thus the accuracy of the filtering algorithm cannot be assessed in this manner. Indeed, lack of true trajectory is one of the primary obstacles in the evaluation of the performance of filtering algorithms. The non-linearity of the model, on the other hand, can be determined without any information about the true trajectory and is also associated with the abilities of algorithms. So far, however, very little attention has been paid to the role of the decision of filtering algorithms based on non-linearity. Thus, this study proposes an alternative characteristic in the assessment of the performance of filtering algorithms, which is the non-linearity of the observation model. This research aims to assess the ability of non-linear characteristic for the choice of an optimal filtering algorithm.

In this research, the data are simulated by the Monte Carlo method. The abilities of filtering algorithms are investigated on the extended Kalman filter (EKF), unscented Kalman filter (UKF), and particle filter (PF). These algorithms are widely utilized in kinematic positioning, and they are appropriate for various levels of non-linearity. The current study evaluated the influence of the algorithm's accuracy on three factors: measurement uncertainty, observation geometry, and the number of observations. These algorithms are also assessed on their computational times according to a certain scenario. Regarding measures of non-linearity, three different indicators are examined for the non-linearity of both system and observation models. The coefficient of determination, $1-R^2$, is utilized as a single indicator to measure the non-linearity of each function of the above models. The M and $1-MVA$, known as the deviation of a non-linear function from linearity and multivariate association, respectively, can be used as indicators to quantify the non-linearity of numerous functions of the above models jointly. The $1-MVA$ indicator is proposed for the first time to quantify the non-linearity of models. From analyses of the accuracy and non-linearity, the relationship between them is determined with changing measurement uncertainty and observation geometry in several scenarios. Based on the established relationship between accuracy and non-linearity, the choice of an optimal algorithm is analyzed through numerical examples.

These results indicate that the accuracy of these algorithms is strongly influenced by measurement uncertainty, observation geometry, and the number of observations. The accuracy obtained by PF is higher than that of UKF and EKF. Conversely, the computational time of EKF is shorter than that of UKF and PF. According to measures of non-linearity, the above-proposed indicators are suitable, and the tendency of non-linearity of a model obtained by these indicators is the same. The non-linearity of the system model is small due to the given small amount of standard deviations of the disturbance quantities. Inversely, the non-linearity of the observation model is high due to high measurement uncertainties, or poor observation geometries. The main finding of this research is that both non-linearity of the observation model and position accuracy are influenced by factors of measurement uncertainty and observation geometry. Therefore, the relationship between the position accuracy and the non-linearity of the observation model is established based on these factors. This relationship is strong, which is assessed by the goodness-of-fit value of the best fitting function. In addition, another important result from the present research is that the fitting function described for this relationship changes due to influencing factors of scenarios. The established relationship constitutes the main limitation of this characteristic in application. As a result, instead of accuracy, the non-linearity of the observation model can be employed for the assessment of algorithms when the true trajectory is not available. However, the optimal algorithm can only be selected using these factors in some special cases. For a general case of arbitrary scenarios' factors, the non-linear characteristic cannot be used for this purpose.

Zusammenfassung

Die Wahl eines optimalen Filteralgorithmus für kinematische Positionierungssysteme stellt eine der am ausführlichsten untersuchten Anwendungen in der Ingenieurgeodäsie dar. Die Möglichkeiten, die ein Filteralgorithmus bietet, werden sehr häufig durch seine Leistungsfähigkeit beurteilt. Die Leistungsfähigkeit wird in dieser Arbeit anhand der Parameter Genauigkeit und Rechenzeit beurteilt. Der Genauigkeitsparameter wird dabei häufig über den Vergleich zwischen der wahren Trajektorie und der durch den Algorithmus geschätzten Trajektorie bestimmt. Jedoch kann es vorkommen, dass die wahre Trajektorie in einer realen Situation nicht bekannt ist und somit die Genauigkeit des Filters nicht auf diese Art und Weise beurteilt werden kann. In der Tat ist dieser Aspekt einer der wichtigsten Hinderungsgründe für eine Beurteilung der Leistungsfähigkeit von Filteralgorithmen. Auf der anderen Seite können Nichtlinearitäten des Modells ohne jegliche Vorinformation über die wahre Trajektorie bestimmt werden. Nichtlinearitäten können ebenfalls mit den Eigenschaften/Parametern des Algorithmus in Verbindung gebracht werden. Diesem Aspekt wird jedoch bislang wenig Beachtung geschenkt. In dieser Arbeit wird ein alternativer Parameter bei der Beurteilung der Leistungsfähigkeit von Filteralgorithmen, die eine Nichtlinearität im Beobachtungsmodell vorweisen, vorgestellt. In der Untersuchung soll der Nichtlinearitätsparameter verwendet werden, um eine entsprechende Wahl eines optimalen Filteralgorithmus vorzunehmen.

In dieser Untersuchung werden die Daten nach der Monte-Carlo Methode simuliert. Zur Untersuchung der Leistungsfähigkeit kommen das Erweiterte Kalmanfilter (EKF), das Unscented Kalmanfilter (UKF) und das Partikel Filters (PF) zum Einsatz. Diese Algorithmen sind bei der Verwendung in der kinematischen Positionsbestimmung weit verbreitet und sind für unterschiedliche Nichtlinearitätsniveaus anwendbar. Diese Dissertation evaluiert den Einfluss der Genauigkeiten der genannten Algorithmen basierend auf den folgenden drei Faktoren: Messunsicherheit, Beobachtungsgeometrie und Anzahl der Beobachtungen. Ferner werden die Algorithmen unter dem Gesichtspunkt der Rechenzeit unter bestimmten Szenarien evaluiert. Bezüglich des Aspekts der Nichtlinearität werden drei unterschiedliche Indikatoren, die sowohl die Modell- als auch die Messgleichungen betreffen, untersucht. Das Bestimmtheitsmaß $1 - R^2$ wird als Indikator für einzelne Funktionen verwendet um die Nichtlinearitäten in den Funktionen der beiden o.g. Modelle zu messen. Das M und das $1 - MVA$, bekannt als die Abweichung der nichtlinearen Modelle von linearen Modellen bzw. die multivariate Assoziation können als Indikatoren genutzt werden, um die Nichtlinearitäten mehrerer Funktionen zusammen zu bewerten. In dieser Arbeit wird zum ersten Mal vorgeschlagen, den Indikator $1 - MVA$ zu nutzen, um die Nichtlinearität des Modells zu beschreiben. Ausgehend von den Genauigkeiten und Nichtlinearitäten wird die Beziehung zwischen ihnen unter sich ändernder Messunsicherheit und Beobachtungsgeometrie in mehreren Szenarien analysiert. Basierend auf der aufgestellten Beziehung wird die Wahl des optimalen Algorithmus anhand numerischer Beispiele getroffen.

Die Ergebnisse zeigen, dass die Genauigkeit der Algorithmen stark von der Messgenauigkeit, der Messgeometrie und der Anzahl der Beobachtungen beeinflusst wird. Die Genauigkeit, die für das PF ermittelt wurde, ist höher als die des UKF und EKF. Umgekehrt ist die Rechenzeit des EKF kürzer als die des UKF und des PF. Bezugnehmend auf die Nichtlinearitätsmaße sind alle oben vorgestellten Indikatoren geeignet. Des Weiteren kann die Tendenz der Nichtlinearität eines Modells mit all diesen Indikatoren erkannt werden. Die Nichtlinearität des Systemmodells ist aufgrund der geringer gegebenen Standardabweichungen der Störgrößen klein. Umgekehrt sind die Nichtlinearitäten des Beobachtungsmodells aufgrund der hohen Messunsicherheiten und der schlechten Beobachtungsgeometrie hoch. Das Ergebnis der Untersuchung zeigt, dass sowohl die Nichtlinearität des Beobachtungsmodells als auch die Positionsgenauigkeit durch die Faktoren der Messunsicherheit und der Messgeometrie beeinflusst werden. Aus diesem Grund wird die Beziehung zwischen der Positionsgenauigkeit und der Nichtlinearität des Beobachtungsmodells mit diesen Faktoren begründet. Die

starke Abhängigkeit zwischen diesen Größen kann durch die Güte der Anpassung der Anpassungsfunktion gezeigt werden. Ein weiteres wichtiges Ergebnis der Untersuchung ist, daß die Änderung der Anpassungsfunktion von den Parametern des jeweiligen Szenarios abhängt. Diese Charakteristik der aufgestellten Beziehung ist gleichzeitig die größte Limitierung in der Anwendung. Somit kann im Ergebnis beim Nichtvorhandensein einer wahren Trajektorie statt der Genauigkeit die Nichtlinearität des Beobachtungsmodells für die Beurteilung des Algorithmus genutzt werden. Jedoch kann die Wahl des optimalen Algorithmus nur in Spezialfällen, bei denen diese oben genannten Parameter gelten, erfolgen. Im Allgemeinfall beliebiger Szenarien kann der Nichtlinearitätsparameter für die Beurteilung nicht herangezogen werden.

1. Introduction

1.1 Motivation

One of the main tasks in kinematic data processing is the choice of algorithm. The performance of a filtering algorithm can be evaluated by a comparison between the true and the estimated value of its algorithm. A variety of parameters are used for the evaluation of the performance of filtering algorithms (Blasch et al. 2006, Li and Zhao 2006). In geodesy, the root mean square error (RMSE) has been widely employed as a general parameter for the assessment of algorithms. However, in order to use this parameter, the true trajectory needs to be provided, but it is frequently unknown in reality. To date, the challenge in the choices of optimal filtering algorithms when the true trajectory is not available constitutes the lack of a proper parameter.

On the other hand, non-linearity of the model is associated with both the equation and measurement uncertainty (Li, 2012), but it is not related to the information of the actual value. It is not difficult to distinguish between linear and non-linear models in theory. However, quantification of non-linearity of a model remains a challenging task. Non-linearity was first quantitatively measured by Beale's indicator (Beale 1960). In that study, a non-linear level was known as a measure to indicate when a non-linear model can be approximated via linear theory. Based on the idea of Beale's indicator, Li (2012) developed a measure of non-linearity for a model in kinematic positioning applications. This measure was also applied for comparing the non-linearity of observation models (Mallick and Ristic 2017), and for evaluating the non-linearity of both dynamic models and measurement models for the purpose of video-based object tracking (Wang et al. 2016). In addition, non-linearity can be identified based on the geometric concept of curvature, termed a curvature measure (Bates and Watts 1980). The curvature measure was utilized to detect the non-linearity of dynamic and observation models in the field of tracking and navigation, such as in Mallick et al. (2005), Niu et al. (2008), and Scala et al. (2007). The evaluation of the linear or non-linear characteristics of the model can also use the coefficient of determination (R^2) (Helton and Davis 2003). In this research, the non-linearity of the model can be determined based on the principle of linear regression analysis. The idea behind this method (R^2) is using a non-linear part, which cannot be accounted for by the linear regression model, as a quantitative non-linearity. The non-linearity value, however, can only deal with a single output variable. By contrast, the multivariate association (MVA) is known as a means of the linear relationship between two sets of variables (Cramer 1974). The multivariate association is directly extended from the multiple regression analysis. This indicator is proposed to be utilized to measure the non-linearity of the model for the first time in this study.

One of the significant challenges for filtering estimation arises from non-linear characteristics of the model. Several approaches exist to overcome the difficulties of non-linear filtering problems. In a linear model with Gaussian process noise and measurement noise, the Kalman filter is well-known to be the optimal solution (Fredrik 2010). Since most of the models are non-linear in different levels of non-linearities, an efficient solution should be proposed in these cases. The KF algorithm can be applied by using a linearization step, which is carried out by employing partial derivatives of non-linear models. These approaches are referred to as the linearized Kalman filter (LKF) and extended Kalman filter (EKF) (Gelb 1979). These methods are able to work well for weakly non-linear models. For a medium level of non-linearity, the unscented Kalman filter (UKF) (Julier and Uhlmann 1997) constitutes an appropriate approach, which is demonstrated to accommodate the second-order derivative in non-linear models. Although the accuracy estimation obtained by UKF is more accurate than those of LKF and EKF, the process and measurement noise assumed to be Gaussian remain the primary limitation of this algorithm. In addition, the particle filter (PF) (Gordon et al. 1993), a popular method for solving non-linear filtering estimation problems, can deal with highly non-linear models without any assumption about the process noise and measurement noise. Consequently, quantification of non-linear levels (i.e., weak, medium, and high) is requisite for effective utilization of these non-linear filtering estimations.

Up to now, finding a potential characteristic in the selection of filtering algorithms in the case of a lack of true trajectory remains a challenge. In this study, non-linearity is proposed as a characteristic for this purpose. It is based on the hypothesis that if the relationship between accuracy and non-linearity is sufficiently strong, non-linearity can be used to replace accuracy as a parameter in the evaluation of filtering algorithms. Therefore, the optimal algorithm can be chosen using the non-linear characteristic, which does not require any information about the true trajectory. A few studies attempted to build a relationship between the performance of the filtering algorithm and non-linearity, such as Verlaan and Heemink (2000), Mallick (2004), and Li (2012). This relationship was only considered in the factor of measurement uncertainty, but a quantitative assessment of this relationship was not performed. Other factors affecting this relationship have also not been considered. This present investigation aims to quantitatively evaluate the relationship between the non-linearity of the observation model and position accuracy obtained by EKF, UKF, and PF. The assessment of the ability to use the non-linearity of the observation model in the decision of the above algorithms is the main goal concerning this study.

1.2 Objectives

The main topics of this thesis are non-linear estimation algorithms, the measure of non-linearity, the establishment of the relationship between accuracy and non-linearity, and the choice of optimal filtering algorithm using the non-linear characteristic. The primary objective of this study is to analyze the ability of a filtering algorithm in different levels of non-linearity. The non-linearities of both system and observation models are determined by different indicators according to kinematic positioning scenarios. Moreover, the relationship between position accuracy and non-linearity of observation is quantitatively analyzed. Finally, the non-linear characteristic for selecting an optimal algorithm is assessed through numerical examples. To achieve these objectives, the following aspects are examined:

- Evaluation of the performance of non-linear estimation algorithms

To assess the position accuracy of a moving object obtained by filtering algorithms, three non-linear estimation algorithms, EKF, UKF, and PF, are investigated in this study. First, the position accuracy of the moving object obtained by these algorithms is explored with a change of measurement uncertainties. In the second case, the position accuracy is evaluated in different observation geometries. Finally, the influence of position accuracy is investigated by changing the number of observations.

- Measures of non-linearity of both system and observation models by utilizing different indicators

To quantitatively measure the non-linearity of a model, three different indicators, $1-R^2$, $1-MVA$, and M , are applied. Non-linearities of the system model and observation model are separately evaluated with their influencing factors. According to the system model, its non-linearity is evaluated by varying velocity, data rate, and orientation change. According to the observation model, the influence of non-linearity is considered with the change of measurement uncertainty and observation geometry.

- Establishment of the relationship between position accuracy and the non-linearity of the observation model

To establish the relationship between accuracy and non-linearity, the position accuracy of the moving object and the non-linearity of the observation model are considered. The two factors of measurement uncertainty and observation geometry, which influence both position accuracy and the non-linearity of the observation model, are considered for the establishment of this relationship. The best function fitting for this relationship is assessed based on its goodness-of-fit. This established relationship is the key in using the non-linear characteristic in the decision of the optimal algorithm in the case of a lack of a true trajectory.

- Assessment of the non-linear characteristic in the selection of the optimal algorithm

To assess the ability to use the non-linearity of the observation model as a characteristic for choosing algorithms, the chosen algorithms by using the 1-MVA parameter will be compared to those using another parameter. The RMSE parameter, which is a popular parameter for evaluation of accuracy in geodesy, is employed for this purpose. Two parameters are used in the same scenarios, in which the true trajectory is assumed to be available. These comparisons are carried out through numerical examples.

1.3 Thesis outline

This thesis comprises six chapters and seven appendixes. Chapter 1 introduces the motivation of the study. A brief background of linear and non-linear models, and the measures of non-linearity are described in Chapter 2. In Chapter 3, a brief overview of filtering algorithms which can deal with non-linear estimation problems is introduced. In addition, the approach of the non-linear system and observation models are presented for the kinematic positioning problem. Chapter 4 assesses the performance of three filtering algorithms, consisting of EKF, UKF, and PF, on simulated data by the Monte Carlo method in terms of accuracy and computational time with kinematic applications. In Chapter 5, the non-linearity of the system model and observation model is examined. The relationship between the position accuracy and the non-linearity of the observation model is also established, according to the change of measurement uncertainty and observation geometry. Numerical examples of the selection of the optimal filtering algorithm using the non-linear characteristic are presented with certain scenarios. The main findings, limitations, and future works are given in Chapter 6.

Appendix A1 presents a classification of accuracy for bearing and range radars in marine applications. The effect of the number of measurements on the position accuracy with a 60° intersection angle is evaluated in Appendix A2. Appendix A3 is to determine the optimal number of MC runs in measuring non-linearity. The determination of the non-linearity of the system model is performed by varying the data rate, velocity, and orientation change in Appendix A4. The fitting function and its coefficients between the position accuracy and the non-linearity of the observation model in cases of changing measurement uncertainty and observation geometry are plotted in Appendix 5 and 6, respectively. Finally, the hypothesis test for the quadratic coefficient of fitting function is carried out in Appendix 7.

2. Background of Non-linear Models and Measures of Non-linearity

Identification of the non-linearity of models is critical for both theory and practice. In filtering estimation, all realistic system and observation models possess some level of non-linearity. The level of non-linearity is one of the most challenging factors to solve in non-linear problems. Therefore, the objective of this chapter is to present linear and non-linear models from theoretical perspectives, and then to introduce indicators for measuring the non-linearity of non-linear models. The structure of this chapter comprises four parts. The first section provides the background of linear and non-linear models. Proper indicators for detecting the non-linearity of a non-linear model are discussed in the subsequent section. The third section proposes a procedure for determining the non-linearity of a non-linear model. In the final section, an empirical example about measures of non-linearity is presented for a simple non-linear function.

2.1 Linear and Non-linear Models

This section presents definitions of linear and non-linear models in a theoretical perspective. The techniques to overcome the non-linear problem, such as linearization, unscented transform, and Monte Carlo simulation, are briefly introduced in the remaining subsections.

2.1.1 Linear Model

The model of observation equations is described by the linear relationship between outputs y_i ($i = 1, 2, \dots, m$) and input variables x_j ($j = 1, 2, \dots, n$) as:

$$y_i = a_{i1}x_1 + a_{i2}x_2 + \dots + a_{in}x_n, i = 1, 2, \dots, m, \quad (2-1)$$

where $a_{i1}, a_{i2}, \dots, a_{in}$ are known scalars.

Equation (2-1) can be written in a matrix-vector form as:

$$\mathbf{y}_{m \times 1} = \mathbf{A}_{m \times n} \mathbf{x}_{n \times 1}, \quad (2-2)$$

$$\text{where } \mathbf{A}_{m \times n} = \begin{pmatrix} a_{11} & \dots & a_{1n} \\ \vdots & \ddots & \vdots \\ a_{m1} & \dots & a_{mn} \end{pmatrix}; \mathbf{y}_{m \times 1} = \begin{pmatrix} y_1 \\ \vdots \\ y_m \end{pmatrix}; \mathbf{x}_{n \times 1} = \begin{pmatrix} x_1 \\ \vdots \\ x_n \end{pmatrix}.$$

Equation (2-2) is the system of m -number of output variables and n -number of input variables.

2.1.2 Non-linear Model

A model is the relationship between output variables and input variables. If this relationship is not linear, this model is known as a non-linear model. There are many models that fit into this framework due to the functional form of the relationship being modeled. The non-linear model of observation equations, in terms of the non-linear relationship between output variables y_i ($i = 1, 2, \dots, m$) and input variables x_j ($j = 1, 2, \dots, n$), can be written as follows:

$$y_i = f_i(x_1, x_2, \dots, x_n), i = 1, 2, \dots, m, \quad (2-3)$$

where $f_i(\cdot)$ is a non-linear equation.

The matrix-vector form of equation (2-3) can also be written in the same way as in equation (2-2) as:

$$\mathbf{y} = \mathbf{f}(\mathbf{x}), \quad (2-4)$$

where $\mathbf{f}(\mathbf{x}) = \begin{pmatrix} f_1(\mathbf{x}) \\ \dots \\ f_m(\mathbf{x}) \end{pmatrix}$ is m -number of non-linear equations.

In geodetic applications, a few cases exist in which the assumption of the linear relationship between output vectors \mathbf{y} and input vector \mathbf{x} in (2-2) holds. For example, in levelling applications, the assumption of linear relation is satisfied. However, in most practical cases, this relationship is non-linear. The following example will clarify this.

Example A

This example gives fundamentally non-linear functions for observations in geodesy. A bearing angle and distance are non-linear functions with respect to coordinates.

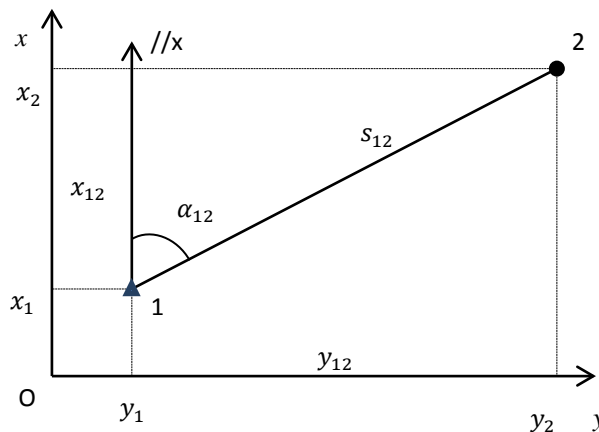


Fig. 2-1. Determination of coordinates x_2 and y_2 by bearing angle and distance in a polar system.

The coordinates of point 1 (x_1, y_1) are known, while the coordinates of point 2 (x_2, y_2) are unknown. The outputs consist of azimuth (bearing angle) and distance measurements which are related to coordinates by (see Fig. 2-1):

$$\alpha_{12} = \text{atan} \left(\frac{y_2 - y_1}{x_2 - x_1} \right), \quad (2-5)$$

$$s_{12} = \sqrt{(x_2 - x_1)^2 + (y_2 - y_1)^2}.$$

The model of observation equations, including azimuth and distance measurements, is a non-linear model with respect to two input variables (unknown parameters) x_2 and y_2 :

$$\begin{pmatrix} \alpha_{12} \\ s_{12} \end{pmatrix} = \begin{pmatrix} \text{atan}\left(\frac{y_2 - y_1}{x_2 - x_1}\right) \\ \sqrt{(x_2 - x_1)^2 + (y_2 - y_1)^2} \end{pmatrix}.$$

2.1.3 Linearization of a Non-linear Model

The linear estimators, such as the least-square method and the standard Kalman filter method, can only be used for the linear model. For non-linear problems, a linearization technique can be utilized to obtain a linear model. The main idea behind linearization is to approximate the formerly non-linear model with a linear one by utilizing Taylor series expansion.

For the relationship between one output variable y and multiple input variables $\mathbf{x} = (x_1, x_2, \dots, x_n)'$, the single-variable function

$$y = f(\mathbf{x}) \quad (2-6)$$

can be expressed in terms of Taylor series as:

$$f(\mathbf{x}) = f(\mathbf{x}^0) + \sum_{i=1}^n \frac{\partial f(\mathbf{x}^0)}{\partial x_i} \Delta x_i + \underbrace{\frac{1}{2} \sum_{i=1}^n \sum_{j=1}^n \frac{\partial^2 f(\mathbf{x}^0)}{\partial x_i \partial x_j} \Delta x_i \Delta x_j + \dots}_{\text{negligible if } \Delta x \text{ small}} \quad (2-7)$$

where $\mathbf{x}^0 = (x_1^0, x_2^0, \dots, x_n^0)'$ is the approximated value of vector \mathbf{x} ; and the difference between \mathbf{x} and \mathbf{x}^0 is $\Delta \mathbf{x} = (\Delta x_1, \Delta x_2, \dots, \Delta x_n)' = (x_1 - x_1^0, x_2 - x_2^0, \dots, x_n - x_n^0)'$.

Assuming that the approximation \mathbf{x}^0 is close to \mathbf{x} , then equation (2-7) can be rewritten in vector form as follows:

$$f(\mathbf{x}) = f(\mathbf{x}^0) + \mathbf{g}' \Delta \mathbf{x} + \frac{1}{2} \Delta \mathbf{x}' \mathbf{H} \Delta \mathbf{x}, \quad (2-8)$$

with \mathbf{g} and \mathbf{H} are the gradient vector and Hessian matrix of function, respectively, which are defined as (Atkinson 1989):

$$\mathbf{g} = \mathbf{g}_f(\mathbf{x}^0) = \frac{d}{dx} f(\mathbf{x}^0) = \begin{pmatrix} \frac{\partial f(\mathbf{x}^0)}{\partial x_1} \\ \vdots \\ \frac{\partial f(\mathbf{x}^0)}{\partial x_n} \end{pmatrix} \text{ and } \mathbf{H} = \mathbf{H}_f((\mathbf{x}^0)) = \frac{d}{dx} \mathbf{g}_f(\mathbf{x}^0) = \begin{pmatrix} \frac{\partial^2 f(\mathbf{x}^0)}{\partial x_1^2} & \dots & \frac{\partial^2 f(\mathbf{x}^0)}{\partial x_1 \partial x_n} \\ \vdots & \ddots & \vdots \\ \frac{\partial^2 f(\mathbf{x}^0)}{\partial x_n \partial x_1} & \dots & \frac{\partial^2 f(\mathbf{x}^0)}{\partial x_n^2} \end{pmatrix}.$$

For the relationship between multiple output variables $\mathbf{y} = (y_1, y_2, \dots, y_m)'$, and multiple input variables $\mathbf{x} = (x_1, x_2, \dots, x_n)'$, the multi-variable function can be expressed in (2-4). The Taylor expansion of the i^{th} ($i=1, 2, \dots, m$) component can be written as:

$$f_i(\mathbf{x}) = f_i(\mathbf{x}^0) + \mathbf{g}'_i \Delta \mathbf{x} + \frac{1}{2} \Delta \mathbf{x}' \mathbf{H}_i \Delta \mathbf{x}. \quad (2-9)$$

If the last term of (2-9), the second-order remainder, is ignored, the linear approximation combining from the first two terms of these m components can be rewritten as (Teunissen and Montenbruck 2017):

$$\mathbf{f}(\mathbf{x}) = \begin{pmatrix} f_1(\mathbf{x}) \\ \vdots \\ f_m(\mathbf{x}) \end{pmatrix} \approx \begin{pmatrix} f_1(\mathbf{x}^0) \\ \vdots \\ f_m(\mathbf{x}^0) \end{pmatrix} + \begin{pmatrix} \frac{\partial f_1(\mathbf{x}^0)}{\partial x_1} & \dots & \frac{\partial f_1(\mathbf{x}^0)}{\partial x_n} \\ \vdots & \ddots & \vdots \\ \frac{\partial f_m(\mathbf{x}^0)}{\partial x_1} & \dots & \frac{\partial f_m(\mathbf{x}^0)}{\partial x_n} \end{pmatrix} \begin{pmatrix} \Delta x_1 \\ \vdots \\ \Delta x_n \end{pmatrix}. \quad (2-10)$$

If the second component on the right-hand side of equation (2-10) is denoted by $\mathbf{J}_f(\mathbf{x}^0)\Delta\mathbf{x}$, and substituting (2-10) into (2-4), the equation in matrix form can then be written as:

$$\mathbf{y} \approx \mathbf{f}(\mathbf{x}^0) + \mathbf{J}_f(\mathbf{x}^0)\Delta\mathbf{x}. \quad (2-11)$$

where $\mathbf{J}_f(\mathbf{x}^0)$ is the Jacobian matrix.

It is necessary to mention that if the difference between \mathbf{y} and m -vector $\mathbf{f}(\mathbf{x}^0)$ is $\Delta\mathbf{y}$, then the formula of the linearized model of observation equations becomes:

$$\Delta\mathbf{y} = \mathbf{J}_f(\mathbf{x}^0)\Delta\mathbf{x}. \quad (2-12)$$

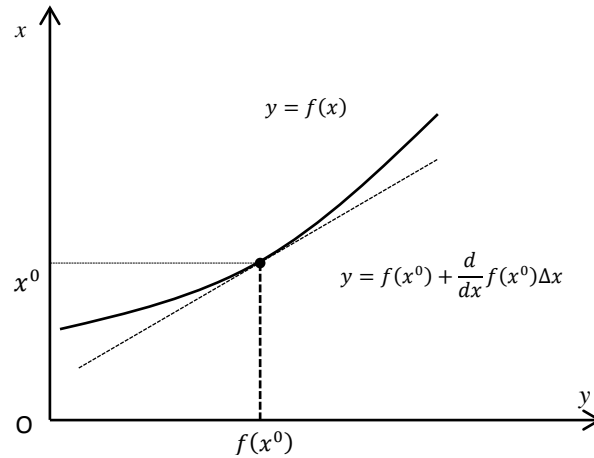


Fig. 2-2. In a one-dimensional formulation, a tangent line approximates to $f(x)$ at x^0 is linear function and which is described by $f(x^0) + \frac{d}{dx}f(x^0)\Delta x$.

Example B

Linearization of a non-linear model is realized in two non-linear observations of distance and azimuth in the configuration of Fig. 2-1. The approximate values for the input variables (unknown parameters) x_2 and y_2 are represented by x_2^0 and y_2^0 . The non-linear observation models in (2-5) are linearized by the following:

$$\frac{\begin{pmatrix} \Delta\alpha_{12} \\ \Delta s_{12} \end{pmatrix}}{(\Delta y)} = \underbrace{\begin{pmatrix} \frac{x_2^0 - x_1}{s_{12}^2} & -\frac{y_2^0 - y_1}{s_{12}^2} \\ \frac{x_2^0 - x_1}{s_{12}} & \frac{y_2^0 - y_1}{s_{12}} \end{pmatrix}}_{J_f(x^0)} \frac{\begin{pmatrix} \Delta x_2 \\ \Delta y_2 \end{pmatrix}}{\Delta x}, \quad (2-13)$$

$$\text{with } \begin{pmatrix} \Delta x_2 \\ \Delta y_2 \end{pmatrix} = \begin{pmatrix} x_2 - x_2^0 \\ y_2 - y_2^0 \end{pmatrix} \text{ and } \begin{pmatrix} \Delta\alpha_{12} \\ \Delta s_{12} \end{pmatrix} = \begin{pmatrix} \alpha_{12} - \text{atan}\left(\frac{y_2^0 - y_1}{x_2^0 - x_1}\right) \\ s_{12} - \sqrt{(x_2^0 - x_1)^2 + (y_2^0 - y_1)^2} \end{pmatrix}.$$

2.1.4 Unscented transform

The unscented transform (UT) method is another way to overcome the non-linear problem without linearization technique, which is discussed in section 2.1.3. The main idea of this method is that the means and covariances of probability distributions are parameterized by a set of appropriately-chosen weighted points. Fig. 2-3 shows the principle of the UT method.

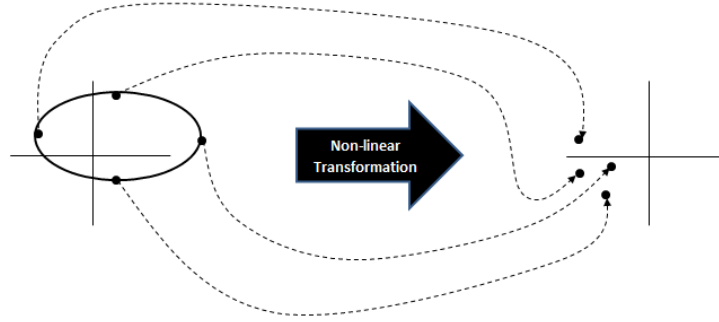


Fig. 2-3. The principle of the unscented transform (Julier and Uhlmann 2004).

Consider propagating n -dimensional random input vector \mathbf{x} through non-linear function $\mathbf{y} = \mathbf{f}(\mathbf{x})$. The mean and covariance matrix of \mathbf{x} are given by $\bar{\mathbf{x}}$ and Σ_{xx} , respectively. To obtain the mean of \mathbf{y} , covariance matrix of \mathbf{y} , and covariance matrix between \mathbf{x} and \mathbf{y} , a matrix of $2n+1$ sigma vectors $\boldsymbol{\gamma}_i$ is generated as:

$$\begin{aligned} \boldsymbol{\gamma}_0 &= \bar{\mathbf{x}} \\ \boldsymbol{\gamma}_i &= \bar{\mathbf{x}} + \left(\sqrt{(n + \lambda_{UT})\Sigma_{xx}}\right)_i, \quad i = 1, 2, \dots, n \\ \boldsymbol{\gamma}_i &= \bar{\mathbf{x}} - \left(\sqrt{(n + \lambda_{UT})\Sigma_{xx}}\right)_{i-n}, \quad i = n + 1, n + 2, \dots, 2n. \end{aligned} \quad (2-14)$$

The corresponding weighted sigma-points are defined as:

$$\begin{aligned}
W_0^m &= \lambda_{UT}/(n + \lambda_{UT}), \\
W_0^c &= \lambda_{UT}/(n + \lambda_{UT}) + (1 - \alpha_{UT}^2 + \beta_{UT}), \\
W_i^m &= W_i^c = 1/2(n + \lambda_{UT}) \quad i = 1, 2, \dots, 2n,
\end{aligned} \tag{2-15}$$

where W^m and W^c are denoted for the weight of mean and weight of covariance, respectively; $(\sqrt{(n + \lambda_{UT})\Sigma_{xx}})_i$ is the i^{th} column of the Cholesky factorization; and $(n + \lambda_{UT})$ is a scaling factor. λ_{UT} is determined by:

$$\lambda_{UT} = \alpha_{UT}^2(n + \kappa_{UT}) - n, \tag{2-16}$$

where the first parameter α_{UT} is set between 10^{-4} and 1, determining the spread of the sigma-points around the mean value; the secondary scaling parameter κ_{UT} is usually set to 0; and, for a Gaussian distribution, the third parameter β_{UT} is 2 (Wan and van der Merwe 2000).

These sigma vectors are propagated through the non-linear function as:

$$\chi_i = f(\gamma_i), \quad i = 0, 1, 2, \dots, 2n. \tag{2-17}$$

Finally, the estimated mean $\hat{\mathbf{y}}$ and estimated covariance matrix $\Sigma_{\hat{\mathbf{y}}\hat{\mathbf{y}}}$, are computed as:

$$\bar{\mathbf{y}} = \sum_{i=0}^{2n} W_i^m \chi_i, \tag{2-18}$$

$$\Sigma_{\hat{\mathbf{y}}\hat{\mathbf{y}}} = \sum_{i=0}^{2n} W_i^c (\chi_i - \bar{\mathbf{y}})(\chi_i - \bar{\mathbf{y}})'. \tag{2-19}$$

In the UT method, a probability density function can be approximated without a linearization step. The assumption of Gaussian distribution is the main disadvantage of this method.

2.1.5 Monte Carlo simulation

The Monte Carlo (MC) simulation is a computational method that relies on the utilization of random samples and probability statistics to approximate required parameters (Buslenko et al. 1966). These parameters (i.e., expected value, variance, and covariance) can be numerically approximated by MC simulation based on the distribution of output variables when the density function of input variables is known. In an MC simulation, a set of samples of input vectors can be generated by using random number generators. A fully deterministic process can be used to generate random numbers (Robert and Casella 2004). It is assumed that a random output vector \mathbf{y} is non-linearly related to a random input vector \mathbf{x} , and the density function of the input vector is known. The quantities of the output vector are calculated by using the non-linear function from the corresponding amounts of input sample vectors. A random distribution of the output quantities is then approximated by an empirical distribution, which is obtained from the output sample vector.

In this section, the MC simulation is presented for computation of the expected value and the covariance of the m -dimensional output vector \mathbf{y} , described in (2-4). First, each input variable of the n -dimensional input vector \mathbf{x} is generated randomly from a probability density function (PDF) with N_{MC} times. Then, the quantities of the m -dimensional vector \mathbf{y} can be calculated by:

$$\mathbf{y}_i = \mathbf{f}(\mathbf{x}_i), \quad i = 1, 2, \dots, N_{MC}, \quad (2-20)$$

where $\mathbf{x}_i = (x_{i1}, x_{i2}, \dots, x_{in})'$ and $\mathbf{y}_i = (y_{i1}, y_{i2}, \dots, y_{im})'$ are the input and output vectors, respectively, at the i^{th} time of N_{MC} number of generated samples in the MC simulation.

Finally, the estimation of statistical quantities, including the mean value and covariance of the output vector, can be computed as:

$$\bar{\mathbf{y}} = \frac{1}{N_{MC}} \sum_{i=1}^{N_{MC}} \mathbf{y}_i \quad (2-21)$$

and

$$\boldsymbol{\Sigma}_{yy} = \frac{1}{N_{MC} - 1} \sum_{i=1}^{N_{MC}} (\mathbf{y}_i - \bar{\mathbf{y}})(\mathbf{y}_i - \bar{\mathbf{y}})', \quad (2-22)$$

where $\bar{\mathbf{y}}$ and $\boldsymbol{\Sigma}_{yy}$ are the mean value and covariance of \mathbf{y} , respectively.

In the MC simulation, the expected value and covariance are more accurate than those achieved by the UT method. Explicitly, a significant number of random samples used in the MC simulation can obtain superior results compared to a small number of sigma-points chosen in a deterministic manner. The accuracy of the estimation values in (2-21) and (2-22) gets better, if N_{MC} gets larger, too. However, the computational time of the simulation increases as the number of samples is increased. One common way of terminating simulation is to continue running until the estimated result becomes stable. In statistical analysis, the required sample can be computed based on the allowable error in the estimation, the confidence level, and the estimated quantity (Hosseini et al. 2011). For example, the typical value of the sample of MC simulation is 5000 in the application of position estimation for mobile robots (Choudhury et al. 2008). To obtain the estimates of the statistical moments (i.e., mean and covariance) of the probability density function with at least three significant digits, 10^5 samples were used in MC simulation in the application of kinematic terrestrial laser scanning (Alkhatib and Kutterer 2013).

2.2 Theory of Measures of Non-linearity

It is not difficult to discern whether a model is linear or non-linear, but quantification of the level of non-linearity remains a problem. Each non-linear filtering algorithm works well on a certain level of non-linearity (i.e., EKF, UKF, and PF are suitable for weak, medium, and high non-linearity, respectively). Up to now, few studies have investigated quantification of these non-linear levels. Consequently, this study will quantitatively analyze non-linear levels for selecting proper filters.

Several indicators exist for measuring non-linearity. The first class of non-linearity measures is known as the test of non-linearity. By this class, the significance value p can reveal non-linearity. However, quantification of the non-linearity is not easy since the result of the test is to reject or accept the hypothesis (Kroll and Emancipator 1993). Another class of non-linearity measures is defined based on curvature studies in differential geometry. Curvature is computed by the ratio between the second-order and the first-order derivatives (Helbig et al. 2000), (Mallick et al. 2005), (O'Brien et al. 2010), and (Niu et al. 2008). However, the main drawback of this method is an omission of higher-order derivatives, which contribute to the non-linearity of models. Moreover, derivatives are not simple to evaluate, or even are non-existent in some cases. Therefore, the two aforementioned classes of non-linearity measure are not considered in this study.

In this research, three indicators for measuring non-linearity are applied. First, the coefficient of determination R^2 (Helton and Davis 2000), (Schwieger 2005), employed as an indicator for evaluating the model, is applied to measure the non-linearity of non-linear models. Although R^2 provides the contribution of each output variable in terms of non-linearity, it does not allow determination of the non-linearity of multiple output variables together. Second, the multivariate association (*MVA*) is used to measure the non-linear relationship between two sets of variables from a theoretical perspective. *MVA*, known as a generalized coefficient of determination, is straightforwardly extended by multiple regression analysis (Hotelling 1936), (Cramer 1946), (Yanai 1974), (Robert and Escoufier 1976), and (Cramer and Nicewander 1979). In this thesis, *MVA* is proposed as an indicator for the first time to be applied for measuring non-linearity of the model. Third, M , developed by Li (2012), is also an appropriate indicator for measuring non-linearity of a model. The main concept behind this method is the mean-square distance between the given non-linear system and a set of all linear models. M is also applied for evaluating the non-linearity of models in Liu and Li (2015), Mallick and Ristic (2017), and Wang et al. (2016). The principles of R^2 , *MVA*, and M will be discussed in the remainder of this chapter, and the numerical computation of these indicators will be analyzed in Chapter 5.

2.2.1 Coefficient of Determination

The coefficient of determination R^2 is one of the most broadly used measures in statistical analysis to evaluate a model. This section will present how R^2 can be developed to measure the non-linear relationship between various input variables and one output variable. Because there is only one output, the index of the output variable is omitted.

In general, linear regression analysis provides a statistical relationship between one output y and multiple independent input variables, x_1, x_2, \dots, x_n , in the following form (Helton and Davis 2003):

$$\hat{y} = b_0 + \sum_{i=1}^n b_i \cdot x_i, \quad (2-23)$$

where b_0, b_1, \dots, b_n are regression coefficients to be estimated; and \hat{y} is the estimated output.

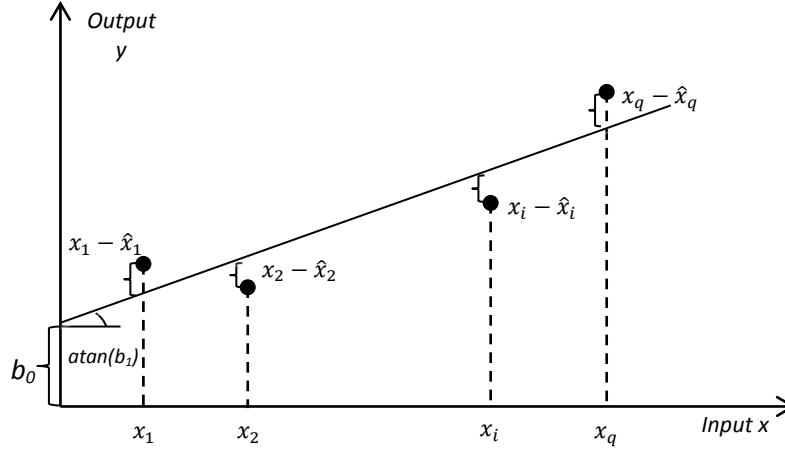


Fig. 2-4. Relationships in regression analysis between x and y (Weisberg 2005).

In order to perform a regression analysis, a total of $n \times q$ realizations for n input quantities x_i and q realizations of the output variables y are required. Supposing that n input variables are independent and have the same accuracy, then the regression coefficients $\mathbf{b} = (b_0 \ b_1 \ \dots \ b_n)'$ can be determined by applying the least-squares method as follows:

$$\mathbf{b} = (\mathbf{X}' \cdot \mathbf{X})^{-1} \cdot (\mathbf{X}' \cdot \mathbf{y}), \quad (2-24)$$

where $\mathbf{X} = \begin{pmatrix} 1 & x_{11} & \dots & x_{1n} \\ 1 & x_{21} & \dots & x_{2n} \\ \vdots & \vdots & \ddots & \vdots \\ 1 & x_{q1} & \dots & x_{qn} \end{pmatrix}$ is a matrix of realizations of the input variable

and $\mathbf{y} = \begin{pmatrix} y_1 \\ y_2 \\ \vdots \\ y_m \end{pmatrix}$ is a vector of realizations of the output variables.

After estimation of the regression coefficient, the estimated output \hat{y}_j is computed by using \mathbf{b} for each line of realization of input variables in matrix \mathbf{X} as:

$$\hat{y}_j = b_0 + \sum_{i=1}^n b_i \cdot x_{ji}, \quad j=1,2,\dots, q. \quad (2-25)$$

For linear regression models, the following covariance decomposition is valid (Helton and Davis 2003):

$$\sum_{j=1}^q (y_j - \bar{y})^2 = \sum_{j=1}^q (\hat{y}_j - \bar{y})^2 + \sum_{j=1}^q (\hat{y}_j - y_j)^2, \quad (2-26)$$

where $\bar{y} = \frac{1}{q} \sum_{j=1}^q y_j$.

If the second term on the right-hand side of (2-26) becomes 0 ($\sum_{j=1}^q (\hat{y}_j - y_j)^2 = 0$), then the analyzed model is a linear model, and the coefficient of multiple determinations is represented as a normalized value:

$$R^2 = \frac{\sum_{j=1}^q (\hat{y}_j - \bar{y})^2}{\sum_{j=1}^q (y_j - \bar{y})^2}. \quad (2-27)$$

R^2 is a criterion for linearity, and its value is in the interval between 0 and 1 (Helton and Davis 2000). $R^2 = 1$ means that the model is linear, while $R^2 < 1$ means that the model is non-linear.

In this study, the value of $1-R^2$ is used as a measure of the non-linearity of a model. This value can be employed for measuring the non-linearity of a model which is a relationship between multiple inputs and a single output, but it cannot be used for a model which is a relationship between multiple inputs and multiple outputs. Consequently, $1-R^2$ is considered as a single indicator for measuring the non-linearity of a model. In order to measure the non-linearity of a model that has multiple output variables, other appropriate indicators should be investigated.

2.2.2 Multivariate Association

Multivariate association (*MVA*), known as the generalized coefficient of determination (Yanai 1974), is employed as a measure of the linear relationship between two sets of variables. Multivariate regression is extended from multiple regression analysis, which is most commonly encountered in the univariate case (a single output variable and a set of input variables) described in subsection 2.2.1. Multivariate regression in the case of more than one output variable is given as (Cramer and Nicewander 1979):

$$\mathbf{Y}_{q \times m} = \mathbf{X}_{q \times n} \mathbf{B}_{n \times m} + \mathbf{E}_{q \times m}, \quad (2-28)$$

where \mathbf{Y} is an $q \times m$ matrix on m output variables for q subjects; \mathbf{X} is a $q \times n$ matrix by n input variables; \mathbf{B} is an $n \times m$ matrix of regression coefficients; and \mathbf{E} is a $q \times m$ matrix of error in prediction or residual.

The matrix \mathbf{E} written in (2-28) is to compute *MVA* that is based on this residual. It is assumed that each row of \mathbf{E} has a multivariate normal distribution, and errors of each row are independent of each other. The matrix of regression coefficients can be expressed by using least-squares estimation under the assumption of independence among input variables as:

$$\mathbf{B} = (\mathbf{X}'\mathbf{X})^{-1}\mathbf{X}'\mathbf{Y}. \quad (2-29)$$

If the matrix of the sum of squares and cross-products of input variables $\mathbf{X}'\mathbf{X}$ is denoted by \mathbf{S}_{xx} and the matrix of the sum of cross-products of input and output variables $\mathbf{X}'\mathbf{Y}$ is denoted by \mathbf{S}_{xy} , then (2-29) is rewritten as follows:

$$\mathbf{B} = \mathbf{S}_{xx}^{-1}\mathbf{S}_{xy}. \quad (2-30)$$

Equation (2-30) is the same as equation (2-24) if each output variable is predicted separately from all input variables in the multiple regression. The matrix of the sum of squares of the output variables $\mathbf{S}_{yy} = \mathbf{Y}'\mathbf{Y}$, and estimated output variables $\mathbf{S}_{\hat{y}\hat{y}}$, is determined by:

$$\mathbf{S}_{\hat{y}\hat{y}} = \hat{\mathbf{Y}}'\hat{\mathbf{Y}} = \mathbf{B}'\mathbf{X}'\mathbf{X}\mathbf{B} = \mathbf{S}_{yx}\mathbf{S}_{xx}^{-1}\mathbf{S}_{xy}. \quad (2-31)$$

From matrices of the sum of the square of input and output variables and the cross-products between them, the *MVA* can be defined by the determinant of these matrices in several approaches (Cramer and Nicewander 1979). These approaches will be described in the next parts.

The relationship between two sets of variables is also measured as a function of a canonical correlation. A comprehensive definition of the canonical correlation ρ can be found in (Anderson 2003). The canonical correlation is a way of measuring the linear relationship between two multiple variables. According to the association between two sets of variables, the correlation matrix is diagonal, and the canonical correlation on the diagonal is maximized. The canonical correlation between two sets of variables \mathbf{x} and \mathbf{y} can be found by solving the following eigenvalue equations:

$$\begin{aligned}\Sigma_{xx}^{-1}\Sigma_{xy}\Sigma_{yy}^{-1}\Sigma_{yx}\widehat{\mathbf{w}}_x &= \rho^2\widehat{\mathbf{w}}_x \\ \Sigma_{yy}^{-1}\Sigma_{yx}\Sigma_{xx}^{-1}\Sigma_{xy}\widehat{\mathbf{w}}_y &= \rho^2\widehat{\mathbf{w}}_y\end{aligned}\quad (2-32)$$

where Σ is the total covariance matrix combined by \mathbf{x} and \mathbf{y} (Borga 1998) as:

$$\Sigma = \begin{bmatrix} \Sigma_{xx} & \Sigma_{xy} \\ \Sigma_{yx} & \Sigma_{yy} \end{bmatrix};$$

the eigenvalue ρ is the canonical correlation, and eigenvectors $\widehat{\mathbf{w}}_x$ and $\widehat{\mathbf{w}}_y$ are the normalized canonical correlations.

The canonical correlation has the same properties as any other correlation. The range of this correlation is from -1 to 1. If this value is close to 0, this indicates no linear association. Inversely, if this absolute value is close to 1, a nearly linear association is indicated.

MVA can be expressed in several ways. In this study, to distinguish the *MVA*, a superscript is used for this indicator. First, Hotelling (1936) suggested that an *MVA*⁽¹⁾ can be solved either by a determinant of covariance or by the canonical correlation. Thus, the *MVA*⁽¹⁾ is equal to the product of the squared canonical correlation, and is also equal to the ratio of the determinant of $\mathbf{S}_{\widehat{y}\widehat{y}}$ to the determinant of \mathbf{S}_{yy} as:

$$MVA^{(1)} = \frac{|\mathbf{S}_{\widehat{y}\widehat{y}}|}{|\mathbf{S}_{yy}|} = \frac{|\mathbf{S}_{yx}\mathbf{S}_{xx}^{-1}\mathbf{S}_{xy}|}{|\mathbf{S}_{yy}|} = \prod_{i=1}^m \rho_i^2. \quad (2-33)$$

Second, the *MVA*⁽²⁾ based on redundancy of measurement can be given by (Hotelling 1936) and (Rozeboom 1965):

$$MVA^{(2)} = 1 - \frac{|\mathbf{S}_{ee}|}{|\mathbf{S}_{yy}|} = 1 - \prod_{i=1}^m (1 - \rho_i^2), \quad (2-34)$$

where $\mathbf{S}_{ee} = \mathbf{S}_{yy} - \mathbf{S}_{\widehat{y}\widehat{y}}$ is the sum of square and cross-products of the error scores.

Third, the form of *MVA*⁽³⁾ based on the multiple correlation coefficient $\mathbf{S}_{\widehat{y}\widehat{y}}/\mathbf{S}_{yy}$ and closely related to

MVA⁽¹⁾ can be defined in Cramer and Nicewander (1979) as:

$$MVA^{(3)} = \frac{|\mathbf{S}_{yy}|^{1/m}}{|\mathbf{S}_{yy}|^{1/m}} = \left(\prod_{i=1}^m \rho_i^2 \right)^{1/m}, \quad (2-35)$$

where m is the smaller dimension of \mathbf{x} and \mathbf{y} .

Similarly, the fourth measure of $MVA^{(4)}$ closely related to $MVA^{(2)}$ and based on the determinate $|\mathbf{S}_{ee}|$ is defined by Rozeboom (1965) as a measure of multivariate association given as:

$$MVA^{(4)} = 1 - \frac{|\mathbf{S}_{ee}|^{1/m}}{|\mathbf{S}_{yy}|^{1/m}} = 1 - \left(\prod_{i=1}^m (1 - \rho_i^2) \right)^{1/m}. \quad (2-36)$$

Fifth, instead of utilizing the determinant of covariance matrices, Yanai (1974) introduced an alternative by utilizing the trace criterion. In this way, the MVA is defined by:

$$MVA^{(5)} = \frac{\text{tr}(\mathbf{S}_{yy}^{-1} \mathbf{S}_{yx} \mathbf{S}_{xx}^{-1} \mathbf{S}_{xy})}{m} = \frac{\sum_{i=1}^m \rho_i^2}{m}. \quad (2-37)$$

According to any two sets of \mathbf{x} and \mathbf{y} variables measured by MVA (Cramer and Nicewander 1979), the values of these measures of MVA will be ordered as follows:

$$MVA^{(1)} \leq MVA^{(3)} \leq MVA^{(5)} \leq MVA^{(4)} \leq MVA^{(2)}.$$

It should be noted that $MVA^{(1)}$ is the product of the squared canonical correlation. Its value is smaller than the smallest canonical correlation or even equals 0 if any of the canonical correlation is equal to 0. Conversely, $MVA^{(2)}$ is larger than the largest canonical correlation. If one of the canonical correlations in (2-34) equals to 1, $MVA^{(2)}$ gets the value of 1 regardless of the values of the other canonical correlations (Cramer and Nicewander 1979). From (2-33) and (2-35), it is inferred that $MVA^{(3)} = (MVA^{(1)})^{1/m}$, and it has a value between the largest and smallest ones of the canonical correlations. Likewise, $MVA^{(4)}$ is closely related to $MVA^{(2)}$. The value of $MVA^{(4)}$ is smaller than or equal to that of $MVA^{(2)}$ because the number of input or output variables m is greater than or equal to 1. $MVA^{(5)}$ is the average squared canonical correlation, which is a reasonable measure with moderate size. This indicator is expressed as a preference in Cramer and Nicewander (1979) since it is an arithmetic mean, and gives the average of the canonical variates between input and output variables. Furthermore, this indicator is the average squared multiple correlation for predicting output variables from input variables. $MVA^{(5)}$ was also successfully examined in the context of the contingency table model and the discriminant analysis model (Serlin 1982).

In this research, $MVA^{(5)}$ will be investigated in the context of measure of non-linearity of the model in Chapter 5. Similar to R^2 , MVA is a normalized value, and measures the linear relationship between two sets of variables. In contrast, $1-MVA$ is used for measuring this non-linear relationship. To evaluate a model which is linear or non-linear, the value of $1-MVA$ can be used. If $1-MVA$ is close to 0, the model is nearly linear. Inversely, if $1-MVA$ is close to 1, the model is non-linear. It is worth noting that all of the multivariate associations mentioned above can be used for the case of random input and output variables (Cramer and Nicewander 1979). The $1-MVA$ is considered as a multiple indicator for quantifying non-linearity of the model.

2.2.3 Non-linearity Measures Based on Deviation from Linear Function

The non-linearity of a non-linear model is measured by using the deviations between this model and the linear model based on a Taylor expansion (Beale 1960). From this concept, the term non-linearity measure was introduced by Desoer and Wang (1980), but it did not apply the measures to any data sets. In this class of non-linearity measures, Allgöwer (1995) proposed a novel approach to calculate this measure using convex optimization. Moreover, the measure of non-linearity considered as a degree of non-linearity is briefly reviewed as follows (Li 2012):

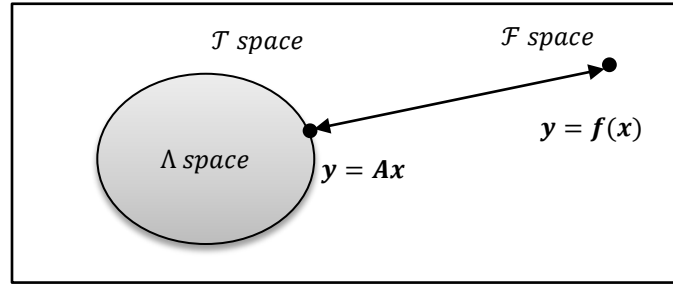


Fig. 2-5. The distance between $y = f(x)$ and its closest linear function, $y = Ax$ of Λ space, known as the distance between \mathcal{F} and Λ (Li 2012).

The function space \mathcal{T} is the set of all function spaces, including all linear functions (see 2-2) in space Λ and all non-linear functions (see 2-4) in space \mathcal{F} . In this case, the definition of measures of non-linearity is expressed in the general and solid deviation from linearity. Instead of using a single point of linear function, there are several points in the linear function subspace Λ to be employed to determine distances from them to a vector of non-linear function f in subspace \mathcal{F} . These distances can be defined in various ways, but the most commonly used method is the greatest lower-bound of the distance between f and each point in Λ . Based on this distance, the non-linearity of the non-linear model is defined as:

$$J = \sqrt{\min_{Ax \in \Lambda} (E(\|x - f(x)\|_2))}, \quad (2-38)$$

where $E(\cdot)$ is the expected value with respect to the input random vector x , and Ax and $f(x)$ have the same dimension. $\|\cdot\|_2$ is the L_2 -norm of the difference between x and $f(x)$.

Equation (2-38) is to apply a numerical method with a finite set of inputs. If the L_2 -norm (Frobenius) in this equation is chosen, the square root of mean square error can be rewritten as:

$$J = \sqrt{E\left((Ax - f(x))'(Ax - f(x))\right)} = \sqrt{\text{tr}(\Sigma_{ff} - \Sigma_{fx}\Sigma_{xx}^{-1}\Sigma'_{fx})}. \quad (2-39)$$

The normalized value is defined as the measure of non-linearity:

$$M = \frac{J}{\sqrt{\text{tr}(\Sigma_{ff})}} = \frac{\sqrt{\text{tr}(\Sigma_{ff} - \Sigma_{fx}\Sigma_{xx}^{-1}\Sigma'_{fx})}}{\sqrt{\text{tr}(\Sigma_{ff})}}, \quad (2-40)$$

where Σ_{xx} and Σ_{ff} are, respectively, the covariance matrices of \mathbf{x} and $f(\mathbf{x})$, and Σ_{fx} is the covariance matrix between $f(\mathbf{x})$ and \mathbf{x} .

If Σ_{ff} and Σ_{fx} are replaced by Σ_{yy} and Σ_{yx} in (2-40), then M can be rewritten as:

$$M = \frac{\sqrt{\text{tr}(\Sigma_{yy} - \Sigma_{yx}\Sigma_{xx}^{-1}\Sigma'_{yx})}}{\sqrt{\text{tr}(\Sigma_{yy})}}, \quad (2-41)$$

where Σ_{yy} and Σ_{yx} are the covariance matrix of \mathbf{y} and covariance matrix between \mathbf{y} and \mathbf{x} , respectively.

M in (2-41) is the non-linearity of the model, which describes the relationship between input vector \mathbf{x} and output vector \mathbf{y} . The measure of non-linearity M ranges from 0 to 1. If M is equal to 0, then the model is linear. The more M deviates from 0 the more non-linear the model is. Similar to the 1-MVA indicator in the previous section, M is another multiple indicator for determining non-linearity of the model.

2.3 Procedure of Measures of Non-linearity

This section presents a procedure for measuring the non-linearity of non-linear models. The level of non-linearity (LoN) of models is an amount that is determined by the non-linear relationship between the input and output variables, as shown in Fig. 2-6. An offline method for measuring non-linearity via Monte Carlo simulation is carried out by three indicators $1-R^2$, $1-MVA$, and M . This procedure will be applied for numerical experiments in section 2.4 and Chapter 5. In section 2.4, the LoN of a non-linear function is evaluated by changing the interval of the input variable. In Chapter 5, the LoN of the system model and the observation model of the filter algorithms (i.e., EKF, UKF, and PF in Chapter 3) are measured separately. A procedure for determination of the non-linearity of both system and observation models was proposed by Dunik et al. (2017), known as the global measure.

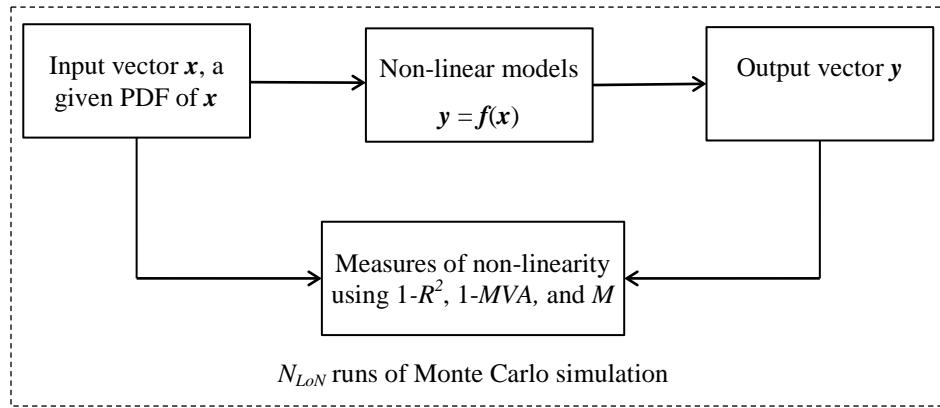


Fig. 2-6. Procedure for determination of the non-linearity of non-linear models. The non-linearity of these models is a non-linear relationship between the vector of input variable \mathbf{x} and the vector of output variables \mathbf{y} . This procedure is carried out by N_{LoN} runs of the Monte Carlo method.

The procedure for the assessment of non-linearity of non-linear models is described as the three steps below:

Step 1: N_{LoN} samples of the input vector \mathbf{x} are sampled under the given PDF. The mean and covariance of the input vector Σ_{xx} is given by:

$$\bar{\mathbf{x}} = \frac{1}{N_{LoN}} \sum_{i=1}^{N_{LoN}} \mathbf{x}_i \quad (2-42)$$

$$\Sigma_{xx} = \frac{1}{N_{LoN} - 1} \sum_{i=1}^{N_{LoN}} (\mathbf{x}_i - \bar{\mathbf{x}})(\mathbf{x}_i - \bar{\mathbf{x}})'$$

Step 2: N_{LoN} samples of the output vector are obtained from their corresponding samples of input vector passing through the non-linear models in (2-4). The mean and covariance of the output vector Σ_{yy} is subsequently given as:

$$\bar{\mathbf{y}} = \frac{1}{N_{LoN}} \sum_{i=1}^{N_{LoN}} \mathbf{y}_i \quad (2-43)$$

$$\mathbf{\Sigma}_{yy} = \frac{1}{N_{LoN} - 1} \sum_{i=1}^{N_{LoN}} (\mathbf{y}_i - \bar{\mathbf{y}})(\mathbf{y}_i - \bar{\mathbf{y}})'$$

The covariance between the input vector and the output one $\mathbf{\Sigma}_{yx}$ is:

$$\mathbf{\Sigma}_{yx} = \frac{1}{N_{LoN} - 1} \sum_{i=1}^{N_{LoN}} (\mathbf{y}_i - \bar{\mathbf{y}})(\mathbf{x}_i - \bar{\mathbf{x}})' \quad (2-44)$$

where $\bar{\mathbf{x}}$ and $\bar{\mathbf{y}}$ denote the mean value of N_{LoN} values of \mathbf{x} and \mathbf{y} , respectively.

Step 3: Finally, the non-linearity of the non-linear models is determined by three indicators, including $1-R^2$, $1-MVA$, and M , as follows:

- The $1-R^2$ can be calculated by (2-27) for each component y_j ($j=1,2,\dots,m$) of the output vector \mathbf{y} in (2-4). It is worth noting that non-linearity can only be dealt with for single component of the output vector.
- The fifth multivariate association, an arithmetic mean of the squared canonical correlation, is used for computation. It is worth noting that the product $\mathbf{\Sigma}_{yy}^{-1}\mathbf{\Sigma}_{yx}\mathbf{\Sigma}_{xx}^{-1}\mathbf{\Sigma}_{xy}$ in (2-37) is equal to the product of covariance matrices corresponding these components as $\mathbf{\Sigma}_{yy}^{-1}\mathbf{\Sigma}_{yx}\mathbf{\Sigma}_{xx}^{-1}\mathbf{\Sigma}_{xy} = \mathbf{\Sigma}_{yy}^{-1}\mathbf{\Sigma}_{yx}\mathbf{\Sigma}_{xx}^{-1}\mathbf{\Sigma}_{xy}$, and thus that non-linearity can be rewritten as:

$$1 - MVA = 1 - \frac{tr(\mathbf{\Sigma}_{yy}^{-1}\mathbf{\Sigma}_{yx}\mathbf{\Sigma}_{xx}^{-1}\mathbf{\Sigma}_{xy})}{m},$$

where m in the denominator is the number of components of the output vector.

This indicator can be used for measuring the non-linearity of all components of the output vector.

- The M quantifies the deviation of a non-linear model from linearity. Non-linearity of the non-linear model in (2-4) is calculated by M , as shown in (2-41). Similar to $1-MVA$, M can be used for quantifying the non-linearity of a model that has multiple output variables.

2.4 Empirical non-linearity

This section aims to differentiate theoretical and empirical non-linearity. In theory, a non-linear function is not difficult to realize by its mathematical equation. If the graph of a function is not a straight line, the function is non-linear. Considering a non-linear function $y = f(x)$ this function is a non-linear relationship between one input variable x , and one output variable y . The level of non-linearity of a non-linear function depends on a given interval of the input variable.

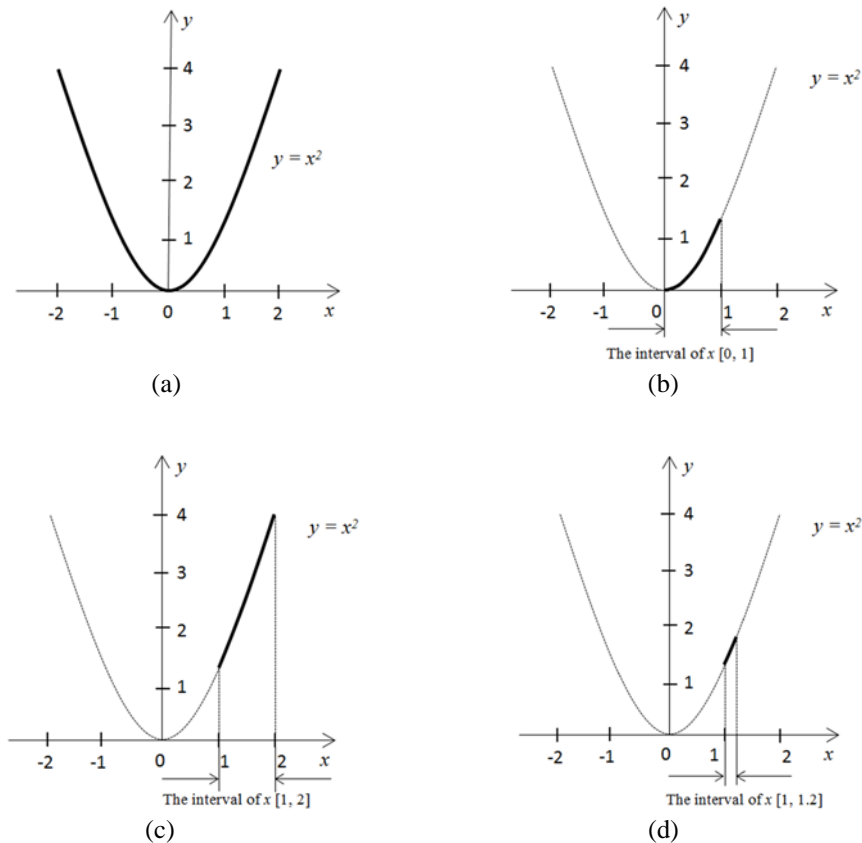


Fig. 2-7. The non-linearity of quadratic function $y = x^2$, with different intervals of the input variable x , is illustrated graphically.

Fig. 2-7(a) gives an example of a simple quadratic function, $y = x^2$, which exhibits a U-shaped curve called a parabola. Graphs of non-linearity of this function due to various intervals of the input variable are compared in Fig. 2-7(a), (b), (c), and (d). The graph of this function shows a parabola and a half-parabola when the corresponding input variable is in the interval $[-2, 2]$ and $[0, 1]$ in Fig. 2-7(a) and (b), respectively. Inversely, in Fig. 2-7(c), the graph is close to a straight line when the corresponding input variable is in the interval $[1, 2]$. In addition, the graph is very close to a straight line when the corresponding input variable is in a small interval of $[1, 1.2]$ in Fig. 2-7(d). Intuitively, non-linearity of this function with different intervals of the input variable will vary. The non-linearity of this function is the highest and smallest according to the given intervals in Fig. 2-7(a) and Fig. 2-7(d), respectively. However, it does not permit us to determine a quantitative analysis of this function in this manner. Thus, an empirical method of quantitative analysis is needed to evaluate the non-linearity of a non-linear function.

In the empirical method, the non-linearity of function $y = x^2$ is quantitatively measured by three indicators $1-R^2$, $1-MVA$, and M . The procedure in section 2.3 is applied for this computation, in which the input and output variables are scalars. N_{LoN} samples of x are randomly generated under the uniform distribution for four certain intervals $[-2, 2]$, $[0, 1]$, $[1, 2]$, and $[1, 1.2]$. N_{LoN} samples of the output variable are derived by these corresponding quantities of the input one through the function $y = x^2$. Then, the variance of x , variance of y , and covariance between x and y are calculated by (2-42), (2-43), and (2-44), respectively. Finally, the non-linearity of this function determined by $1-R^2$, $1-MVA$, and M is simulated with $N_{LoN} = 10^4$ (see Appendix A3), and is shown in Fig. 2-8.

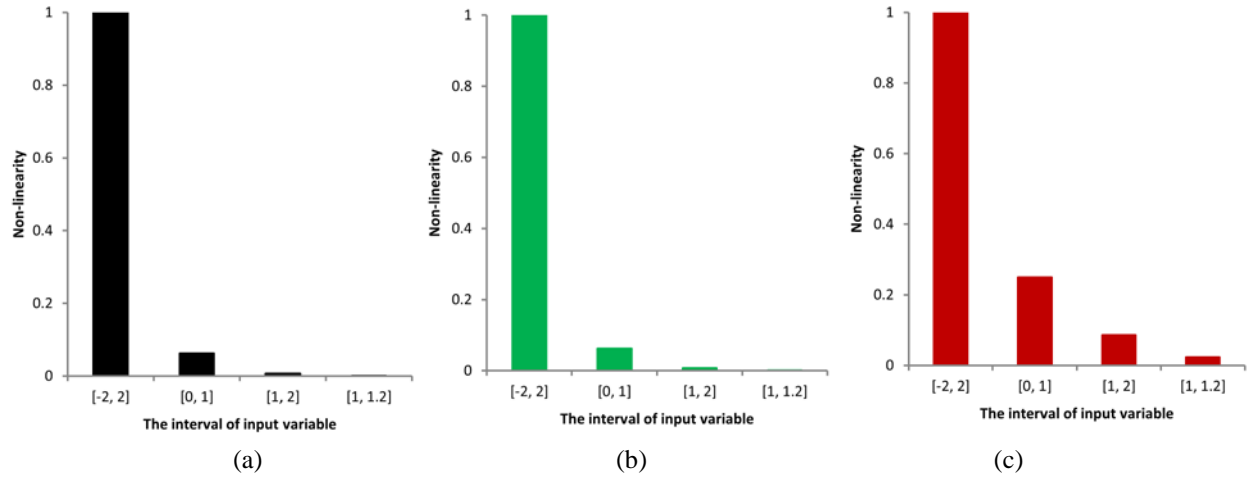


Fig. 2-8. The non-linearity of quadratic function $y = x^2$, with different intervals of the input variable x , is quantitatively measured by $1-R^2$, $1-MVA$, and M .

Fig. 2-8 shows a comparison of the non-linearity of function $y = x^2$ due to varying intervals of x . The quantity of non-linearity of this function measured by three indicators is the highest according to the interval $[-2, 2]$. Inversely, this value is the smallest according to the interval $[1, 1.2]$. These results are in agreement with the qualitative analysis, as previously mentioned. In addition, the non-linearity values indicated by $1-R^2$ and $1-MVA$ are similar (see Fig. 2-8(a) and (b)). This result is consistent with the theory that the MVA is a straightforward extension from R^2 , and they are precisely the same when the output variable is a scalar. Determination of non-linearity using M , on the other hand, is higher in value (see Fig. 2-8(c)), but its behavior is similar to that determined by utilizing $1-R^2$ and $1-MVA$. In the following chapter the intervals of non-linear functions are defined by the defined standard deviations of the input variables, mainly the measurement.

3. Filtering Algorithms for Positioning

The primary goal of this chapter is to provide an introduction to filtering algorithms that are useful for most practical applications. These filtering algorithms are developed for solving non-linear characteristics of both system and observation models. Non-linearity significantly rises not only by the mathematical form of non-linear functions, but also by measurement uncertainty. Especially, in the case of using low-cost sensors, the high uncertainty obtained from these measurements leads to high non-linearity. To date, processing data from low-cost sensors by non-linear filters in kinematic applications remains a challenge. Therefore, the first section of this chapter will present the principle of non-linear filtering algorithms. In the second section, several non-linear system and observation models focusing on kinematic positioning applications will be presented. Quantitative analyses of the abilities of these algorithms investigated according to the above non-linear system and observation models will be presented in Chapter 4.

3.1 Non-linear Filtering Algorithms

The estimation problem of a non-linear stochastic system has long constituted an attractive topic for researchers. For a linear system and Gaussian noise, the Kalman filter (KF) is an optimal solution for estimation (Kalman 1960). For non-linear issues, generally, the systems need to be linearized around approximated (nominal) or estimated (predicted) states prior to using KF. This is referred to as linearized Kalman filter and extended Kalman filter, respectively (Gelb 1979). Another method for non-linear filtering which uses the Kalman filter without linearization is known as unscented Kalman filter (UKF). Instead of linearization, UKF (Julier and Uhlmann 1997) uses selected sigma-points (see section 2.1.4) to draw the required probability density function (PDF), which allows us to obtain the first and second moments (mean and covariance) from these samples. However, the noise model is still assumed to be Gaussian. For non-linear estimations with a possible non-Gaussian noise distribution, the particle filter (PF) is the most suitable approach (Gordon et al. 1993). In this approach, mean and covariance quantities are approximated directly from a large number of sample points. This section summarizes the principle of the above filtering algorithms consisting of KF, LKF, EKF, UKF, and PF.

3.1.1 Kalman filter

The KF is proposed to solve the problem of estimating the state vector of a linear stochastic system by using linear observations with respect to the state vector (Kalman 1960). For a discrete time form, the stochastic system model with additive white Gaussian noise is described by the following equations:

$$\mathbf{y}_{k+1} = \mathbf{T}_k \mathbf{y}_k + \mathbf{B}_k \mathbf{u}_k + \mathbf{S}_k \boldsymbol{\xi}_k, k = 1, 2, \dots, \quad (3-1)$$

where \mathbf{y}_k is the n_y -dimensional state vector; \mathbf{u}_k is an n_u -dimensional known input vector or deterministic vector (i.e., acting forces); the subscript k indicates a value at time t_k ; \mathbf{T}_k is an $n_y \times n_y$ transition matrix; \mathbf{B}_k is an $n_y \times n_u$ matrix of acting force; \mathbf{S}_k is an $n_y \times n_\xi$ matrix of disturbance quantities; and $\boldsymbol{\xi}_k$ is the n_ξ -dimensional vector of Gaussian process noise ($E[\boldsymbol{\xi}_k] = 0$) with covariance of disturbance in the state equation:

$$E[\boldsymbol{\xi}_k \cdot \boldsymbol{\xi}_k'] = \boldsymbol{\Sigma}_{\xi\xi_k}.$$

The observation model is:

$$\mathbf{l}_{k+1} = \mathbf{A}_{k+1}\mathbf{y}_{k+1} + \boldsymbol{\eta}_{k+1}, k = 1, 2, \dots, \quad (3-2)$$

where \mathbf{A}_{k+1} is an $n_l \times n_y$ design matrix; and $\boldsymbol{\eta}_k$ is the n_l -dimensional vector of Gaussian observation noise ($E[\boldsymbol{\eta}_k] = 0$) with covariance:

$$E[\boldsymbol{\eta}_{k+1} \cdot \boldsymbol{\eta}'_{k+1}] = \boldsymbol{\Sigma}_{\boldsymbol{\eta}\boldsymbol{\eta}_{k+1}}.$$

The process and observation noises are assumed to be independent of the initial state vector \mathbf{y}_0 . The initial state vector is a random variable, which is distributed by a Gaussian density function with appropriated covariance matrix $\boldsymbol{\Sigma}_{\mathbf{y}\mathbf{y}_0}$.

The estimation of KF for a dynamic model with an acting force can be found in Berg and Miller (2010) and Heunecke (1995). The thesis aims to apply this algorithm for applications of kinematic positioning in which the acting force are frequently unknown. Thus, the procedure of the standard Kalman filter that solved the system model without an acting force is presented in Fig. 3.1 by the following steps.

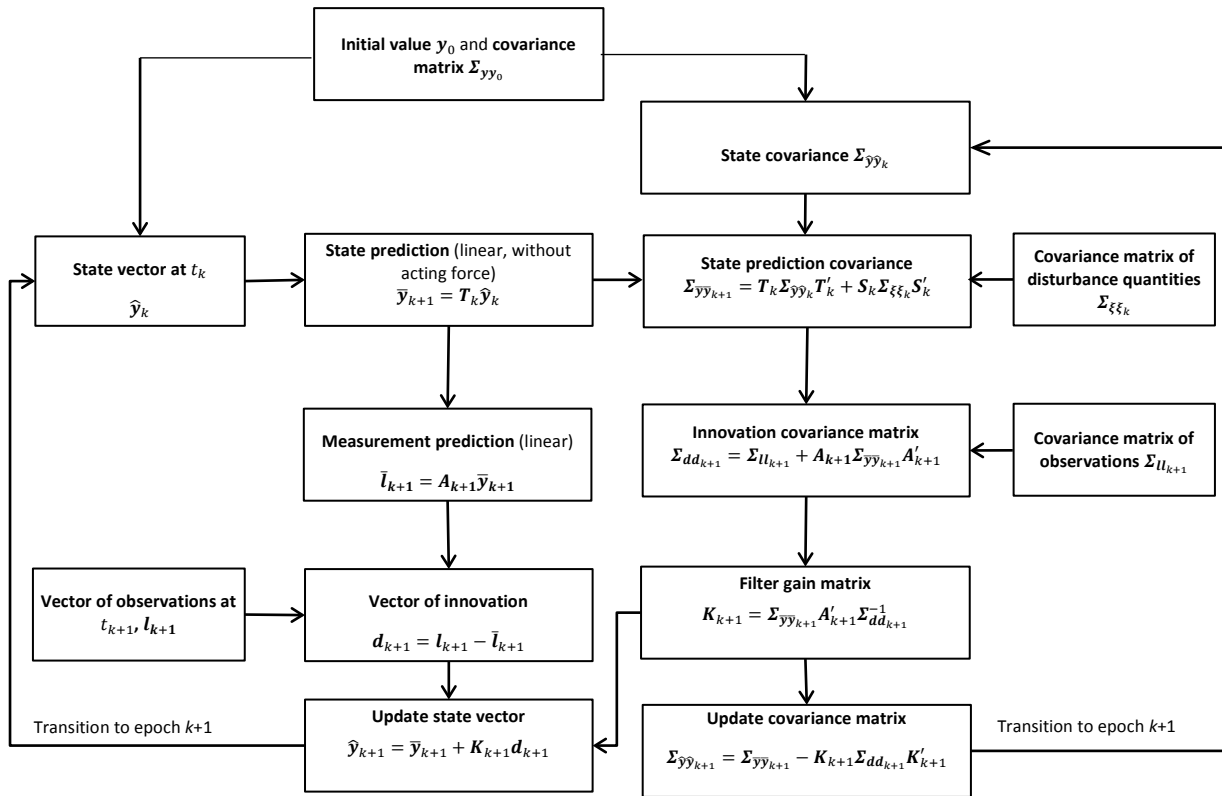


Fig. 3-1. Scheme of standard KF without acting force for linear estimation.

The two steps of the procedure of KF can be summarized as follows:

1. Prediction step

The predicted state vector at t_{k+1} from the state vector at t_k (3-1) can be written as:

$$\bar{\mathbf{y}}_{k+1} = \mathbf{T}_k \hat{\mathbf{y}}_k. \quad (3-3)$$

Propagation of the state's covariance without acting force is expressed by:

$$\Sigma_{\bar{y}\bar{y}_{k+1}} = T_k \Sigma_{\hat{y}\hat{y}_k} T_k' + S_k \Sigma_{\xi\xi_k} S_k' \quad (3-4)$$

2. Update step

The predicted state vector at t_{k+1} is transformed into the observation space using (3-2):

$$\bar{l}_{k+1} = A_{k+1} \bar{y}_{k+1}, \quad (3-5)$$

which is employed for calculation of the innovation vector:

$$d_{k+1} = l_{k+1} - \bar{l}_{k+1}. \quad (3-6)$$

The corresponding covariance matrix of the innovation can be determined by:

$$\Sigma_{dd_{k+1}} = A_{k+1} \Sigma_{\bar{y}\bar{y}_{k+1}} A_{k+1}' + \Sigma_{u_{k+1}}, \quad (3-7)$$

where $\Sigma_{u_{k+1}}$ is the covariance matrix of the measurements.

The updated state vector at t_{k+1} and its covariance matrix are computed as follows:

$$\hat{y}_{k+1} = \bar{y}_{k+1} + K_{k+1} d_{k+1}, \quad (3-8)$$

$$\Sigma_{\hat{y}\hat{y}_{k+1}} = \Sigma_{\bar{y}\bar{y}_{k+1}} - K_{k+1} \Sigma_{dd_{k+1}} K_{k+1}', \quad (3-9)$$

with the Kalman gain matrix:

$$K_{k+1} = \Sigma_{\bar{y}\bar{y}_{k+1}} A_{k+1}' \Sigma_{dd_{k+1}}^{-1}. \quad (3-10)$$

Overall, the KF is the optimal algorithm in situations with linear system and linear observation relationships. However, most real-world applications are non-linear at some level. The following subsections will deal with this issue of the non-linear problem at different levels of non-linearity.

3.1.2 Linearized Kalman filter

The main purpose of the linearized Kalman filter (LKF) is to deal with the non-linearity issue (Vaispacher et al. 2015). The use of partial derivatives as a linear approximation of non-linear relations constitutes the central idea of this method. A Taylor series, generally, is used to expand a non-linear function f about an approximate (or known) vector \mathbf{y}^o that is close to vector \mathbf{y} with the existence of the partial derivatives:

$$f(\mathbf{y}) = f(\mathbf{y}^o) + \left. \frac{\partial f}{\partial \mathbf{y}} \right|_{\mathbf{y}=\mathbf{y}^o} (\mathbf{y} - \mathbf{y}^o) + \text{higher - order terms.} \quad (3-11)$$

For non-linear estimation, the discrete time of the system model in (3-1) is replaced by:

$$\mathbf{y}_{k+1} = \boldsymbol{\phi}(\mathbf{y}_k, \boldsymbol{\xi}_k), \quad (3-12)$$

and the observation model in (3-2) is also represented by a non-linear function as:

$$\mathbf{l}_{k+1} = \boldsymbol{\theta}(\mathbf{y}_{k+1}, \boldsymbol{\eta}_{k+1}), \quad (3-13)$$

where $\boldsymbol{\phi}$ and $\boldsymbol{\theta}$ are non-linear functions of the state vector. The linearization technique is applied to obtain a simple approximation solution according to non-linear system and observation functions. If the second- and higher-order terms are neglected, then the first-order approximation coefficients (Jacobian matrix) of the transition, disturbance, and design matrices (not including the forcing matrix) are:

$$\mathbf{T}_k = \left. \frac{\partial \boldsymbol{\phi}}{\partial \mathbf{y}} \right|_{\mathbf{y}=\mathbf{y}_k^o}; \quad \mathbf{S}_k = \left. \frac{\partial \boldsymbol{\phi}}{\partial \boldsymbol{\xi}} \right|_{\boldsymbol{\xi}=\boldsymbol{\xi}_k}; \quad \mathbf{A}_{k+1} = \left. \frac{\partial \boldsymbol{\theta}}{\partial \mathbf{y}} \right|_{\mathbf{y}=\mathbf{y}_{k+1}^o}. \quad (3-14)$$

$\delta \mathbf{y} = \hat{\mathbf{y}} - \mathbf{y}^o$ is denoted for the difference between the estimated state vector $\hat{\mathbf{y}}$ and the approximate state vector \mathbf{y}^o . The procedure of LKF, as shown in Fig. 3-2, can be described as the following two steps:

1. Prediction step

The predicted state vector $\bar{\mathbf{y}}_{k+1}$ at t_{k+1} is combined by the predicted approximate vector \mathbf{y}_{k+1}^o , which passes through the non-linear prediction function $\boldsymbol{\phi}$ and from the difference $\delta \mathbf{y}_{k+1}$, transformed by transition matrix \mathbf{T}_k as:

$$\bar{\mathbf{y}}_{k+1} = \mathbf{y}_{k+1}^o + \delta \mathbf{y}_{k+1}, \quad (3-15)$$

where $\delta \mathbf{y}_{k+1} = \mathbf{T}_k \delta \mathbf{y}_k$; and $\mathbf{y}_{k+1}^o = \boldsymbol{\phi}(\mathbf{y}_k^o)$.

The propagation of the state's covariance uses (3-4).

2. Update step

The predicted observation at t_{k+1} is also linearized using (3-11):

$$\bar{\mathbf{l}}_{k+1} = \boldsymbol{\theta}(\mathbf{y}_{k+1}^o) + \mathbf{A}_{k+1} \delta \mathbf{y}_{k+1}. \quad (3-16)$$

The innovation vector and its covariance matrix can be determined by (3-6) and (3-7), respectively. The updated state vector at t_{k+1} is computed by substituting (3-16) back into (3-8) as:

$$\hat{\mathbf{y}}_{k+1} = \bar{\mathbf{y}}_{k+1} + \mathbf{K}_{k+1} \left(\mathbf{l}_{k+1} - (\boldsymbol{\theta}(\mathbf{y}_{k+1}^o) + \mathbf{A}_{k+1} \delta \mathbf{y}_{k+1}) \right). \quad (3-17)$$

Finally, the covariance matrix of the updated state is calculated by (3-9) and (3-10).

and

$$\bar{l}_{k+1} = \theta(\bar{y}_{k+1}). \quad (3-20)$$

A procedure of the EKF can be achieved by substituting (3-19) and (3-20) into (3-3) and (3-5), respectively, of the KF process in subsection 3.1.1. A graph of the EKF process is presented in Fig. 3-3.

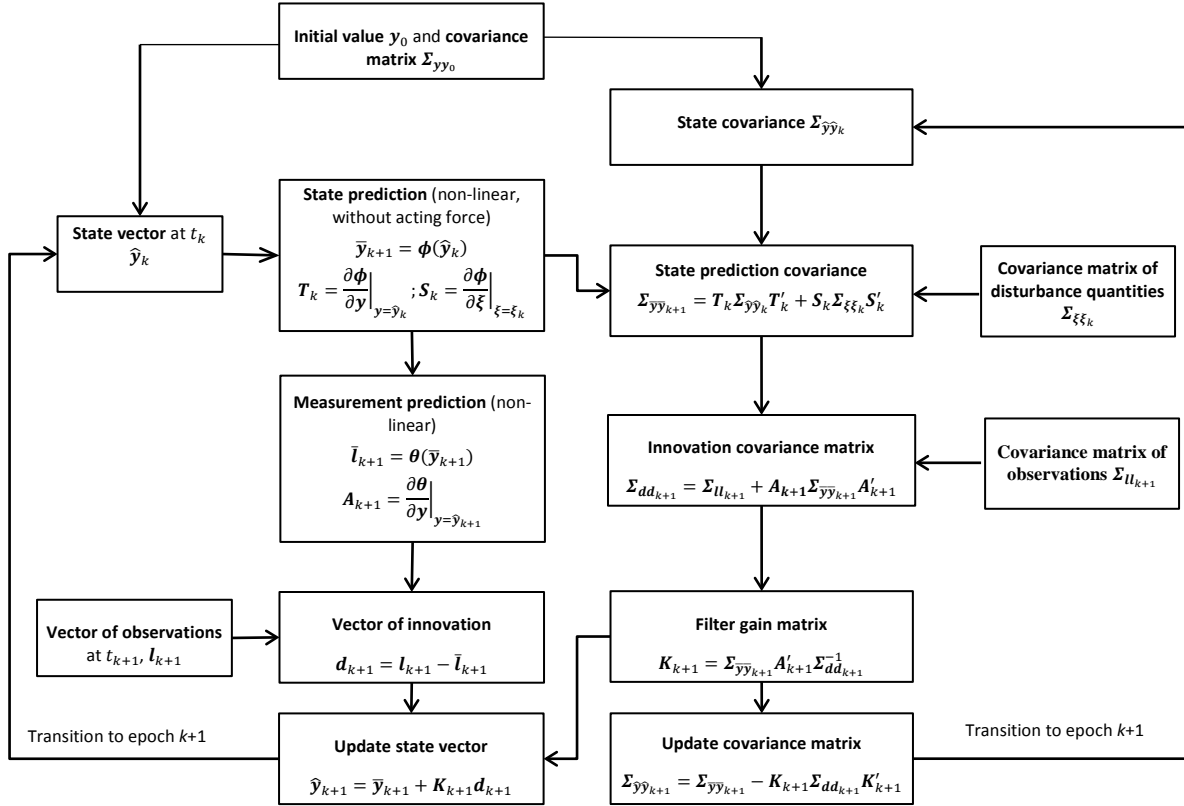


Fig. 3-3. Scheme of EKF without acting force for non-linear estimation.

Overall, although the EKF can be used for non-linear estimation generally, in the case of high non-linearity, EKF that uses a first-order Taylor expansion is insufficient. Three potential disadvantages of EKF for handling highly non-linear functions are that: (1) The linearization can lead to unstable filters if the intervals are inadequately small; (2) the first-order derivation can be complicated, or even non-existent, in some applications; and (3) its linearization approximation can make the filtering algorithm diverge (i.e., a too-large measurement uncertainty or very high non-linearities). These disadvantages are the same as those of LKF discussed in section 3.1.2.

3.1.4 Unscented Kalman filter

The main idea behind the unscented Kalman filter (UKF) is that it uses a set of individually sampled points to parameterize mean and covariance (Julier et al. 1995). The UKF is based on the UT method presented in section 2.1.4, in which the number of input n is replaced by n_y in this case. The UT transform is to generate $(2n_y+1)$ sigma-points for the UKF algorithm. The procedure of UKF (in Fig. 3-4) for the system and observation functions in (3-11) and (3-12), respectively, can be expressed as the following steps:

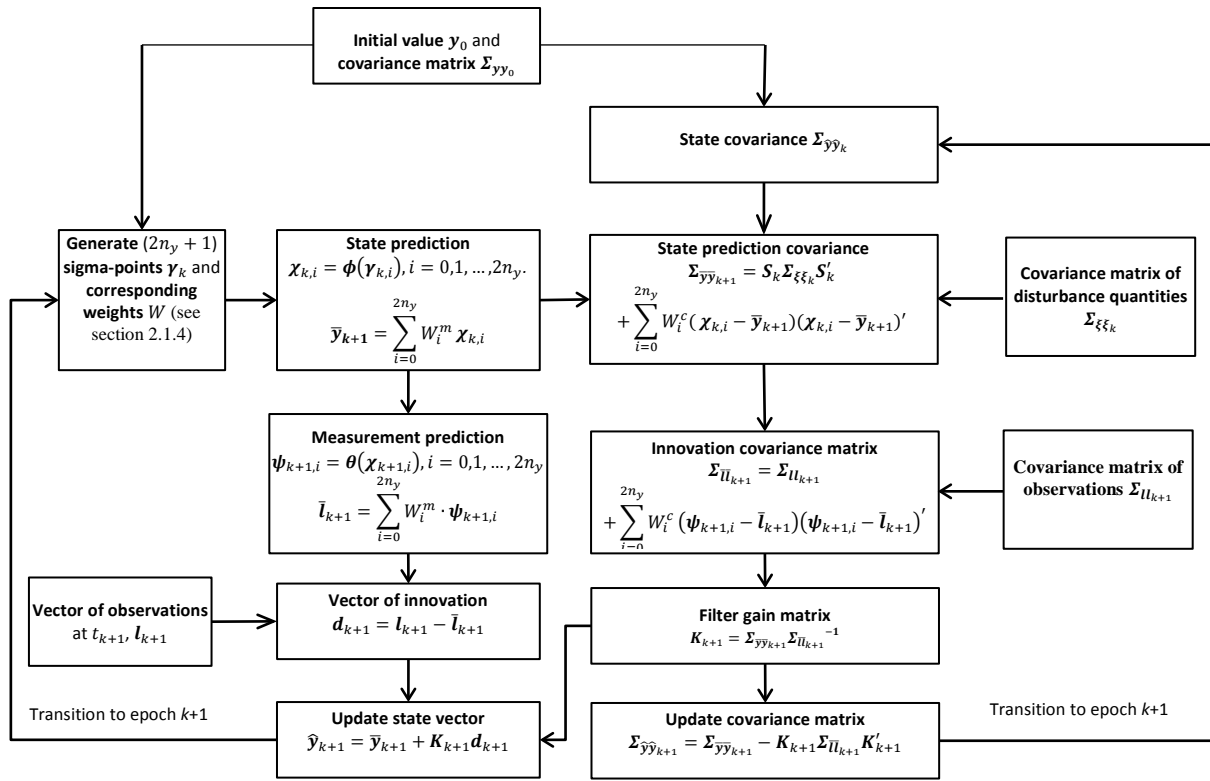


Fig. 3-4. Scheme of UKF without acting force for non-linear estimation.

1. Prediction step

Each sigma-point passes through the non-linear prediction function ϕ at epoch k as shown in (3-11):

$$\chi_{k,i} = \phi(\gamma_{k,i}), i = 0, 1, 2, \dots, 2n_y. \quad (3-21)$$

From the weights and sigma points (see (2-14) and (2-17)), as mentioned in section 2.1.4, the mean value and the covariance matrix of the predicted state vector at epoch $k+1$ can be expressed by utilizing these sigma-points after transforming them by the following equations (without acting forces):

$$\bar{y}_{k+1} = \sum_{i=0}^{2n_y} W_i^m \chi_{k,i}, \quad (3-22)$$

$$\Sigma_{\bar{y}\bar{y}_{k+1}} = S_k \Sigma_{\xi\xi_k} S_k' + \sum_{i=0}^{2n} W_i^c (\chi_{k,i} - \bar{y}_{k+1})(\chi_{k,i} - \bar{y}_{k+1})'.$$

2. Update step

The sigma-points are transmitted through the non-linear observation function θ in (3-12):

$$\boldsymbol{\psi}_{k+1,i} = \boldsymbol{\theta}(\boldsymbol{\chi}_{k,i}), i = 0, 1, 2, \dots, 2n_y, \quad (3-23)$$

where $\boldsymbol{\psi}$ is a matrix of the output sigma-points.

From these output sigma-points and their weights, the predicted observations can be calculated by:

$$\bar{\mathbf{l}}_{k+1} = \sum_{i=0}^{2n_y} W_i^m \boldsymbol{\psi}_{k+1,i}. \quad (3-24)$$

Julier and Uhlmann (1997) described how the innovation covariance matrix is determined by adding the covariance of measurement noise $\boldsymbol{\Sigma}_{\mathbf{u}_{k+1}}$ at epoch $k+1$ and the covariance matrix of the posterior sigma-points as:

$$\boldsymbol{\Sigma}_{\bar{\mathbf{u}}_{k+1}} = \boldsymbol{\Sigma}_{\mathbf{u}_{k+1}} + \sum_{i=0}^{2n_y} W_i^c (\boldsymbol{\psi}_{k+1,i} - \bar{\mathbf{l}}_{k+1})(\boldsymbol{\psi}_{k+1,i} - \bar{\mathbf{l}}_{k+1})', \quad (3-25)$$

$$\mathbf{K}_{k+1} = \boldsymbol{\Sigma}_{\bar{\mathbf{y}}\bar{\mathbf{y}}_{k+1}} \boldsymbol{\Sigma}_{\bar{\mathbf{u}}_{k+1}}^{-1}.$$

The updated state vector and the covariance matrix of the state vector are computed as:

$$\hat{\mathbf{y}}_{k+1} = \bar{\mathbf{y}}_{k+1} + \mathbf{K}_{k+1} \mathbf{d}_{k+1},$$

$$\boldsymbol{\Sigma}_{\hat{\mathbf{y}}\hat{\mathbf{y}}_{k+1}} = \boldsymbol{\Sigma}_{\bar{\mathbf{y}}\bar{\mathbf{y}}_{k+1}} - \mathbf{K}_{k+1} \boldsymbol{\Sigma}_{\bar{\mathbf{u}}_{k+1}} \mathbf{K}_{k+1}'. \quad (3-26)$$

The complete procedure of UKF is depicted in Fig. 3-4. Although the UKF is similar to the Monte Carlo (MC) method by using a set of samples to parameterize the first and second moments of probability distributions, this method draws the samples in a deterministic algorithm instead of the random manner of the MC method. The small number of sigma-points approximated by a Gaussian distribution may lead to a gross distortion of the true trajectory or divergence of the filter. As a result, the UKF is considered as a balanced solution in terms of computational complexity, but it is not sufficient for coping with the non-Gaussian distribution of uncertainties.

3.1.5 Particle filter

The particle filter (PF) is widely employed for non-linear and non-Gaussian models. The central idea of the PF is to approximate the posterior PDF of the state vector as a set of random samples. The mean and covariance can be obtained from a precise posterior PDF, which is generated by a great number of samples. This method is known under the names of the bootstrap method, condensation algorithm (Isard and Blake 1998), and sequential Monte Carlo. The first paper on the sequential MC method was presented by Hammersley and Morton (1954). However, the PF began to be commonly used with the seminal paper of Gordon et al. (1993). Here, resampling, an important step, is introduced, which created a novel method, known as sampling importance resampling (SIR) or particle filter. This method is closely related to the bootstrap procedure which was introduced by Efron (1979). Numerous versions of PF existed at that time. For example, Pitt and Shephard (1999) introduced the auxiliary particle filter for dealing with tailed measurement densities to transcend some limitations of SIR. Doucet et al. (2001) developed a new

extension of the importance sampling technique, named sequential importance sampling (SIS). In the scope of this thesis, PF theory based on the SIR algorithm will be described below.

A posterior PDF of the predicted state vector \mathbf{y}_{k+1} , $p(\mathbf{y}_{k+1}|\mathbf{L}_k)$, can be determined by using a probability model of state evolution $p(\mathbf{y}_{k+1}|\mathbf{y}_k)$, as follows:

$$p(\mathbf{y}_{k+1}|\mathbf{L}_k) = \int p(\mathbf{y}_{k+1}|\mathbf{y}_k)p(\mathbf{y}_k|\mathbf{L}_k)d\mathbf{y}_k, \quad (3-27)$$

where \mathbf{L}_k denotes the set of all observations received up to and including \mathbf{l}_k : $\mathbf{L}_k = \{\mathbf{l}_i, i = 1, 2, \dots, k\}$; and a filtering probability density $p(\mathbf{y}_k|\mathbf{L}_k)$ for the Bayesian inference is given by:

$$p(\mathbf{y}_k|\mathbf{L}_k) = \frac{p(\mathbf{l}_k|\mathbf{y}_k)p(\mathbf{y}_k|\mathbf{L}_{k-1})}{p(\mathbf{l}_k|\mathbf{L}_{k-1})}. \quad (3-28)$$

The PF approximates the probability density function $p(\mathbf{y}_k|\mathbf{L}_k)$ by a significant number of N_{PF} independent particles $\mathbf{y}_{k,i}$, $i=1, 2, \dots, N_{PF}$, and their associated weights $W_{k,i}$, $i=1, 2, \dots, N_{PF}$, where the sum of all weights is proportional to unity. The PF updates the state vector and the corresponding weights recursively with each new measurement. In (3-28), the normalization factor $p(\mathbf{l}_k|\mathbf{L}_{k-1})$ is usually unknown. However, this factor is not essential for this method, since the probability density function $p(\mathbf{y}_k|\mathbf{L}_k)$, can be sufficiently evaluated by:

$$p(\mathbf{y}_{k+1}|\mathbf{L}_k) \propto p(\mathbf{l}_k|\mathbf{y}_k)p(\mathbf{y}_k|\mathbf{L}_{k-1}), \quad (3-29)$$

In theory, a Monte Carlo method can be used to approximate the uncertainty of arbitrary probability density functions. However, in this thesis, only the Gaussian distribution is used. The likelihood function $p(\mathbf{l}_k|\mathbf{y}_k)$ is computed by considering the measurement standard deviation (STD) σ under the assumption of a Gaussian distribution:

$$p(\mathbf{l}_k|\mathbf{y}_k) = \frac{1}{\sqrt{2\pi}\sigma} e^{-\frac{(\mathbf{l}_k-\mathbf{y}_k)^2}{2\sigma^2}} \quad (3-30)$$

and $p(\mathbf{y}_k|\mathbf{L}_{k-1})$ is approximated with particles which are known to constitute the main idea of the PF method, according to:

$$p(\mathbf{y}_k|\mathbf{L}_{k-1}) \approx \frac{1}{N_{PF}} \sum_{i=1}^{N_{PF}} \delta(\mathbf{y}_k - \mathbf{y}_{k,i}), \quad (3-31)$$

where $\delta(\cdot)$ is the delta-Dirac function.

However, this approach suffers from divergence phenomena, in which almost all of the particles' weights have a value of 0, except one non-zero weight, after a few steps. This problem can be handled by a resampling step. Several resampling algorithms were analyzed and compared by Hol et al. (2006). The SIR algorithm is briefly described by the following procedure:

Step 1: N_{PF} particles $\mathbf{y}_{0,i}$, $i=1,2,\dots, N_{PF}$ are drawn depending on the Gaussian distribution $p(\mathbf{y}_0)$ at time $t_k = 0$.

Step 2: The weights $W_{k,i} = p(\mathbf{l}_k | \mathbf{y}_{k,i})$ are calculated by (3-30), and normalised weights can be defined as:

$$\tilde{W}_{k,i} = \frac{W_{k,i}}{\sum_{j=1}^{N_{PF}} W_{k,j}}, i = 1, 2, \dots, N_{PF}. \quad (3-32)$$

Step 3: A new set of particles $\mathbf{y}_{k,i}^*$, $i=1,2,\dots, N_{PF}$ are rearranged from the current set $\mathbf{y}_{k,i}$, $i=1,2,\dots, N_{PF}$ by the resampling method (see Fig. 3-5).

Step 4: At time t_{k+1} , new particles $\mathbf{y}_{k+1,i}$, $i=1,2,\dots, N_{PF}$ are drawn, which are based on the prediction function (3-1) as follows:

$$\mathbf{y}_{k+1,i} = \boldsymbol{\phi}(\mathbf{y}_{k,i}^*, \boldsymbol{\xi}_{k,i}), i = 1, 2, \dots, N_{PF},$$

where the process noise $\boldsymbol{\xi}_{k,i}$ is simulated by a Gaussian distribution; and the acting force $\mathbf{u}_{k,i}$ is ignored.

Step 5: Increase time $t_k := t_{k+1}$ and repeat from step 2.

The updated state vector and the covariance of the state vector of the SIR algorithm are computed by:

$$\begin{aligned} \hat{\mathbf{y}}_k &= E[\mathbf{y}_k | \mathbf{L}_k] = \int \mathbf{y}_k p(\mathbf{y}_k | \mathbf{L}_k) d\mathbf{y}_k \approx \sum_{i=1}^{N_{PF}} W_{k,i} \mathbf{y}_{k,i} \text{ or } \frac{1}{N_{PF}} \sum_{i=1}^{N_{PF}} \mathbf{y}_{k,i}^*, \\ \boldsymbol{\Sigma}_{\hat{\mathbf{y}}_k \hat{\mathbf{y}}_k} &= E[(\mathbf{y}_k - \hat{\mathbf{y}}_k)(\mathbf{y}_k - \hat{\mathbf{y}}_k)' | \mathbf{L}_k] = \int (\mathbf{y}_k - \hat{\mathbf{y}}_k)(\mathbf{y}_k - \hat{\mathbf{y}}_k)' p(\mathbf{y}_k | \mathbf{L}_k) d\mathbf{y}_k \\ &\approx \sum_{i=1}^{N_{PF}} W_{k,i} (\mathbf{y}_{k,i} - \hat{\mathbf{y}}_k)(\mathbf{y}_{k,i} - \hat{\mathbf{y}}_k)' \text{ or } \frac{1}{N_{PF}} \sum_{i=1}^{N_{PF}} (\mathbf{y}_{k,i}^* - \hat{\mathbf{y}}_k)(\mathbf{y}_{k,i}^* - \hat{\mathbf{y}}_k)'. \end{aligned} \quad (3-33)$$

The larger the number of particles in the simulation, the more precise the updated state vector and covariance of the state vector will be obtained. In typical experiments, the chosen number of the particle is similar to the number of samples in the Monte Carlo simulation, as presented in section 2.1.5. For instance, a 5000 sample chosen to ensure to obtain the performance of the particle filter was used in the application of terrain-aided navigation (Beddar-Wiesing and Bieshaar 2020). The trajectory of the moving object in the horizontal plane is estimated by the bootstrap filter with 4000 samples (Gordon et al. 1993).

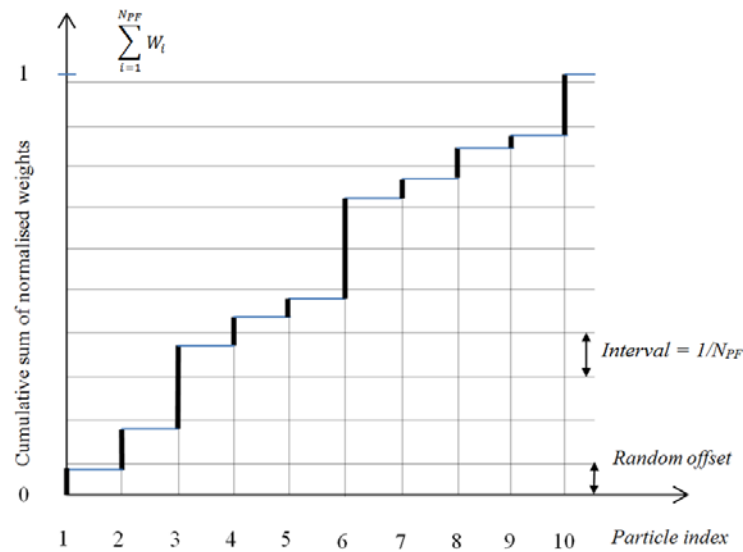


Fig. 3-5. A graphical illustration of the systematic resampling method with 10 particles ($N_{PF}=10$). A starting point with random offset is chosen randomly from the uniform distribution $U[0, 1/N_{PF}]$, and the interval is proportional to $1/N_{PF}$. The vertical axis of the graph illustrates the weight W_i , which is increased by the cumulative sum of the normalized weight $W_i = \sum_{j=1}^i W_j$. For this situation, shown in this figure, particle number 6 is chosen three times, particle number 3 and 10 are chosen twice, and particle number 2, 4, and 8 are chosen once. Thus, the resampled set consists of particle indexes 2, 3, 3, 4, 6, 6, 6, 8, 10, and 10 (Pham and Schwieger 2016).

Although the SIR-PF constitutes a perfect solution for solving non-linear and non-Gaussian filtering problems in terms of estimation performance, it possesses the main disadvantage in practice of its computational complexity.

3.2 Computational complexity

In this section, the computational complexity of the EKF, UKF, and PF is discussed in theory. Computational complexity is defined here as a function of the dimensions of the matrices. The basic operations required for computing these algorithm equations are matrix addition, matrix subtraction, matrix transpose, matrix inversion, and matrix multiplication. Computational complexity, commonly denoted by $O(\cdot)$, plays an essential role in practice, especially in real-time kinematic applications. An analysis of the computational complexity of a discrete Kalman filter in this way can be found in Mendel (1971). Both LKF and EKF only differ from KF in the computational complexity of the two linearized functions of the system (prediction) and observation. Because of the previously mentioned disadvantages of both KF and LKF, they are not popular in practice. EKF, UKF, and PF, on the other hand, are broadly used in pragmatic situations. An investigation of EKF's computational cost for an autonomous vehicle application was presented in Samsuri et al. (2015). The computational complexity of the three algorithms for a mobile robot localization application was discussed in Madrigal and Claraco (2013). In that study, the total computational complexity of both EKF and UKF depends on the dimension of both the state vector and observation vector. The unique difference in the computational complexity between EKF and UKF is the cost of computing the system and observation functions, for which the computing cost of these functions of EKF is in terms $O(\boldsymbol{\phi})$ and $O(\boldsymbol{\theta})$, while that of UKF is in terms $O(n_y \cdot \boldsymbol{\phi})$ and $O(n_y \cdot \boldsymbol{\theta})$. In these denotations, $O(\boldsymbol{\phi})$ and $O(\boldsymbol{\theta})$ are the computing cost of the system model and the observation model, respectively, and n_y is the dimension of the state vector. Obviously, the computing cost of UKF is n_y times more than that of EKF concerning the computing cost of functions. Moreover, it can be determined that EKF propagates one point, while UKF propagates several sigma-points throughout both the system model and the observation model. The computational complexity of PF is denoted by $O(N_{PF})$ and is the highest among the above three algorithms. This is because many particles are propagated throughout both the system model and the observation model. The computational complexity of PF depends on the number of particles since the PF is based on Monte Carlo methods, which rely on the law of large numbers. A large number of particles used for this algorithm leads to a considerable amount of time for computation. However, the main disadvantage of PF due to computational time can be decreased by the power of contemporary computers. The computational time of the three algorithms will be compared in Chapter 4.

3.3 Non-linear System and Observation Models

The system model and the observation model are used in two corresponding steps, including time update and measurement update of an estimation algorithm. The goal of the system model is to propagate the state vector forward in time and to determine how this vector varies with time. The observation model is to update the state vector with a set of measurements and to identify how measurements vary with the state vector. The state vector of filtering algorithm, which is the set of output variables, as mentioned in section 3.1, will be presented in this section.

The state of a system is defined as a minimum set of variables such that the knowledge of these values and the input variables and the equation describing the system's dynamic, will provide the future state and the output of the system (Khameneh 2015). When the present state variables of a system and the values of the input variable are known, the state variables identify the future behavior of the system. The state variables can be chosen in different ways to describe a system. These variables are often selected such that they are appropriate for the physical quantities of the system, which can easily measure. The most suitable states in estimation by Kalman filter depends on the application (Vanicek and Krakiwsky 1986). For static applications, such as in surveying, the position is estimated, but the velocity is not necessary. For kinematic applications, the state is a set of data describing exactly where an object is located in space, and how it is moving. For example, regarding slow-moving objects, such as marine application, land vehicle, and machine guidance construction, both the position and velocity are needed to be estimated. Regarding fast-moving objects, such as fighter aircraft and space launch vehicles, the acceleration has also to be determined. Furthermore, in the integration of GNSS and inertial navigation system (INS) application, the advisable state vector is chosen by rover position, velocity, attitude quaternion, accelerometer biases, gyroscope biases, and the receiver clock error (Teunissen and Montenbruck 2017).

In this study, the state vector is designed to show the motion of a moving object. The motion may be described by time-varying coordinates called the trajectory. The orientation and velocity are additional parameters to describe the motion. This state vector of four output variables including two coordinates, orientation, and velocity was developed in Aussems (1999) and Eichhorn (2005) and then it is applied in Garcia et al. (2010) and Ramm (2008). Besides, to illustrate the change of orientation of the moving object between two measuring epochs, the orientation change can be considered as a parameter of the state vector. Thus, the state vector with five above parameters can be defined as (Schweitzer 2012):

$$\mathbf{y} = (x \quad y \quad \varphi \quad v \quad \Delta\varphi)' \quad (3-34)$$

where x and y are coordinates in the horizontal plane, φ is the orientation, v is the velocity, and $\Delta\varphi$ is orientation change.

This state vector will be employed in the establishment of the system model in the following sections.

3.3.1 Non-linear System Models

The system models can be described as linear or non-linear models. For the linear system model, a constant velocity movement, known as the Wiener velocity model, is widely employed (Bar-Shalom et al. 2001), (Alkhatib et al. 2008), and (Särkkä 2013). In this thesis, non-linear system models are considered. The straight line and circle models that describe the system behavior of vehicle movement on the plane are non-linear models. These models, based on Aussems (1999), are presented by Eichhorn (2005). The comparison between these models according to data rate, curvature radius, and velocity can be found in Schweitzer (2012). These models are applied for modeling the system behaviors of a moving object in Chapters 4 and 5, and described in the following.

a. Straight-line model

The straight linear model is a simplification of a moving object in reality. In the plane, it is assumed that an object moves on the straight line between two points with a constant velocity, and the measuring epochs are realized at these points. The geometric model between two consecutive epochs from k to $k+1$ is illustrated in Fig. 3-6.

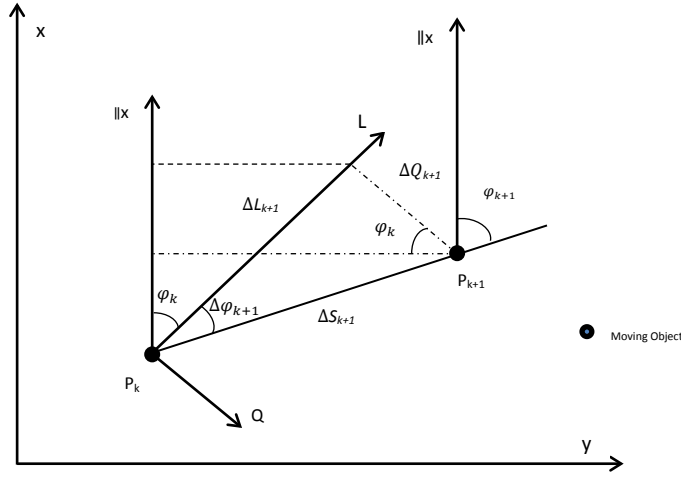


Fig. 3-6. Straight-line model (Aussems 1999).

From the estimated state vector at epoch k , $\hat{\mathbf{y}}_k = (\hat{x}_k \ \hat{y}_k \ \hat{\varphi}_k \ \hat{v}_k \ \Delta\hat{\varphi}_k)'$, the predicted position of the next epoch, which is similar to the polar survey method, is given as:

$$\bar{x}_{k+1} = \hat{x}_k + \Delta L_{k+1} \cdot \cos(\hat{\varphi}_k) - \Delta Q_{k+1} \cdot \sin(\hat{\varphi}_k) \quad (3-35)$$

$$\bar{y}_{k+1} = \hat{y}_k + \Delta L_{k+1} \cdot \sin(\hat{\varphi}_k) + \Delta Q_{k+1} \cdot \cos(\hat{\varphi}_k)$$

where two values $(\Delta L_{k+1}, \Delta Q_{k+1})$ of the moving object system (L, Q) can be computed through the distance and the angle between two epochs (see Fig. 3-5):

$$\Delta L_{k+1} = \Delta S_{k+1} \cdot \cos(\Delta\bar{\varphi}_{k+1}) \quad (3-36)$$

$$\Delta Q_{k+1} = \Delta S_{k+1} \cdot \sin(\Delta\bar{\varphi}_{k+1}),$$

where ΔS_{k+1} is the distance of the movement of the object between two epochs k and $k+1$, and \bar{x}_{k+1} , \bar{y}_{k+1} , $\bar{\varphi}_{k+1}$, \bar{v}_{k+1} , and $\Delta\bar{\varphi}_{k+1}$ are components of the predicted state vector $\bar{\mathbf{y}}_{k+1}$ at epoch $k+1$.

Substituting (3-36) into (3-35) yields:

$$\bar{x}_{k+1} = \hat{x}_k + \Delta S_{k+1} \cdot \cos(\Delta\bar{\varphi}_{k+1}) \cdot \cos(\hat{\varphi}_k) - \Delta S_{k+1} \cdot \sin(\Delta\bar{\varphi}_{k+1}) \cdot \sin(\hat{\varphi}_k) \quad (3-37)$$

$$\bar{y}_{k+1} = \hat{y}_k + \Delta S_{k+1} \cdot \cos(\Delta\bar{\varphi}_{k+1}) \cdot \sin(\hat{\varphi}_k) + \Delta S_{k+1} \cdot \sin(\Delta\bar{\varphi}_{k+1}) \cdot \cos(\hat{\varphi}_k).$$

Equation (3-37) can be rewritten as:

$$\bar{x}_{k+1} = \hat{x}_k + \Delta S_{k+1} \cdot (\cos(\Delta\bar{\varphi}_{k+1}) \cdot \cos(\hat{\varphi}_k) - \sin(\Delta\bar{\varphi}_{k+1}) \cdot \sin(\hat{\varphi}_k)) \quad (3-38)$$

$$\bar{y}_{k+1} = \hat{y}_k + \Delta S_{k+1} \cdot (\cos(\Delta\bar{\varphi}_{k+1}) \cdot \sin(\hat{\varphi}_k) + \sin(\Delta\bar{\varphi}_{k+1}) \cdot \cos(\hat{\varphi}_k)).$$

Substituting $\Delta S_{k+1} = \hat{v}_{k+1} \cdot \Delta t$ into (3-38), the equation can be rewritten as:

$$\begin{aligned}\bar{x}_{k+1} &= \hat{x}_k + \hat{v}_{k+1} \cdot \Delta t \cdot \cos(\hat{\varphi}_k + \Delta\bar{\varphi}_{k+1}) \\ \bar{y}_{k+1} &= \hat{y}_k + \hat{v}_{k+1} \cdot \Delta t \cdot \sin(\hat{\varphi}_k + \Delta\bar{\varphi}_{k+1}).\end{aligned}\tag{3-39}$$

Hence, the predicted state vector $\bar{\mathbf{y}}_{k+1} = \Phi(\hat{\mathbf{y}}_k)$ is modeled by the following equations:

$$\begin{aligned}\bar{x}_{k+1} &= \hat{x}_k + \hat{v}_{k+1} \cdot \Delta t \cdot \cos(\hat{\varphi}_k + \Delta\bar{\varphi}_{k+1}) \\ \bar{y}_{k+1} &= \hat{y}_k + \hat{v}_{k+1} \cdot \Delta t \cdot \sin(\hat{\varphi}_k + \Delta\bar{\varphi}_{k+1}) \\ \bar{\varphi}_{k+1} &= \hat{\varphi}_k + \Delta\bar{\varphi}_{k+1} \\ \bar{v}_{k+1} &= \hat{v}_k \\ \Delta\bar{\varphi}_{k+1} &= \Delta\hat{\varphi}_k.\end{aligned}\tag{3-40}$$

The transition matrix, including the derivatives of the system equations concerning the state variables, is given as:

$$\mathbf{T} = \begin{bmatrix} 1 & 0 & t_{13} & t_{14} & t_{15} \\ 0 & 1 & t_{23} & t_{24} & t_{25} \\ 0 & 0 & 1 & 0 & 1 \\ 0 & 0 & 0 & 1 & 0 \\ 0 & 0 & 0 & 0 & 1 \end{bmatrix},\tag{3-41}$$

where

$$\begin{aligned}t_{13} &= -\bar{v}_{k+1} \cdot \Delta t \cdot \sin(\hat{\varphi}_k + \Delta\bar{\varphi}_{k+1}) \\ t_{14} &= \Delta t \cdot \cos(\hat{\varphi}_k + \Delta\bar{\varphi}_{k+1}) \\ t_{15} &= -\bar{v}_{k+1} \cdot \Delta t \cdot \sin(\hat{\varphi}_k + \Delta\bar{\varphi}_{k+1}) \\ t_{23} &= \bar{v}_{k+1} \cdot \Delta t \cdot \cos(\hat{\varphi}_k + \Delta\bar{\varphi}_{k+1}) \\ t_{24} &= \Delta t \cdot \sin(\hat{\varphi}_k + \Delta\bar{\varphi}_{k+1}) \\ t_{25} &= \bar{v}_{k+1} \cdot \Delta t \cdot \sin(\hat{\varphi}_k + \Delta\bar{\varphi}_{k+1}).\end{aligned}\tag{3-42}$$

The influence of disturbance acceleration, a and rotation rate $\dot{\varphi}$ are modeled stochastically using disturbance matrix S satisfying $E(\xi) = E(a, \dot{\varphi}) = 0$. The state vector is a function of acceleration, which is written as:

$$\begin{aligned}\bar{x}_{k+1} &= \hat{x}_k + a \cdot \frac{\Delta t^2}{2} \cdot \cos(\hat{\varphi}_k + \Delta\bar{\varphi}_{k+1}) \\ \bar{y}_{k+1} &= \hat{y}_k + a \cdot \frac{\Delta t^2}{2} \cdot \sin(\hat{\varphi}_k + \Delta\bar{\varphi}_{k+1})\end{aligned}\tag{3-43}$$

and the state vector is a function of rotation rate, which is expressed by:

From (3-35), the posterior positions can be computed by prior positions using three values, including $\hat{\varphi}_k$, ΔL_{k+1} , and ΔQ_{k+1} , in which $\hat{\varphi}_k$ is the orientation of the object at epoch k . Two remaining values are calculated by a radius R and orientation change $\Delta\bar{\varphi}_{k+1}$ as:

$$\begin{aligned}\Delta L_{k+1} &= R \cdot \sin(\Delta\bar{\varphi}_{k+1}), \\ \Delta Q_{k+1} &= R \cdot (1 - \cos(\Delta\bar{\varphi}_{k+1})).\end{aligned}\tag{3-47}$$

Thus, the state vector of the moving object at epoch $k+1$ is written as follows:

$$\begin{aligned}\bar{x}_{k+1} &= \hat{x}_k + \frac{\bar{v}_{k+1} \cdot \Delta t}{\Delta\bar{\varphi}_{k+1}} (\sin(\hat{\varphi}_k + \Delta\bar{\varphi}_{k+1}) - \sin\hat{\varphi}_k) \\ \bar{y}_{k+1} &= \hat{y}_k + \frac{\bar{v}_{k+1} \cdot \Delta t}{\Delta\bar{\varphi}_{k+1}} (\cos\hat{\varphi}_k - \cos(\hat{\varphi}_k + \Delta\bar{\varphi}_{k+1})) \\ \bar{\varphi}_{k+1} &= \hat{\varphi}_k + \Delta\bar{\varphi}_{k+1} \\ \bar{v}_{k+1} &= \hat{v}_k \\ \Delta\bar{\varphi}_{k+1} &= \Delta\hat{\varphi}_k.\end{aligned}\tag{3-48}$$

The transition matrix T is given in the form of (3-41) with:

$$\begin{aligned}t_{13} &= \bar{v}_{k+1} \cdot \Delta t \cdot \frac{\cos(\hat{\varphi}_k + \Delta\bar{\varphi}_{k+1}) - \cos\hat{\varphi}_k}{\Delta\bar{\varphi}_{k+1}} \\ t_{14} &= \Delta t \cdot \frac{\sin(\hat{\varphi}_k + \Delta\bar{\varphi}_{k+1}) - \sin\hat{\varphi}_k}{\Delta\bar{\varphi}_{k+1}} \\ t_{15} &= \bar{v}_{k+1} \cdot \Delta t \cdot \frac{\cos(\hat{\varphi}_k + \Delta\bar{\varphi}_{k+1})}{\Delta\bar{\varphi}_{k+1}} + \bar{v}_{k+1} \cdot \Delta t \cdot \frac{\sin\hat{\varphi}_k - \sin(\hat{\varphi}_k + \Delta\bar{\varphi}_{k+1})}{\Delta\bar{\varphi}_{k+1}^2} \\ t_{23} &= \bar{v}_{k+1} \cdot \Delta t \cdot \frac{\sin(\hat{\varphi}_k + \Delta\bar{\varphi}_{k+1}) - \sin\hat{\varphi}_k}{\Delta\bar{\varphi}_{k+1}} \\ t_{24} &= -\Delta t \cdot \frac{\cos(\hat{\varphi}_k + \Delta\bar{\varphi}_{k+1}) - \cos\hat{\varphi}_k}{\Delta\bar{\varphi}_{k+1}} \\ t_{25} &= \bar{v}_{k+1} \cdot \Delta t \cdot \frac{\sin(\hat{\varphi}_k + \Delta\bar{\varphi}_{k+1})}{\Delta\bar{\varphi}_{k+1}} - \bar{v}_{k+1} \cdot \Delta t \cdot \frac{\cos\hat{\varphi}_k - \cos(\hat{\varphi}_k + \Delta\bar{\varphi}_{k+1})}{\Delta\bar{\varphi}_{k+1}^2}.\end{aligned}\tag{3-49}$$

The disturbance matrix containing the derivative of the system equations by different disturbance variables is defined as:

$$\mathbf{S} = \begin{bmatrix} s_{11} & s_{12} & 0 & \Delta t & 0 \\ s_{21} & s_{22} & \Delta t & 0 & \Delta t \end{bmatrix}',\tag{3-50}$$

with

$$\begin{aligned}
s_{11} &= \frac{\Delta t^2}{2 \cdot \Delta \bar{\varphi}_{k+1}} \cdot (-\sin \hat{\varphi}_k + \sin(\hat{\varphi}_k + \Delta \bar{\varphi}_{k+1})) \\
s_{21} &= \frac{\Delta t^2}{2 \cdot \Delta \bar{\varphi}_{k+1}} \cdot (\cos \hat{\varphi}_k - \cos(\hat{\varphi}_k + \Delta \bar{\varphi}_{k+1})) \\
s_{12} &= \frac{\bar{v}_{k+1} \cdot \Delta t}{\dot{\varphi}} \cdot \cos(\hat{\varphi}_k + \dot{\varphi} \cdot \Delta t) - \frac{\bar{v}_{k+1}}{\dot{\varphi}^2} \cdot (-\sin \hat{\varphi}_k + \sin(\hat{\varphi}_k + \dot{\varphi} \cdot \Delta t)) \\
s_{22} &= \frac{\bar{v}_{k+1} \cdot \Delta t}{\dot{\varphi}} \cdot \sin(\hat{\varphi}_k + \dot{\varphi} \cdot \Delta t) - \frac{\bar{v}_{k+1}}{\dot{\varphi}^2} \cdot (\cos \hat{\varphi}_k - \cos(\hat{\varphi}_k + \dot{\varphi} \cdot \Delta t)).
\end{aligned} \tag{3-51}$$

Finally, the covariance matrix of disturbance quantities is described in (3-46).

As mentioned previously, the matrix derivatives T and S are only applied for the EKF algorithm, but not for UKF and PF.

The circle model used for modeling a system is closer to reality than the straight line model. However, the difference between these models is negligible (Schweitzer 2012). In addition, the computation of the circle model is more complicated than that of the straight-line model, and the circle model cannot be applied when the object moves in an exact straight line.

3.3.2 Non-linear Observation Models

This section presents the non-linear observation models, which are used for modeling measurements of sensors. Distance and bearing angle constitute basic measurements in positioning and navigation, which can be provided by such sensors. The observation model that includes these measurements is highly non-linear with respect to the state vector. The distance measurement and bearing angle measurement equations at epoch k can be written as:

$$s_k = \sqrt{(x_k - X_o)^2 + (y_k - Y_o)^2} \tag{3-52}$$

$$\alpha_k = \text{atan} \left(\frac{y_k - Y_o}{x_k - X_o} \right), \tag{3-53}$$

where $P(X_o, Y_o)$ are known coordinates of reference point P; and (x_k, y_k) are unknown coordinates of the moving object at epoch k .

For the aim of calculation in this thesis, a moving object tracked by a radar system is chosen as an example. In general, a moving object can be tracked by multiple radars that are located at different reference points. Two bearing radars and two range radars located at reference points are considered in this example. The measurements which can be provided from these radars include two true bearing angles (α_1, α_2) and two distances (s_1, s_2). Several variant forms of observation models can be established from the combination of these measurements. In this section, three observation models, including the observation model combining two bearing angles, two distances, and two bearing angles and two

distances, are considered. These observation models will be applied for analysis in Chapter 4 and 5, and are described as follows:

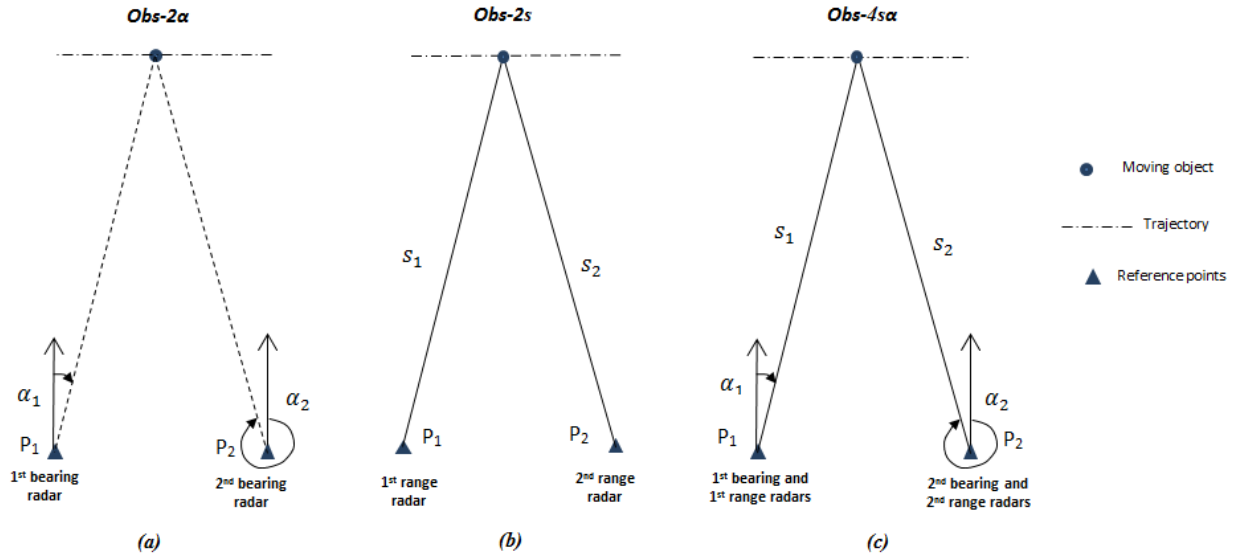


Fig. 3-8. A moving object is tracked by multiple radars in three cases. In the first case, the measurements are two simultaneous bearing angles α_1 and α_2 (a). The second case is two simultaneous distances s_1 and s_2 (b). In the third case, four simultaneous measurements, including two angles and two distances, are obtained as α_1 , α_2 , s_1 , and s_2 (c).

a. Observation model of two bearing angles (*Obs-2 α*)

The observation model with two bearing angles, which is a basic form in the field of positioning and navigation, is denoted by *Obs-2 α* (Fig. 3-8(a)). This model was also employed for a non-linear tracking problem (Niu et al. 2008). Two sensors are fixed at reference points P_1 and P_2 (ground stations), which simultaneously provide bearing angular measurements (α_1 , α_2) to the moving object, so that the observation model at epoch k can be expressed by:

$$\mathbf{l}_k = (\alpha_{1,k} \quad \alpha_{2,k})', \quad (3-54)$$

where $\alpha_{1,k}$ and $\alpha_{2,k}$ are computed by (3-53).

The design matrix \mathbf{A} is linearized by the observation model with respect to the individual state variable as follows:

$$\mathbf{A} = \begin{bmatrix} \frac{-\Delta y_{1,k}}{s_1^2} & \frac{\Delta x_{1,k}}{s_1^2} & \mathbf{0}_{1 \times 3} \\ \frac{-\Delta y_{2,k}}{s_2^2} & \frac{\Delta x_{2,k}}{s_2^2} & \mathbf{0}_{1 \times 3} \end{bmatrix}, \quad (3-55)$$

where $\Delta x_{1,k} = x_k - X_o^{(P1)}$; $\Delta y_{1,k} = y_k - Y_o^{(P1)}$; $\Delta x_{2,k} = x_k - X_o^{(P2)}$; $\Delta y_{2,k} = y_k - Y_o^{(P2)}$; and s_1 and s_2 are distances from P_1 and P_2 to the moving object, respectively.

Assuming that the measurement values are non-correlated and their measurement accuracies are equivalent, $\sigma_{\alpha_1} = \sigma_{\alpha_2} = \sigma_{\alpha}$, the corresponding covariance matrix of these measurements is then calculated as:

$$\Sigma_{ll} = \begin{bmatrix} \sigma_{\alpha}^2 & 0 \\ 0 & \sigma_{\alpha}^2 \end{bmatrix}. \quad (3-56)$$

b. Observation model of two distance measurements (Obs-2s)

The observation model of two distances (*Obs-2s*) is also a common form in the field of positioning and navigation. In general, this observation model is created by two distances (s_1, s_2) from two separate range sensors. To keep the geometries of *Obs-2s* and *Obs-2 α* unchanged, two range sensors are fixed at P_1 and P_2 , respectively, in Fig. 3-8(b). Assuming that a moving object is observed synchronously by these measurements, the vector of the observation model at epoch k can then be expressed by:

$$\mathbf{l}_k = (s_{1,k} \quad s_{2,k})', \quad (3-57)$$

where $s_{1,k}$ and $s_{2,k}$ are used in (3-52).

The design matrix \mathbf{A} for this observation function is:

$$\mathbf{A} = \begin{bmatrix} \frac{\Delta x_{1,k}}{s_1} & \frac{\Delta y_{1,k}}{s_1} & \mathbf{0}_{1 \times 3} \\ \frac{\Delta x_{2,k}}{s_2} & \frac{\Delta y_{2,k}}{s_2} & \mathbf{0}_{1 \times 3} \end{bmatrix}, \quad (3-58)$$

where $\Delta x_k = x_k - X_o$; $\Delta y_k = y_k - Y_o$; and s_1 and s_2 are the distances between the moving object and sensor 1 and sensor 2, respectively.

The corresponding covariance matrix of distance measurements, in which these measurement values are assumed to be non-correlated, is calculated as:

$$\Sigma_{ll} = \begin{bmatrix} \sigma_s^2 & 0 \\ 0 & \sigma_s^2 \end{bmatrix}, \quad (3-59)$$

with the standard deviations of two distance measurements assumed to be similar $\sigma_{s_1} = \sigma_{s_2} = \sigma_s$.

c. Observation model of two distances and two bearing angles (Obs-4s α)

Obs-4s α comprises two distances and two angles. This model is used when a moving object is observed from multiple range and bearing radars. In order to be fair in the comparison between observation models, the geometry of the *Obs-4s α* is kept unchanged compared to *Obs-2s* or *Obs-2 α* . In this model, two range and bearing static sensors are also fixed at P_1 and P_2 in Fig. 3-8(c). In general, four measurements of distances and bearing angles can be observed synchronously or asynchronously. However, in this study, all measurements are assumed to be synchronous. The vector of the observation model at epoch k can be expressed as:

$$\mathbf{l}_k = (s_{1,k} \quad \alpha_{1,k} \quad s_{2,k} \quad \alpha_{2,k})'. \quad (3-60)$$

It is assumed that these measurement values are non-correlated, and measurement accuracy is similar for distance sensors, as well as angle sensors. The corresponding design matrix \mathbf{A} and the covariance matrix Σ_{ll} are presented as:

$$\mathbf{A} = \begin{bmatrix} \frac{\Delta x_{1,k}}{s_1} & \frac{\Delta y_{1,k}}{s_1} & \mathbf{0}_{1 \times 3} \\ -\frac{\Delta y_{1,k}}{s_1^2} & \frac{\Delta x_{1,k}}{s_1^2} & \mathbf{0}_{1 \times 3} \\ \frac{\Delta x_{2,k}}{s_2} & \frac{\Delta y_{2,k}}{s_2} & \mathbf{0}_{1 \times 3} \\ -\frac{\Delta y_{2,k}}{s_2^2} & \frac{\Delta x_{2,k}}{s_2^2} & \mathbf{0}_{1 \times 3} \end{bmatrix}; \Sigma_{ll} = \begin{bmatrix} \sigma_s & 0 & 0 & 0 \\ 0 & \sigma_\alpha & 0 & 0 \\ 0 & 0 & \sigma_s & 0 \\ 0 & 0 & 0 & \sigma_\alpha \end{bmatrix}. \quad (3-61)$$

4. Accuracy and Computational Time of Kinematic Positioning

Accuracy and computational time of filtering algorithms have constituted a major research topic in kinematics for several decades (Bar-Shalom et al. 2001 and Wen et al. 2014). In kinematic positioning, the position, velocity, and acceleration of a moving object are determined by utilizing sensors' observations, such as bearing angle (azimuth), relative angle, distance, possible range rate, and coordinates. The large error contained in measurements of low-cost sensors leads to a reduction in the object's position accuracy. This issue can be improved by processing the data with suitable algorithms to a certain extent. The computational time of a filtering algorithm associated with its accuracy is another critical issue. The computational time of the algorithm plays an essential role in practice, especially in real-time applications. Numerous investigations of the computational time of filtering algorithms exist, such as Mendel (1971), Karlsson et al. (2005), and Samsuri et al. (2015). In order to select the most suitable algorithm, three algorithms, including EKF, UKF, and PF, are evaluated on various system and observation models in this research. Position accuracy and computational time are used as the primary and secondary parameters, respectively, in this evaluation.

The structure of this chapter is as follows. Section 4.1 presents the estimation filtering algorithm for kinematic position accuracy for each of three influencing factors investigated: (1) measurement uncertainty; (2) observation geometry; and (3) number of measurements. In section 4.2, the computational time of these algorithms is analyzed with a single run. The summary is presented in section 4.3.

4.1 Kinematic Position Accuracy

To evaluate the accuracy of a filtering algorithm, the root mean square error (RMSE) is often used in geodesy and navigation positioning. The RMSE is the root means square of the difference between the true trajectory and estimated one from a filtering algorithm. All components of the state vector, including coordinates, orientation, velocity, and orientation change can be evaluated by RMSE. However, in geodesy or geography, horizontal position accuracy (i.e., accuracy of both x and y coordinates) is commonly utilized. The procedure to evaluate the horizontal accuracy achieved by a filtering algorithm is described as follows:

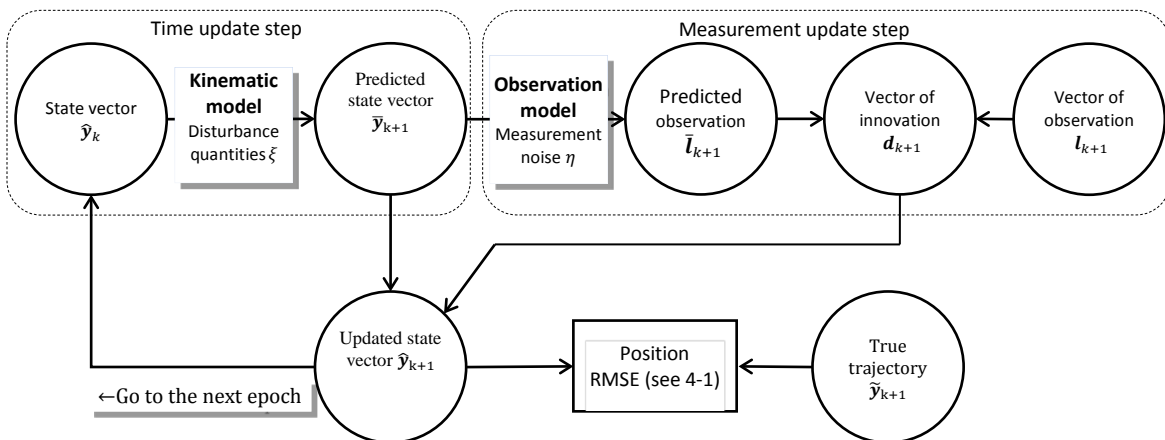


Fig. 4-1. Position RMSE is used for evaluating a filtering algorithm from epoch k to epoch $k+1$.

The state vector is obtained in two steps (Fig. 4-1). In the first step, the predicted state vector at epoch $k+1$ is predicted by using the system model from the state vector at epoch k . In the second step, the updated state vector is obtained from the current vector of observation l_{k+1} and the predicted observation \hat{l}_{k+1}

derived from the observation model and the predicted state vector. This vector is calculated via the observation model and corresponding observation noise. Thus, the state vector at time $k+1$ and its covariance matrix are computed based on both of the above epochs. The position RMSE at a particular cycle in a loop of N_{Epo} times is given as:

$$\text{RMSE} = \sqrt{\frac{\sum_{k=0}^{N_{Epo}} ((\tilde{x}_{k+1} - \hat{x}_{k+1})^2 + (\tilde{y}_{k+1} - \hat{y}_{k+1})^2)}{N_{Epo}}}, \quad (4-1)$$

where N_{Epo} is the number of measuring epochs; \tilde{x} and \tilde{y} are the north and east coordinates, respectively, of the true trajectory; and \hat{x} and \hat{y} are the estimations of corresponding coordinates by the filtering algorithm.

In this section, a scenario for the evaluation of position RMSE of the moving object is discussed. Then, this accuracy parameter (RMSE) is determined by changing factors, including measurement uncertainty, observation geometry, and the number of measurements in the following subsections.

4.1.1 Introduction of Scenarios

In positioning and tracking applications, moving objects are frequently tracked by one or more sensors. These sensors, such as active or passive radars, radio detection finders, acoustic radars, infrared sensors and other types of sensors, are employed for determining the kinematics (typically positions, velocity, and orientations) of moving objects. Several combinations of observation models can be used by these sensors' measurements (i.e., distance and bearing angle). These observation models can be combined from a single measurement or multiple measurements. In submarine surveillance, the bearing observation was applied by using passive sonar measurements from a ship (Bar-Shalom et al. 2001). The distance-only observation was also used by employing a passive inverse synthetic aperture radar (ISAR) (Ristic et al. 2004). In the ground moving object indicator (GMTI) radar, the observation model includes bearing angle (azimuth), distance, and Doppler or range-rate. One application of this radar for aircraft and ground-moving surveillances can be found in Mallick et al. (2015). Moreover, the observation model, including one distance and one bearing angle from a single radar or two bearing angles from two sensors, was used for tracking issues (Niu et al. 2008).

In this section, scenarios are designed by the following parameters: a moving object is assumed to be tracked by two radars located at the reference points. This object moves from the west to the east in the x - y plane with a constant velocity of 5 m/s (18 km/h). Due to the slow movement of the object, the data rate (sampling time) of measurement Δt is assumed to be 1 s, and the moving object is observed during the period of 100 s. The shortest distance from the moving object to radars is approximately $s = 1$ km (Fig. 4-2). The observations of these scenarios are assumed in three cases of two bearing angles, two distances, and both two bearing angles and two distances corresponding with three observation models, as described in section 3.3.2. Regarding the scenario of two bearing angles (see Fig. 3-8(a)), two radars can provide information about the bearing angle, which is an angle between true north and a line pointed directly at an object. This angle is measured in a clockwise direction from the true north in the horizontal plane, which is called the true bearing of a radar object (Bole et al. 2005). Two bearing angles are assumed to be synchronous, and their measurement accuracies are equal to 1° . Regarding the scenario of two distances (see Fig. 3-8(b)), assumed that two distances synchronously provided by two range radars with 20 m of measurement accuracy. Regarding the scenario of two bearing angles and two distances, the measurement accuracies of bearing angle and distance (see Fig. 3-8(c)) are also assumed to be 1° of and 20 m, respectively. Because of the above assumptions about the velocity and object trajectory, the standard deviations of process noise, including acceleration a_ξ and rotational rate φ_ξ , for modeling the moving object are subjected to a very small amount with $a_\xi = 0.01$ m/s² and $\varphi_\xi = 0.01$ rad/s². Both process noise

and measurement noise are assumed to be Gaussian. Because of the given trajectory of the moving object, the straight-line system model in section 3.2.1 is applied for the system model, which is the non-linear model with respect to the state vector. In addition, the non-linear observation models which are bearing angle and distance measurements concerning the state vector are applied. The initial state vector is based on one-point initialization. The initial state vector is the first observed position, orientation, velocity, and orientation change $y_0 = (1100 \text{ m}, 100 \text{ m}, 90^\circ, 1 \text{ m/s}, 0.01^\circ)'$. The covariance matrix of the initial state vector is:

$$\Sigma_{yy_0} = \begin{pmatrix} 10m^2 & 0 & 0 & 0 & 0 \\ 0 & 10m^2 & 0 & 0 & 0 \\ 0 & 0 & (1^\circ)^2 & 0 & 0 \\ 0 & 0 & 0 & (1m/s)^2 & 0 \\ 0 & 0 & 0 & 0 & (0.1^\circ)^2 \end{pmatrix}. \quad (4-2)$$

All simulations in this chapter are carried out by three filtering algorithms, consisting of EKF, UKF, and PF. To obtain reliable RMSE values, these algorithms are simulated by 300 independent Monte Carlo runs, and the number of particles using PF, $N_{PF} = 3 \times 10^4$. A detailed explanation of the optimal value of PF can be found in section 4.2.

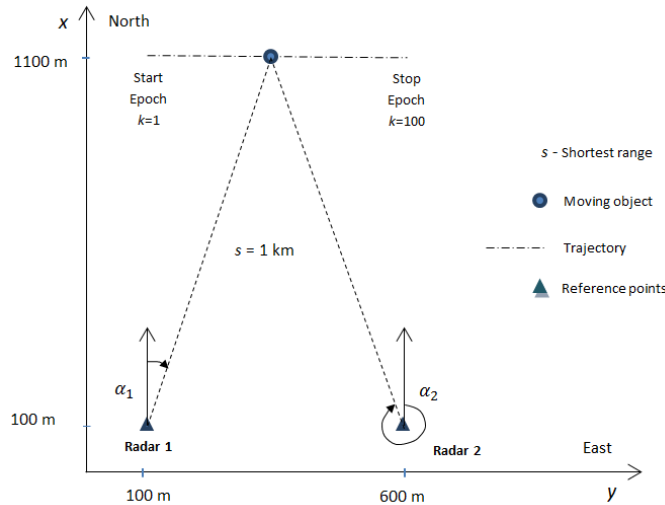


Fig. 4-2. Geometry of object trajectory and two bearing angles from radars located at (100 m, 100 m) and (600 m, 100 m), respectively.

4.1.2 Impact of Measurement Uncertainty on Position Accuracy

The uncertainty of radar measurements is one of the essential factors in the performance of kinematic position accuracy of moving objects. However, the influence of measurement uncertainty on position accuracy depends on the factors of scenarios. The kinematic positioning accuracies obtained by EKF, UKF, and PF are investigated for a wide range of uncertainty of bearing angles. The accuracy (or uncertainty) of the bearing angle varies in different radar systems. The accuracy of a bearing angle depends on both the internal signal processing method and external conditions. Currently, the standard deviation (STD) of bearing angle σ_α obtained by a radar system typically ranges from 0.05° to 3° , or even up to 10° (see Appendix A1). In order to evaluate kinematic position accuracy, depending on measurement uncertainty, the scenario of two bearing angles in section 4.1.1 is used for $0.2^\circ \leq \sigma_\alpha \leq 2^\circ$. This range of

measurement uncertainty is chosen because it is suitable for the specifications of measurement accuracy of the radar and is sufficiently large for comparing the performance between filtering algorithms.

This evaluation examines the performance of these algorithms as a function of the uncertainty of bearing angle measurement. Fig. 4-3 shows the averaged value of RMSE of EKF, UKF, and PF over 100 epochs. The RMSE values of these three algorithms increase with increasing measurement uncertainty (or STD of measurement). The RMSE of PF is the smallest for the whole interval of surveyed measurement uncertainty. Similar results are discussed in Konatowski et al. (2016) and Doucet et al. (2001). Moreover, the RMSE of UKF is also smaller than that of EKF for all surveyed measurement uncertainties. This result is consistent with the work of Julier and Uhlmann (1997), who reported that UKF achieves higher accuracy than that of EKF due to measurement uncertainty.

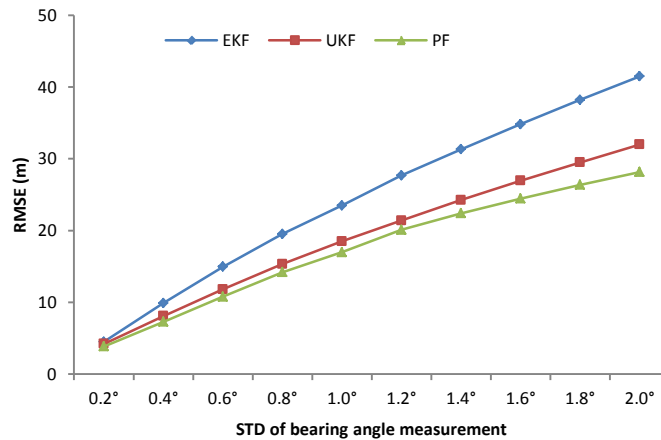


Fig. 4-3. Position RMSEs obtained by EKF, UKF, and PF versus bearing angle accuracy.

This evaluation can also reveal the improvement in performance relative to EKF. The improvement factor, based on position RMSE, is defined as:

$$\text{Improvement} = \frac{(\text{RMSE}_{\text{EKF}} - \text{RMSE}_{\text{filter}})}{\text{RMSE}_{\text{filter}}} \cdot 100\%, \quad (4-3)$$

where $\text{RMSE}_{\text{filter}}$ is position RMSE of UKF or PF.

Table 4-1. Performance comparison among EKF, UKF, and PF in varying measurement uncertainty.

σ_{α}	Improvement (%)	
	UKF vs. EKF	PF vs. EKF
0.2°	7%	17%
0.4°	22%	36%
0.6°	26%	38%
0.8°	27%	38%
1.0°	27%	38%
1.2°	29%	38%
1.4°	29%	40%
1.6°	29%	42%
1.8°	30%	45%
2.0°	30%	47%

The important aspect of this evaluation is the improvement of both PF and UKF compared to EKF. PF achieves the best performance, obtaining 17% to 47% as STD is increased from 0.2° to 2° . Similarly, the value of improvement of UKF rises continuously from 7% to 30%. These results are consistent with the analysis of bearing-only tracking for the maneuvering case (Ristic et al. 2004). The improvement of PF and UKF becomes larger in the case of high uncertainty. In contrast, these improvement values are only slightly different in the case of low uncertainty.

The behavior of these algorithms can be explained as follows. Since STD of bearing angle measurement increases, the cross-range observability of the moving object decreases. This leads to that the approximation point for local linearization of EKF is far from ideal (or not linear to ideal). The Jacobian matrix of the observation model then becomes incorrect, which affects the innovation covariance matrix, the gain matrix, and the state estimates. By contrast, the principles of both UKF and PF are based on deterministic and random sampling approaches, respectively. The results indicate that UKF and PF are able to handle medium and high non-linearity, respectively.

The posterior probability density function of measurement noise also becomes non-Gaussian since it undergoes a non-linear transformation. PF is suitable for solving non-Gaussian noise in this case. These reasons explain the better performances of PF in the context of measurement uncertainty in comparison with those of both UKF and EKF.

4.1.3 Impact of Observation Geometry on Position Accuracy

Observation geometry is another factor affecting the position accuracy of a moving object. However, the extent of this influence depends on the parameters of the scenario. In this study, the impact of observation geometry on position accuracy is evaluated for three algorithms in a certain scenario. The scenario in section 4.1 is used with varying distance s , which is the shortest distance between two stationary radars and the moving object. According to a particular value of s in this scenario, the observation geometry can be characterized by the intersection angle γ in Fig. 4-4.

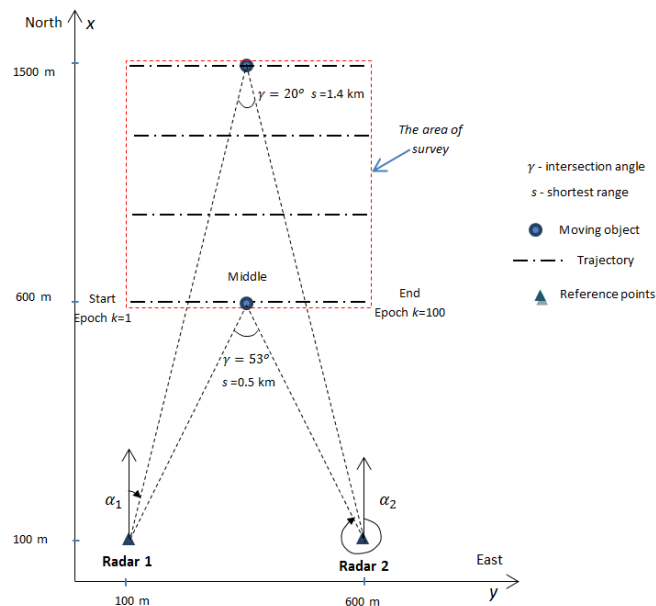


Fig. 4-4. Radars track a moving object with varying its observation geometry, which is characterized by the shortest distance s and intersection angle γ . The example shows two cases of observation geometry with the shortest distance $s = 1.4$ km (or $\gamma = 20^\circ$) and $s = 0.5$ km (or $\gamma = 53^\circ$).

Although certain observation geometry will optimize tracking performance in terms of position accuracy, this subject of the optimization of geometry will not be examined in this research. In this evaluation, suppose that the object moves on the trajectory satisfying the shortest distance s that is from 0.5 km to 1.4 km. The corresponding intersection angle at the moving object decreases from 53° to 20° . These values of s and γ are selected because they are sufficiently large to compare the performance of three filtering algorithms without divergence phenomenon. The effect of observation geometry on position accuracy determined by EKF, UKF, and PF is presented as the following analyses.

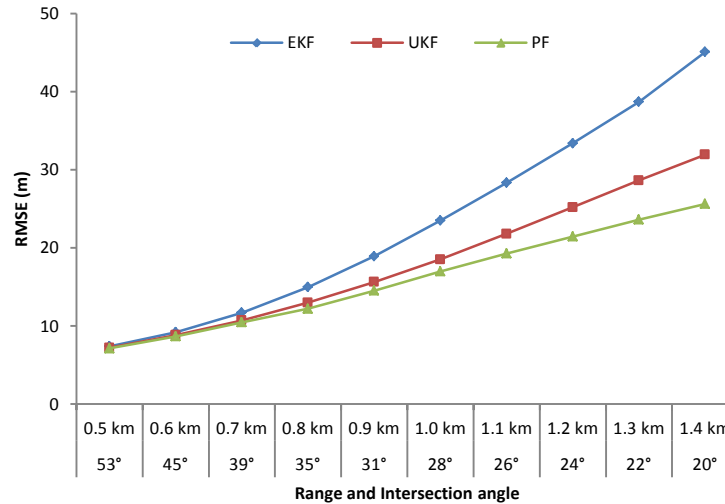


Fig. 4-5. The position RMSE of a moving object versus observation geometry, which is characterized by intersection angle.

Fig. 4-5 shows the averaged position RMSEs of three algorithms over 100 epochs with changing intersection angle. The position RMSE values of these three algorithms increase with decreasing value of intersection angle γ (or increasing the shortest distance s). The position RMSE of PF is the smallest followed by UKF. Inversely, the position RMSE of EKF is the highest.

Table 4-2. Performance comparison among EKF, UKF, and PF in varying the observation geometry.

s (km)	γ	Improvement (%)	
		UKF vs. EKF	PF vs. EKF
0.5	53°	3%	4%
0.6	45°	4%	6%
0.7	39°	9%	12%
0.8	35°	15%	23%
0.9	31°	21%	30%
1.0	28°	27%	38%
1.1	26°	30%	47%
1.2	24°	33%	56%
1.3	22°	35%	64%
1.4	20°	41%	76%

Note: the value of intersection angle γ is presented at the middle point of the trajectory.

The improvement in RMSE of PF compared to EKF increases from 4% to 76% with decreasing intersection angle γ (or increasing the shortest distance s). These values of UKF compared to EKF are 3% and 41%, respectively. Performances in terms of RMSE improvement tend to be similar to those in section 4.1.2 when varying measurement error. Similar results have been reported in the context of unmanned aerial vehicle navigation (UAV) in Veth (2013).

The behavior of the RMSE of these algorithms is mainly due to the geometrical reasons (Atkinson 1989). In the above-mention scenarios, the observation geometry is good if the shortest distance s is large or the intersection angle γ is small. Inversely, the geometry is bad if the shortest distance s is small or the intersection angle γ is large.

Furthermore, the posterior density function becomes more non-Gaussian due to non-linear transformation. In this case, PF again achieves excellent performance because it is proper to handle high and non-Gaussian uncertainty of measurement. Both EKF and UKF can obtain desirable results, which is similar to the analysis in section 4.1.2.

4.1.4 Impact of Number of Measurements on Position Accuracy

The position accuracy of an object can be enhanced by more measurements from multiple radars. A multiple radar system consists of several single radars providing measurements, such as bearing, range, and range-rate (or radial velocity). In reality, multiple radars are frequently employed in order to improve the position accuracy of the object (Bar-Shalom 1990, Heidger et al. 2004, Curry 2005). For multiple radars, all measurements are transmitted from single sensors to a fusion center. These measurements may be synchronous or asynchronous, meaning that the sampling times of all of the radars are the same or arbitrary. According to asynchronous measurements, time-alignment must be considered prior to fusing. Several methods that were proposed for fusing asynchronous data can be found in Li et al. (2017). In this research, synchronous measurements are considered, whereby all data are assumed to be similar in sampling time and received at the same time. To evaluate the improvement in position accuracy due to the numbers of observed radars, three observation models, *Obs-2 α* , *Obs-2s*, and *Obs-4s α* , as presented in section 3.3.2, are compared in this part. These scenarios in section 4.1.1 are used for these evaluations. This supposed value is proper for specifications of range radars (see Appendix A1) and comparable to the measurement accuracy of the angular radars in the above-given range between radars and the moving object.

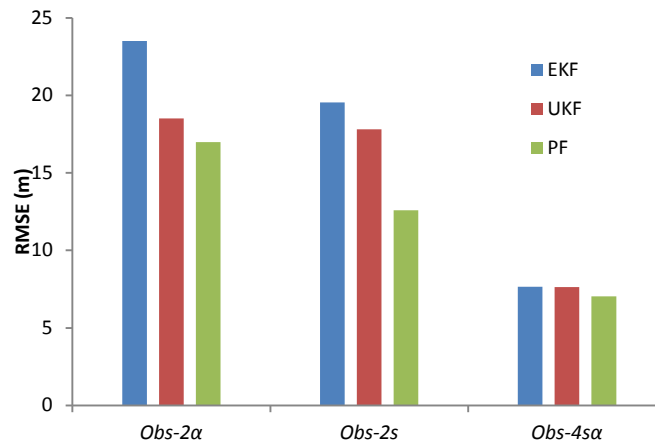


Fig. 4-6. The averaged position RMSE of the moving object is obtained by EKF, UKF, and PF over 100 epochs. The RMSE values of these algorithms are calculated in the above three cases.

Fig. 4-6 shows the comparison about the position RMSEs in three scenarios. It is clear that the more measurements that are observed, the higher position accuracy that can be obtained. This result also suggests that the distance scenario is better than the bearing measurement scenario in the positioning of moving objects. These results agree with the analyses of the relation between the vessel's position and the number and type of measurements in theory proposed in Swierczynski and Czuplewski (2015). However, the contribution of this work is a comparison of position RMSE according to particular algorithms. The RMSEs of EKF, UKF, and PF decrease 2.9, 2.5, and 2.5 times, respectively, in the comparison between *Obs-4sa* and *Obs-2a*. Reductions in RMSE of EKF, UKF, and PF are 2.6, 2.3, and 1.8 times, respectively, in the comparison between *Obs-4sa* and *Obs-2s*. It is worth noting that the above factors of reduction in RMSE are determined in a particular scenario (i.e., $s = 1$ km and $\gamma = 28^\circ$). These factors of reduction in RMSE change dramatically by observation geometry. For example, when the intersection angle is approximately $\gamma = 60^\circ$, these factors are approximately 1.5 times (see Appendix A2). In addition, the improvement in position accuracy depends on the algorithms used. Table 4-3 shows the improved accuracy of three algorithms when the number of measurements increases. In observation models *Obs-2s* and *Obs-2a* using two measurements, the enhanced efficiency of UKF is 19% and 10%, respectively. Likewise, these values of PF are 26% and 55%, respectively. In contrast, in the observation *Obs-4sa* using four measurements, the improvement accuracies of UKF and PF decrease to 0.3% and 9%, respectively. These results suggest that the improvements in UKF and PF compared to EKF are less in the case of many measurements from multiple radars. In other words, EKF is a suitable algorithm in this case due to its short computational time.

Table 4-3. Improvement in accuracy in three cases of observation models.

Observation model	Improvement (%)	
	UKF vs. EKF	PF vs. EKF
<i>Obs-2s</i>	10%	55%
<i>Obs-2a</i>	19%	26%
<i>Obs-4sa</i>	0.3%	9%

4.2 Computational complexity

The performance of the filtering algorithm in the previous section is solely discussed regarding the important parameter of RMSE. However, computational complexity is another critical parameter. Both parameters contribute to the ability of the filtering algorithm. As mentioned in Chapter 3, computational complexity only indicates the algorithms' complexity from a theoretical perspective. In practice, the actual computational time (execution time) of an algorithm is needed, and this can be obtained by empirical calculations. This issue is addressed in Fredrik (2010) and Elvira et al. (2017). In this study, the computation is performed on a desktop PC with an Intel Core i7-5820K, 3.30 GHz of CPU, and 64 GB of RAM, and running MATLAB version R2019a. The scenario of two bearing angle in section 4.1.1 is used for the evaluation of the computational time of three algorithms, EKF, UKF, and PF, which is presented in Table 4-4. Both EKF and UKF are simulated with one run, and PF uses a 3×10^4 particle, which is determined as described in the following:

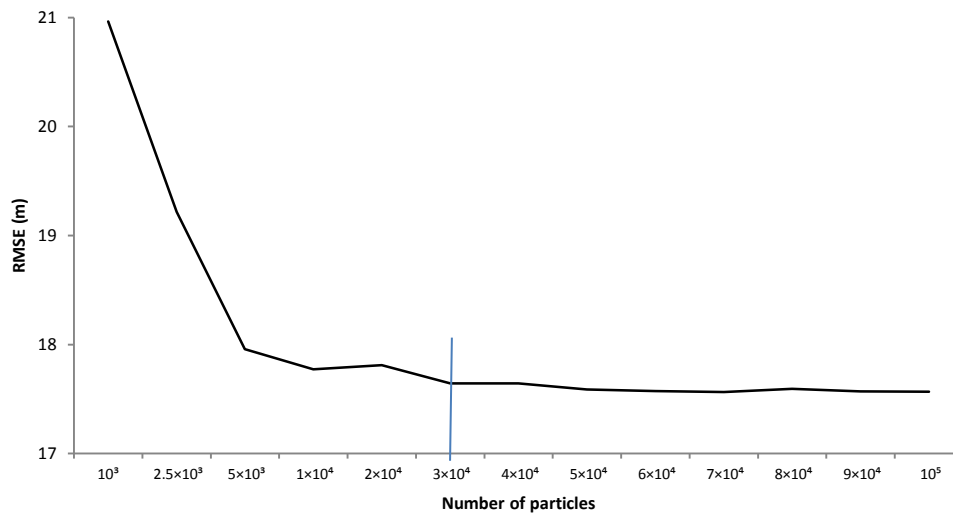


Fig. 4-7. Position RMSE versus the number of particles for $10^3 \leq N_{PF} \leq 10^5$.

Fig. 4-7 presents the experimental computation of position RMSE of PF for varying values of the number of particles. The position RMSE of PF decreases with an increase in the number of particles in the interval $[10^3, 10^5]$. The position RMSE considerably decreases when the number of PF increases from 10^3 to 5×10^3 , but then this value slightly decreases in the interval $[5 \times 10^3, 3 \times 10^4]$ of particles. The position RMSE does not reduce when the number of particles is higher than 3×10^4 . Thus, $N_{PF} = 3 \times 10^4$ is considered as an optimal value for this experiment. This behavior of estimated accuracy of PF due to the varying number of particles is consistent with the theory. However, it should also be noted that the optimal value of the particle depends on required accuracy and factors of scenarios, such as quantity of measurement uncertainty.

Table 4-4. Computational time of EKF, UKF, and PF.

Time	EKF	UKF	PF
Time for a single run of the algorithm	0.014 s	0.018 s	67 s
Proportion of computational time	1x	1.4x	4785x

Table 4-4 shows that the computational time of UKF and PF are 1.4 and 4785 times longer than the one for EKF, respectively. The difference in computational time between PF and the other two algorithms is high. To meet the real-time processing requirement, generally, the rate of incoming sensor data should be

lower than the update rate of the algorithm. In this experiment, both EKF and UKF can be used for real-time applications since the computational time of these algorithms (< 0.02 s) is smaller than the data rate ($\Delta t = 1$ s). In contrast, PF is unable to be applied for this issue because the computational time of this algorithm is approximately 67 times higher than the data rate. For this reason, computational inefficiency due to a large number of particles of PF remains a challenge in real-time applications. To reduce the computational time of PF, numerous solutions can be utilized, such as reduction of the dimension of the state vector, parallel and distributed computing, and adjusting the number of particles (Wang et al. 2017). In the present study, the computational time of PF is controlled based on the approach of adjusting the number of particles. The concept behind this approach is that the number of particles is reduced to a minimum value, so that the PF still can meet the requirement of accuracy.

4.3 Summary

Three influencing factors on position accuracy: measurement uncertainty, observation geometry, and number of measurements, are analyzed in this chapter. First, high measurement uncertainties cause a major reduction of position accuracy. Second, the magnitude of both intersection angle at moving object and the distance are the main effects on position accuracy in terms of observation geometry. According to a bad observation geometry, in which the moving object is far from radars, and the intersection angle is small, the position of the moving object becomes less accurate. Third, the position accuracy can be improved to a certain extent when using more measurements in the case of multiple radars. However, the extent of this improvement depends on the scenario, such as the intersection angle and the type of measurements.

This chapter also compares performances in terms of position accuracy and computational time among EKF, UKF, and PF. According to position accuracy, PF is superior compared to those of UKF and EKF. The key strength of PF is its ability to cope well with high measurement uncertainty and bad observation geometry. However, these results also suggest that the burden in computational time of PF remains a challenge in real-time applications. EKF, on the other hand, is preferred for implementations of measurement with high accuracy since its computational time is small and the accuracy is comparable if the uncertainty of the measurement is small. This algorithm should also be applied for multiple radar systems when the number of measurements is sufficiently large. Furthermore, although the computation time of UKF is not much different from that of EKF, the accuracy obtained by UKF is relatively higher than that of EKF. Hence, UKF should be considered as a potential algorithm in practical applications.

5. Choice of Filtering Algorithms using Non-linear Characteristic

In general, the optimal filtering algorithm is defined based on different parameters. The most straightforward parameter is RMSE, which is calculated by the difference between the true and estimated values. This issue is investigated in Chapter 4. In reality, however, the true trajectory is usually unknown. Thus, it is necessary to use an alternative approach to assess the ability of the filtering algorithm in this case. This problem is investigated by utilizing non-linearity as a characteristic, which can be measured without information about the true trajectory. The structure of this chapter includes three sections as follows. Section 5.1 will present the measure of non-linearity of the model for two cases of the system model and the observation model. In section 5.2, the relationship between the non-linearity of the observation model and position accuracy is established. Section 5.3 provides numerical examples about choosing the optimal filtering algorithm based on the non-linear characteristic.

5.1 Measures of Non-linearity

A measure of non-linearity is a mean to quantify the proportion of non-linearity between the input and output of a non-linear model (Allgöwer 1995). Measures of non-linearity have attracted attention in the field of kinematic positioning (Dunik et al. 2013, Wang et al. 2016, and Mallick et al. 2005). The highly non-linear characteristic is a challenge in the estimation since each filtering algorithm operates well at a certain level of non-linearity. Non-linearity may arise from the system model (Li and Jilkov 2005) and the observation model with their corresponding noises, particularly high noises from low-cost sensors. As a consequence, the measure of non-linearity plays a vital role in choosing a proper filter algorithm with a certain non-linear model. The non-linearity of both system (kinematic) and observation models can be investigated jointly (Li 2012, Dunik et al. 2013). However, the proportion of non-linearity between the system model and the observation model can change due to practical situations. To determine the importance of these models, the non-linearity of the system model and observation model are measured separately. To obtain reliable results, these evaluations are performed with sample sizes of $N_{LoN} = 10^4$ using the given scenarios in section 4.1.1. This chosen value is optimal for determining non-linearity by these indicators (see Appendix A3). The following parts will present how the non-linearity of system and observation models is measured.

Fig. 5-1 presents the procedure of measures of non-linearity of system and observation models based on the procedure of Kalman filter (see Chapter 3). The measures of non-linearity for a model, as represented in section 2.3, can be applied for both system and observation models in this part. The non-linearity of the system model is the proportion of the non-linearity relationship between the state vector $\hat{\mathbf{y}}_k$ and the predicted state vector $\bar{\mathbf{y}}_{k+1}$. Hence, the corresponding input and output of the system model in the procedure of measures of non-linearity (see section 2.3) are the state vector $\hat{\mathbf{y}}_k$ and the predicted state vector $\bar{\mathbf{y}}_{k+1}$, respectively. Similarly, the input vector and output vector of the non-linearity of the observation model are the predicted state vector $\bar{\mathbf{y}}_{k+1}$ and the predicted observation $\bar{\mathbf{l}}_{k+1}$, respectively.

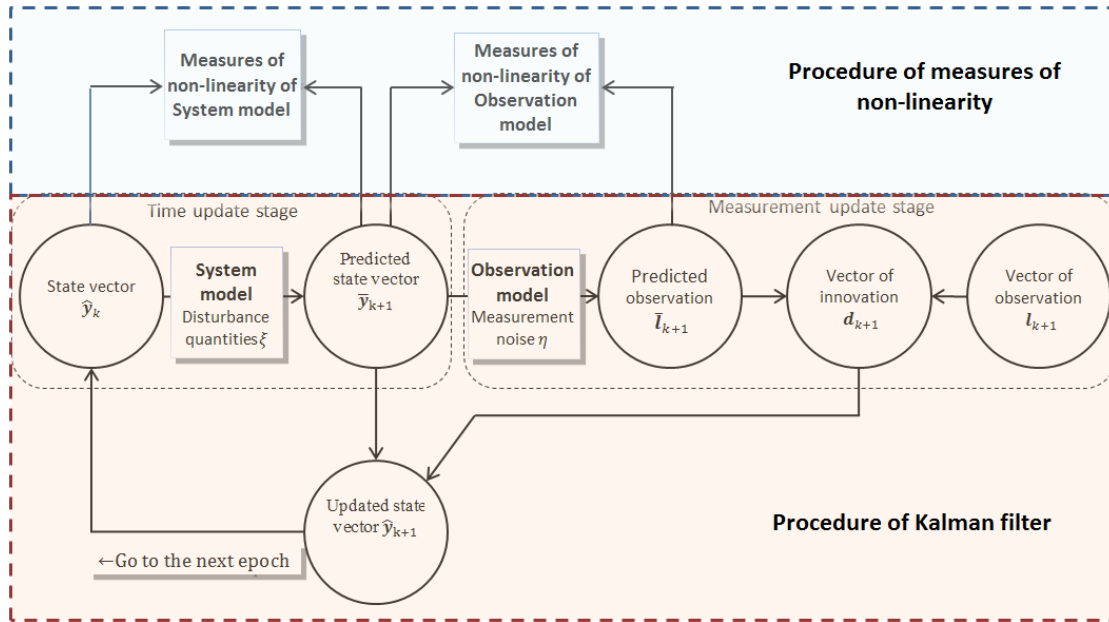


Fig. 5-1. Procedure for determination of the non-linearity of the system and observation models from epoch k to epoch $k+1$. Measures of non-linearity of these above models corresponding to two steps of the Kalman filter procedure are illustrated on the top.

5.1.1 Non-linearity of the system model

This section aims to measure the non-linearity of the system model by varying its factors, such as velocity, data rate, and orientation change. The scenario of two bearing angles in section 4.1.1 is also used for these evaluations. The straight linear model applied for modeling the kinematic behavior of a moving object is non-linear concerning the state vector. In (3-40), the first two equations are non-linear, and the last three equations are linear. Consequently, two non-linear equations about x and y are considered for analysis of the non-linearity of the system model using both single and multiple indicators, as mentioned in Chapter 2. The non-linearity of the system model can be quantified by multiple indicators, $1-MVA$ and M . To distinguish non-linearity between component x and y , the single indicator $1-R^2$ is employed.

a. Impact of velocity on non-linearity of the system model

This part examines the non-linearity of the system model as a function of velocity. The velocity of the moving object is simulated in the interval between 1 m/s and 40 m/s. The $1-R^2$ s of x and y components only increase approximately 0.01 with the rise in this velocity interval in Fig. 5-2(a). A similar trend of non-linearity of the system model quantified by multiple indicators $1-MVA$ and M can be seen in Fig. 5-2(b). Both $1-MVA$ and M increase only approximately 0.01 with the increase of velocity.

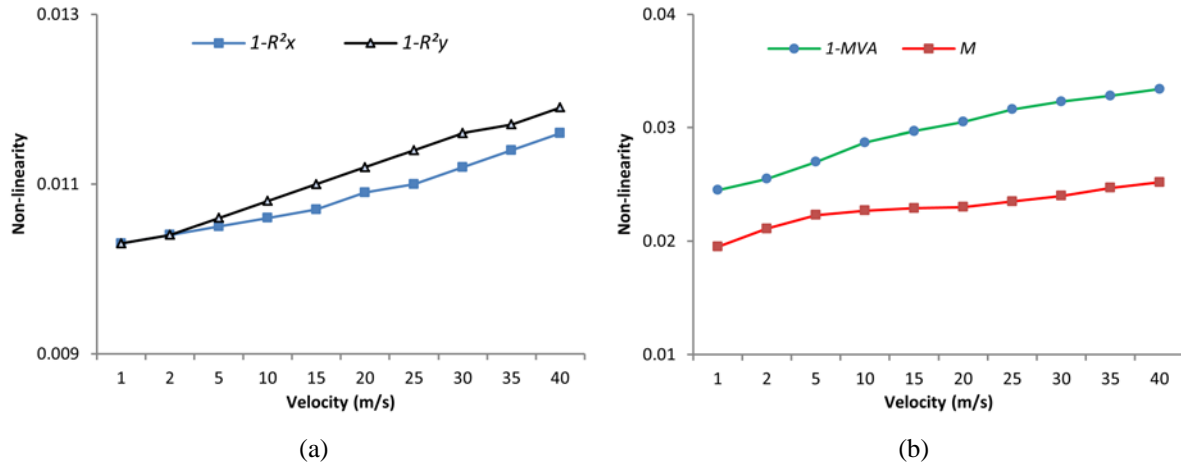


Fig. 5-2. Non-linearity of the system model versus velocity for the single indicator $1-R^2$ (a) and for multiple indicators $1-MVA$ and M (b). It is worth to note that the non-linearity values in the vertical axis are at a different scale.

b. Impact of data rate on non-linearity of the system model

In this section, non-linearity for the case of a change of data rate (sampling time) is presented. The data rate Δt is simulated in the interval [0.01 s, 5 s] or [100 Hz, 0.2 Hz]. Fig. 5-3(a) indicates that $1-R^2$'s of x and y components increase nearly 0.01 with the increase of data rate from 0.01 s to 5 s. Similarly, $1-MVA$ and M increase approximately 0.03 and 0.05, respectively, with the growth of data rate in Fig. 5-3(b).

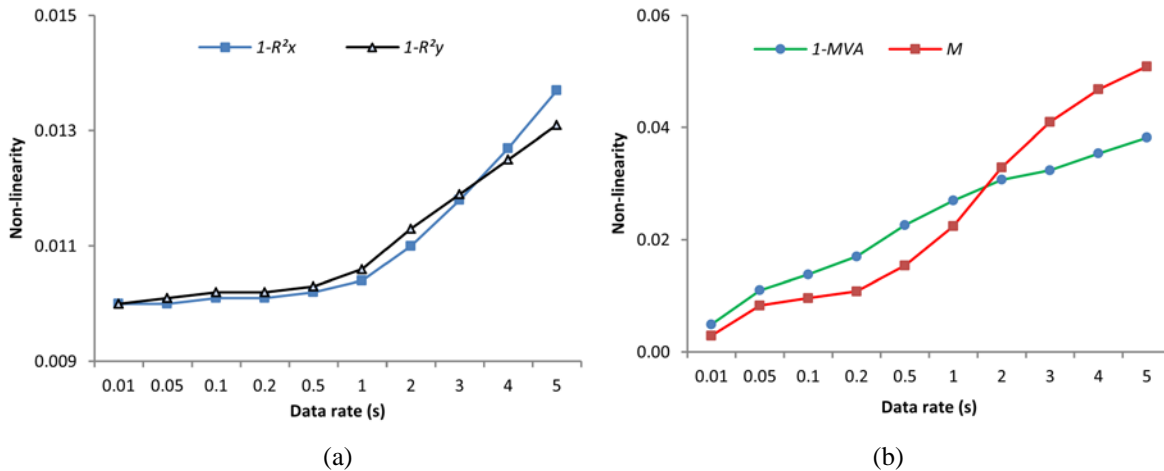


Fig. 5-3. Non-linearity of the system model versus data rate for the single indicator $1-R^2$ (a) and for multiple indicators $1-MVA$ and M (b). Note that the non-linearity quantities in the vertical axis of these graphs are not at the same scale.

c. Impact of orientation change on non-linearity of the system model

Fig. 5-3 presents the non-linearity of the system model versus the orientation change for $0^\circ \leq \Delta\varphi \leq 9^\circ$. The $1-R^2$'s of x and y components increase nearly 0.01 according to the growth of $\Delta\varphi$ from 0° to 9° (Fig. 5-4(a)). The non-linearity of the system model measured by $1-MVA$ and M also increases approximately 0.01 and 0.02, respectively, it $\Delta\varphi$ increases from 0° to 9° in Fig. 5-4(b).

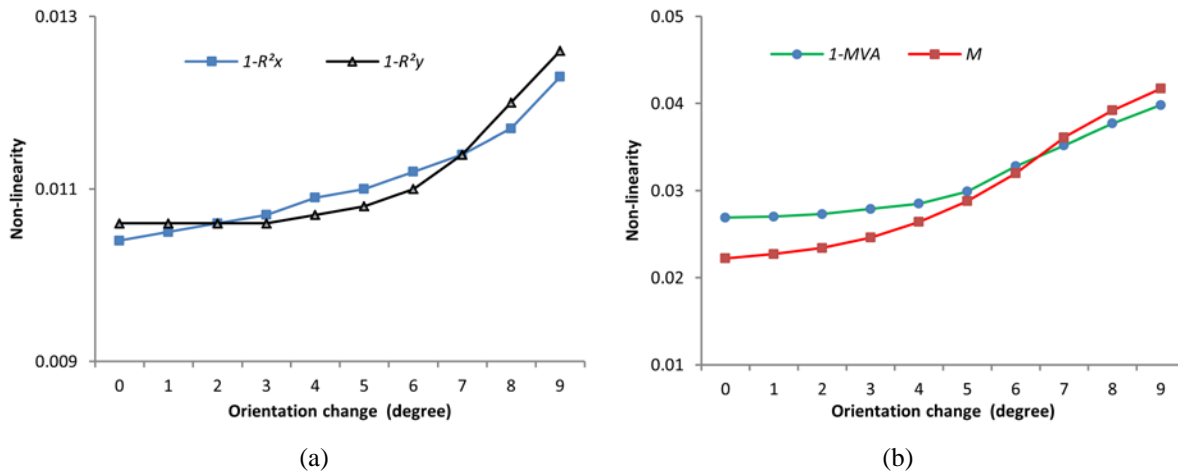


Fig. 5-4. Non-linearity of the system model versus orientation change for the single indicator $1-R^2$ (a) and for multiple indicators $1-MVA$ and M (b). It is worth note that the non-linearity values in the vertical axis of two charts are at a different scale.

d. Summary

This section investigates non-linearity of the system model and its influencing factors, including velocity, data rate, and orientation change on its value. The non-linearity of the system model is small (< 0.05), which means that this model is nearly linear. Another important result to emerge from these evaluations is that the change of this value according to the varying factors is also relatively small (approximately 0.01 to 0.05). These results are in accordance with the theory of non-linearity, as mentioned in Chapter 2. In these evaluations, the system model is non-linear in terms of mathematical equations. However, the quantity of non-linearity of this model is small due to the small standard deviations of disturbance quantities from given scenarios. Moreover, the behavior tendency of non-linearity of the system model due to the above three factors can be explained as follows. From the straight-line model used for the system model in (3-40), large values of both data rate and velocity cause less accuracy of the predicted state vector. In addition, this model is perfect for a straight trajectory when $\Delta\varphi$ is equal to 0° . This is because, when $\Delta\varphi$ differs from 0° , the accuracy of the predicted state vector becomes worse. The lower accuracy of the predicted state vector accounts for the high non-linearity of this model. It should be noted that the quantity of non-linearity and its change would become larger if high standard deviations of disturbance quantities are introduced. For example, when the standard deviation of disturbance quantities increases four times, the non-linearity and its change increase approximately two times (see Appendix A4).

5.1.2 Non-linearity of the observation model

This section aims to analyze the behavior of non-linearity of the observation model with its influencing factors. As explained in Chapter 4, the accuracy of estimation is a function of measurement uncertainty, observation geometry, and the number of measurements. Both the accuracy of estimation and non-linearity are associated (Verlaan and Heemink 2000) and (Li 2012). It is worth noting that the non-linearity of the observation model is unchanged due to an increase in the number of observations. Consequently, the non-linearity of the observation model will be analyzed with a change of measurement uncertainty and observation geometry only. Other factors that could affect the non-linearity of the observation model are not presented in this study. Note that assumptions that are used for the assessment

of position RMSE according to measurement uncertainty and observation geometry, as shown in Chapter 4, are also used for these evaluations as follows.

a. Impact of measurement uncertainty on non-linearity

Low-cost sensors may cause high measurement uncertainties, resulting in an increase in the level of non-linearity. Therefore, the objective of this section is to measure how the non-linearity of the observation model changes by measurement uncertainty. The scenario of two bearing angles in section 4.1.1 is also used for this evaluation, in which measurement uncertainty is in the interval from 0.2° to 2° . The following analysis will present the non-linearity of the observation model due to measurement uncertainty.

Fig. 5-5 shows that all three indicators increase with the growth of measurement uncertainty. The $1-R^2$ of each bearing angle increases by approximately 0.30. In addition, the $1-MVA$ and M rise approximately 0.33 and 0.42, respectively. The behavioral tendency of $1-MVA$ is similar to that of $1-R^2$. These results are in agreement with the theory that the MVA is extended from R^2 . On the other hand, M increases to a greater extent compared to the two different indicators. Overall, measurement uncertainty constitutes the essential factor that influences non-linearity of the observation model, especially in the case of high uncertainty in low-cost sensors' measurements.

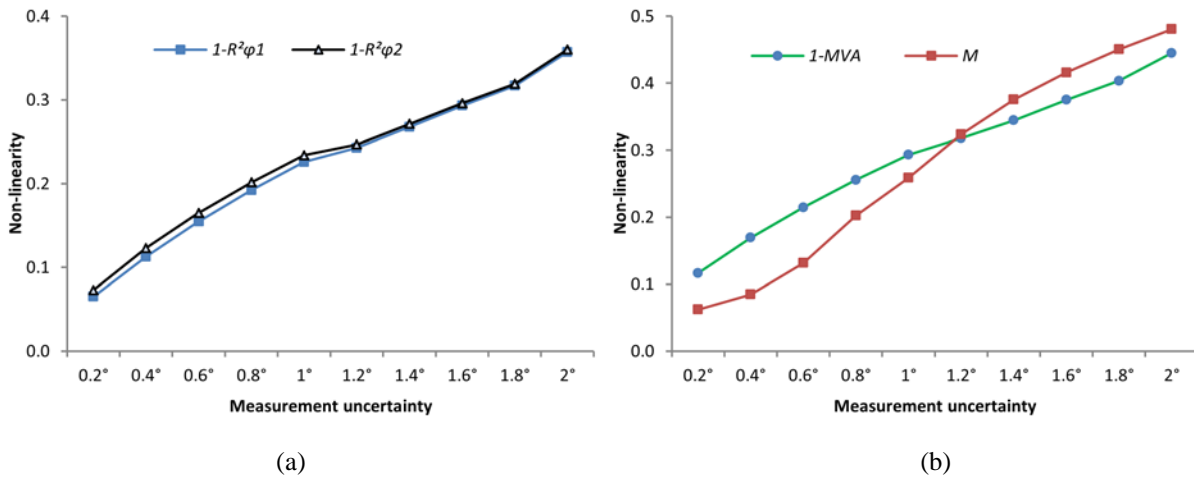


Fig. 5-5. Variation of the three indicators $1-R^2$, $1-MVA$, and M with the uncertainty of bearing angle. $1-R^2$ measures the non-linearity of each bearing angle separately (a), while $1-MVA$ and M measure the non-linearity of both bearing angles jointly (b). Note that the non-linearity values in the vertical axis of these graphs are at a different scale.

b. Impact of observation geometry on non-linearity

In this evaluation, the non-linearity of the observation model is considered as a function of observation geometry. The scenario of two bearing angles in section 4.1.1 is still the same as that used thus far, but the range is set in the interval between 0.5 km and 1.4 km, or the intersection angle in the interval $[53^\circ, 20^\circ]$, which is similar to the analysis in section 4.1.3. The above three indicators, including $1-R^2$, $1-MVA$, and M , are independently measured for non-linearity due to observation geometry as follows.

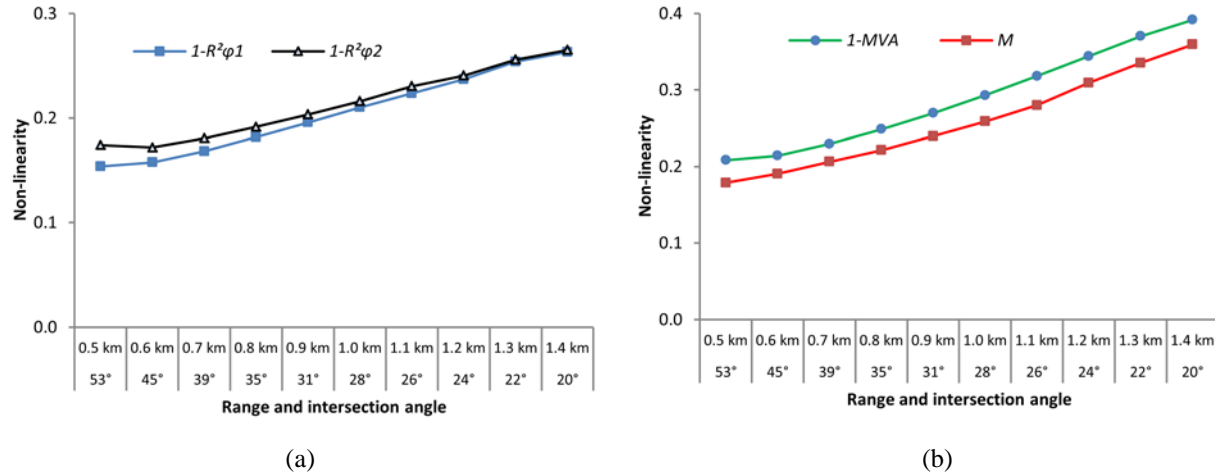


Fig. 5-6. Non-linearity of the observation model measured by the single indicator $1-R^2$ (a) and multiple indicators $1-MVA$ and M (b) versus range or intersection angle. It is worth noting that the non-linearity quantities in the vertical axis are not at the same scale.

The non-linearity of the observation model considerably increases with increasing range or decreasing intersection angle. The increases in non-linearity obtained by the three indicators $1-R^2$, $1-MVA$, and M are approximately 0.10, 0.18, and 0.18, respectively, for the range interval [0.5 km, 1.4 km] or intersection angle interval [53°, 20°]. Again, the tendencies of the three indicators are similar in the evaluation of the non-linearity of the observation model with varying observation geometry.

c. Impact of both measurement uncertainty and observation geometry on non-linearity

As mentioned previously, the non-linearity of the observation model is a function of two factors: measurement uncertainty (STD of measurement) and observation geometry. In the previous sections, a separate evaluation of the non-linearity of the observation model is carried out for each factor. In this section, a joint evaluation of the non-linearity of the observation model is performed with those two factors together. This evaluation is conducted with varying measurement uncertainty in the interval [0.2°, 2°] and varying range between radars and the moving object in the interval [0.5 km, 1.4 km], or intersection angle in the interval [53°, 20°]. Three indicators, $1-R^2$, $1-MVA$, and M , are employed to investigate the non-linearity of the observation model. The behavior of non-linearity when changing both the above factors is illustrated by 100 combinations of range and uncertainty in Fig. 5-7. This figure shows the behavior of non-linearity for varying both measurement uncertainty and observation geometry. In this graph, non-linearity is represented by the height on the surface of measurement uncertainty and range. The non-linearity of the observation model increases with increasing both measurement uncertainty and range. Although there is a small difference in quantities of non-linearity between these indicators, the trends of non-linearity determined by these indicators are similar. For varying ranges between radars and the moving object, non-linearity moderately changes according to small measurement uncertainties, but remarkably changes according to large measurement uncertainties. Inversely, for varying measurement uncertainties, non-linearity dramatically varies with the entire surveyed range. The maximum quantities of non-linearity measured by $1-R^2$, $1-MVA$, and M reach nearly 0.43, 0.57, and 0.57, respectively, according to $\sigma_\alpha = 2^\circ$ and $s = 1.4$ km. The changes of these values are approximately 0.35, 0.46, and 0.47, respectively, corresponding to the above three indicators, when measurement uncertainty and range vary from the minimum value to the maximum value in their intervals.

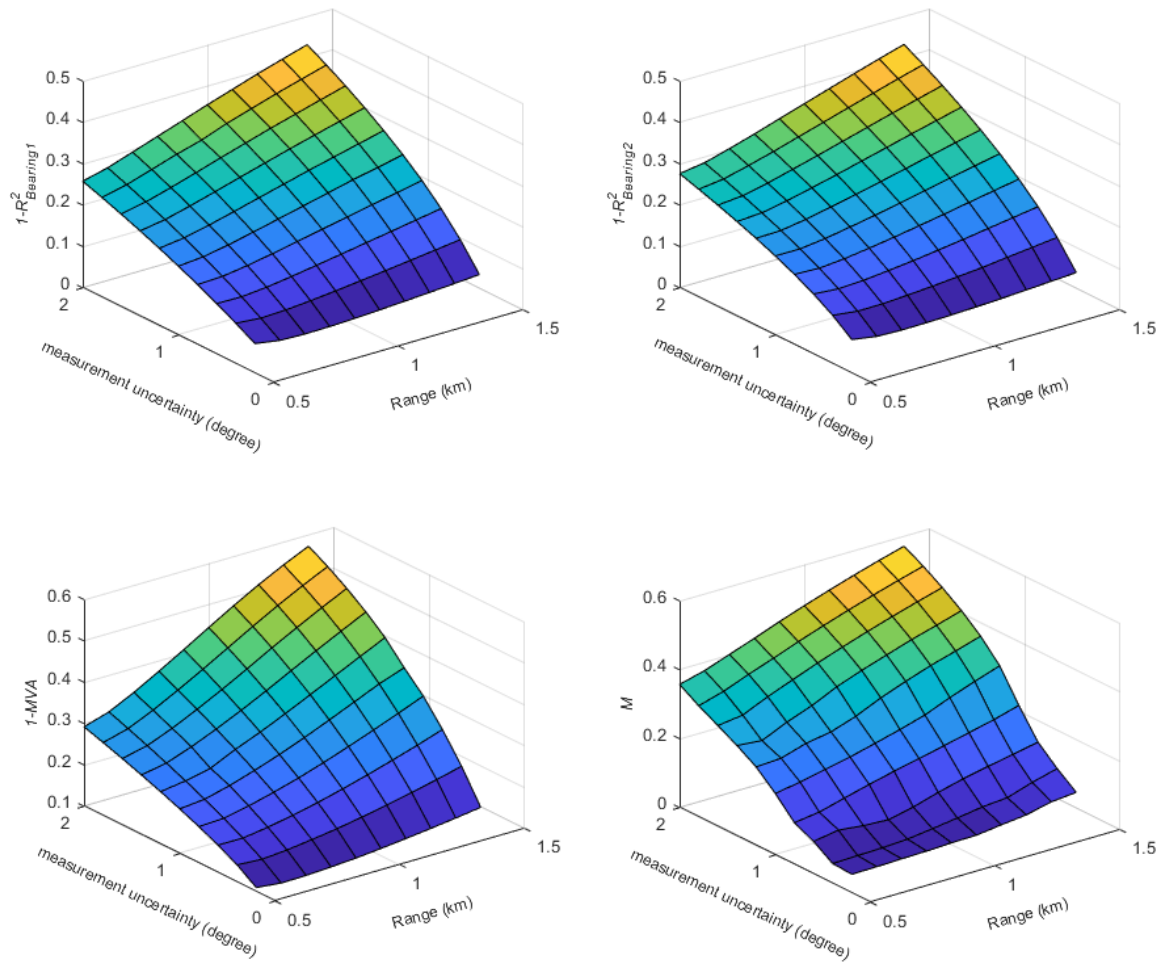


Fig. 5-7. Non-linearity of the observation model is a function of the factors of measurement uncertainty and range between radars and the moving object. The non-linearity obtained by $1-R^2$ for the first and second bearing angles is specified in the top-left and top-right corner, respectively. The non-linearity achieved by $1-MVA$ and M is presented in the bottom-left and bottom-right corner, respectively.

d. Summary

In this section, the non-linearity of the observation model and its influencing factors, including measurement uncertainty and observation geometry, are investigated. The non-linearity of the observation model is high and outstandingly changed by the above factors. First, the non-linearity of the observation model can reach approximately 0.6 due to high measurement uncertainties or poor observation geometry from the given scenarios. This means that the observation model is highly non-linear. This result is in accordance with the theory of non-linearity, as analyzed in Chapter 2. In this evaluation, the mathematical equation of the observation model is non-linear, and given measurement uncertainty to be high, corresponding to low-cost sensors' measurement of these scenarios. Second, the strong change in the non-linearity of the observation model is due to a large interval of both measurement uncertainty and intersection angle.

5.2 Relationship between Non-linearity and Position Accuracy

The purpose of this section is to elucidate the relationship between the position accuracy and the non-linearity of the observation model. A few studies have attempted to demonstrate this relationship, such as Verlaan and Heemink (2000), Mallick (2004), and Li (2012). However, the factors affecting this relationship remain unclear, and a quantitative relationship has not yet been established. The current study will provide a quantitative analysis of the relationship between the position accuracy and the non-linearity of the observation model. As discussed in the previous section, $1-R^2$ was only be used to determine the non-linearity of a single output variable of the observation model, and is unable to be used for identifying this relationship. Conversely, the multiple indicators $1-MVA$ and M can provide the measure of non-linearity of all output variables of the observation model. The trends of non-linearity obtained by these indicators are similar, as shown in section 5.1, and the difference in their quantities is small. As a consequence, both $1-MVA$ and M can be used for analyzing non-linearity and establishing the above relationship. In this section, the relationship between position accuracy and non-linearity determined by $1-MVA$ is presented.

Suppose that a relationship between them exists, which is generally described by the equation $1-MVA=f(RMSE)$. The function chosen for this relationship may be one of the basic functions, such as a linear function, an exponential function, and polynomial functions with different orders. This section aims to identify the fitting function between $1-MVA$ and position RMSE. The fitting function can be found by using both graphic and numerical methods. In the graphical method, a scatter plot is used to provide a visual depiction of the behavior of the entire data. A rough estimate can be obtained by the graphical method, and it can be used as initial estimates for numerical methods. However, the coefficient of the fitting function cannot be determined by this method. They can be determined by the numerical method. To evaluate how the function fits the data of $1-MVA$ and RMSE, the goodness-of-fit (GOF), which is defined by the sum of the discrepancy between data and expected values from the chosen function, is used. If the fitting function is linear, the GOF is exactly the coefficient of determination R^2 , as shown in section 2.2.1. In this study, the combination of the graphic method and the numerical method is applied to determine the fitting function in the two following steps. First, a scatter plot of data about the relationship between $1-MVA$ parameter and RMSE parameter can be drawn on a graph in the form of dots. From the tendency of these dots, a particular function can be chosen as a fitting function for approximating the relationship between these parameters. After utilizing the graphical method, the coefficients of the given function and its corresponding GOF value are determined.

This determination of the relationship between $1-MVA$ and RMSE will be evaluated on the two influencing factors of measurement uncertainty and observation geometry in the three following cases. First, the variation of observation geometry is evaluated for this relationship. In the second case, an investigation of this relationship is carried out with varying measurement uncertainty. Finally, this relationship is assessed in changing both measurement uncertainty and observation geometry in the third case.

5.2.1 Variation of measurement uncertainty

The relationship between $1-MVA$ and RMSE is investigated according to varying measurement uncertainty. This scenario of two bearing angles has also been applied in section 4.1.1 with 10 different values of measurement uncertainties, for $0.2^\circ \leq \sigma_\alpha \leq 2.0^\circ$. In this scenario, the shortest distance between radars and the moving object is 1 km or the intersection angle is 28° . Establishment of the relationship between $1-MVA$ and RMSE is based on the combination of both graphic and numerical methods, as described as follows.

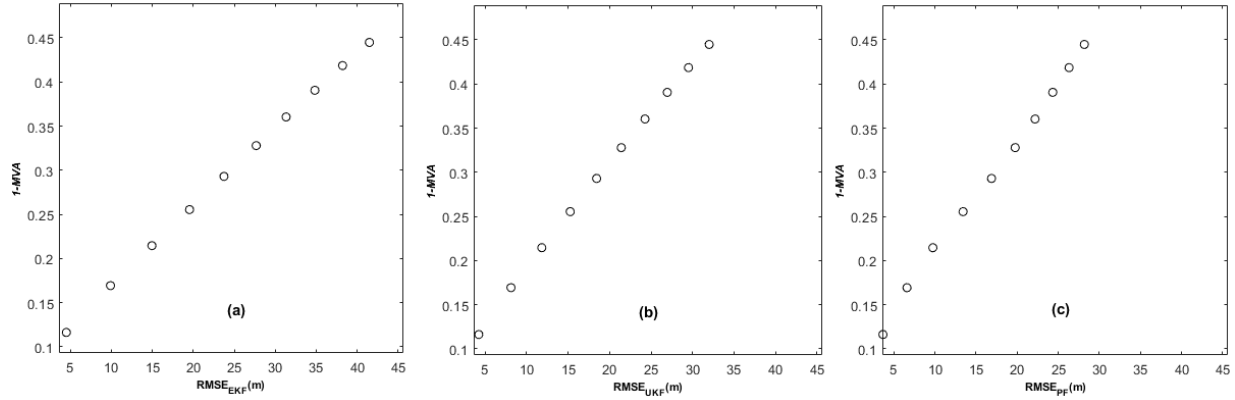


Fig. 5-8. Relationship between 1-MVA and RMSE of EKF, UKF, and PF in (a), (b), and (c), respectively, in different measurement uncertainties.

Fig. 5-8 shows the relationship between 1-MVA and RMSE of three algorithms, EKF, UKF, and PF. Since all three data exhibit a linear trend, a linear function is an appropriate choice for modeling these data. The linear function in (2-1) is applied for the fitting function in the numerical method, in which the input x and the output y are replaced by RMSE and 1-MVA, respectively as follows:

$$1 - MVA = b_0 + b_1 \cdot RMSE, \quad (5-1)$$

where b_0 and b_1 are intercept and slope coefficients, respectively.

In the numerical method, the intercept and slope coefficients of linear functions can be estimated using the least-square method. The coefficients of the fitting function and their GOF values are listed in Table 5-1.

Table 5-1. Determination of coefficients b_0 and b_1 of the linear function and their GOFs in different measurement uncertainties.

Algorithms	Fitting function	Coefficients		GOF R^2
		b_0	b_1	
EKF	Linear function	0.0807	0.0088	0.9995
UKF	Linear function	0.0734	0.0118	0.9990
PF	Linear function	0.0791	0.0128	0.9967

In Table 5-1, the GOF values are higher than 0.99, which means that the linear function is sufficient for describing this relationship. The slope coefficient b_1 of the fitting function for the relationship between 1-MVA and RMSE, according to PF, is the highest (Fig. 5-8(c)), which means that the rate of change in 1-MVA per unit change in the RMSE, according to PF, is the fastest. Inversely, the slope coefficient of fitting function in this relationship, according to EKF, is the smallest (Fig. 5-8(a)), which means that the rate change in 1-MVA per unit change in the RMSE, according to EKF, is the lowest.

In this section, other scenarios are also used for the evaluation for this relation, in which measurement uncertainty are varied in ten levels from 0.2° to 2° but the distance or intersection angle is given at one particular value, for $0.5 \text{ km} \leq s \leq 1.4 \text{ km}$ or $28^\circ \leq \gamma \leq 53^\circ$ (see Appendix A5 for details). The determination of fitting functions and their GOFs for these scenarios are similar to the previously mentioned procedure and also summarized in Appendix A5. It is worth noting that, according to scenarios $s = 0.5 \text{ km}$ and $s = 0.6 \text{ km}$, the data of scatter plots follow parabolic patterns. Consequently, the quadratic model (second-order polynomial function) that best fits the data is given by:

$$1 - MVA = b_0 + b_1 \cdot RMSE + b_2 \cdot RMSE^2, \quad (5-2)$$

where b_0 , b_1 , and b_2 are the coefficients.

For all scenarios, the GOF values are higher than 0.99, which indicates that the proposed fitting functions are satisfied for establishment of the relationship between 1-*MVA* and RMSE in the case of varying measurement uncertainty. The important result that emerges from these evaluations is that coefficients of fitting functions describing this relationship are not the same among the above scenarios.

5.2.2 Variation of observation geometry

This section aims to establish the relationship between 1-*MVA* and RMSE due to the change of observation geometry. The scenario that is used for this evaluation is similar to the scenario of two bearing angles in section 4.1.1. Both 1-*MVA* and RMSE is evaluated in ten different observation geometries. These observation geometries is surveyed with the corresponding distance in the interval [0.5 km, 1.4 km] or the corresponding intersection angle in the interval [53°, 20°]. The fitting functions for this relationship can also be solved in a similar manner to that discussed in section 5.2.1.

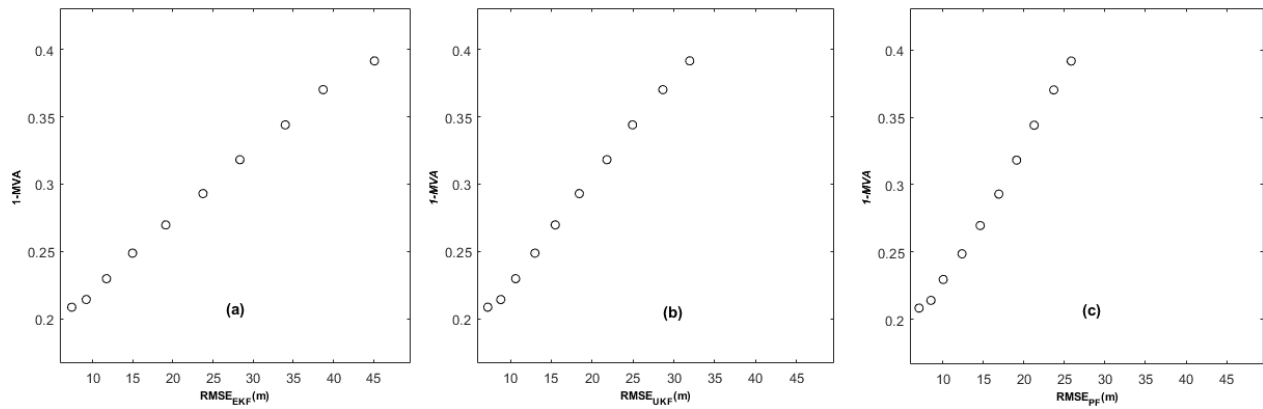


Fig. 5-9. Relationship between 1-*MVA* and RMSE of EKF, UKF, and PF in (a), (b), and (c), respectively, in different observation geometries.

Fig. 5-9 shows the relationship between 1-*MVA* and RMSE of EKF, UKF, and PF by scatter plots. Since the data of the scatter plot in Fig. 5-9(a) follows a linear pattern, a linear function is better for modeling this data. The data of scatter plots in Fig. 5-9(b) and Fig.5-9(c) follow quadratic patterns so that quadratic functions should be used to model these data.

Table 5-2. Determination of coefficients b_0 and b_1 of the linear function and their GOFs in different observation geometries.

Algorithms	Fitting function	Coefficients			GOF R^2
		b_0	b_1	b_2	
EKF	Linear function	0.1720	0.0050	-	0.9973
UKF	Linear function	0.1501	0.0077	-	0.9987
PF	Linear function	0.1286	0.0101	-	0.9954
UKF	Quadratic function	0.1384	0.0093	-4.771×10^{-5}	0.9971
PF	Quadratic function	0.1469	0.0076	6.688×10^{-5}	0.9960

In the numerical method, the quadratic coefficient b_2 of a quadratic function using for modeling the relationship between 1-*MVA* and RMSE of UKF and PF algorithms (5-2) is small, and it has been shown that the quadratic coefficient can be ignored (see Appendix A7). Besides, the GOF values when using the quadratic function and linear function are almost the same. Thus, the linear function is considered as a potential fitting function in order to simplify in this case. The form of a linear equation in (5-1) is also employed in the numerical evaluation. The coefficients of fitting functions and their GOF values measured by R^2 are determined in Table 5-2. The GOF values of these fitting functions are higher than 0.99, meaning that the linear function is the best fitting function for the relationship between 1-*MVA* and RMSE in case of varying observation geometry. In addition, the rate of change in 1-*MVA* per unit change in RMSE, according to PF, is faster than those of both UKF and EKF since the slope coefficient b_1 of PF (Fig. 5-9(c)) is higher than those of UKF and EKF (Fig. 5-9(a) and (b)).

Other scenarios also used the same factors as those in this scenario, but the uncertainty of bearing angle is given at different values in the angle range from 0.2° to 2° step with 0.2° (see Appendix A6 for details). Determination of fitting functions and their GOF values is carried out similarly to section 5.2.1, except that the quadratic function (5-2) is selected for describing the relationship between 1-*MVA* and RMSE of PF according to the scenario $\sigma_\alpha = 0.2^\circ$. The linear function is selected as a fitting function for all remaining scenarios. From the numerical analysis, the GOF values of all scenarios are higher than 0.97, indicating that these chosen fitting functions are appropriate for these evaluations. The rates of change in 1-*MVA* per unit change in RMSE of EKF, UKF, and PF are consistent with the analyses mentioned in section 5.2.1. The significant result of these evaluations is that coefficients of fitting function modeling for this relationship are not the same among the above scenarios.

5.2.3 Variations of both measurement uncertainty and observation geometry

This section aims to establish the relationship between 1-*MVA* and RMSE with simultaneously varying both measurement uncertainty and observation geometry. This relationship is examined when these influencing factors are varied in three different ranges as the following.

First, the measurement uncertainty is altered in 10 equal steps between 0.2° and 2° , and the observation geometry is changed in 10 equal steps between 0.5 km and 1.4 km of the distance. Determination of the best function fitting of the above relationship is also dealt with by a combination of the graphical method and the numerical method, as presented the previous subsections (see 5.2.1 and 5.2.2).

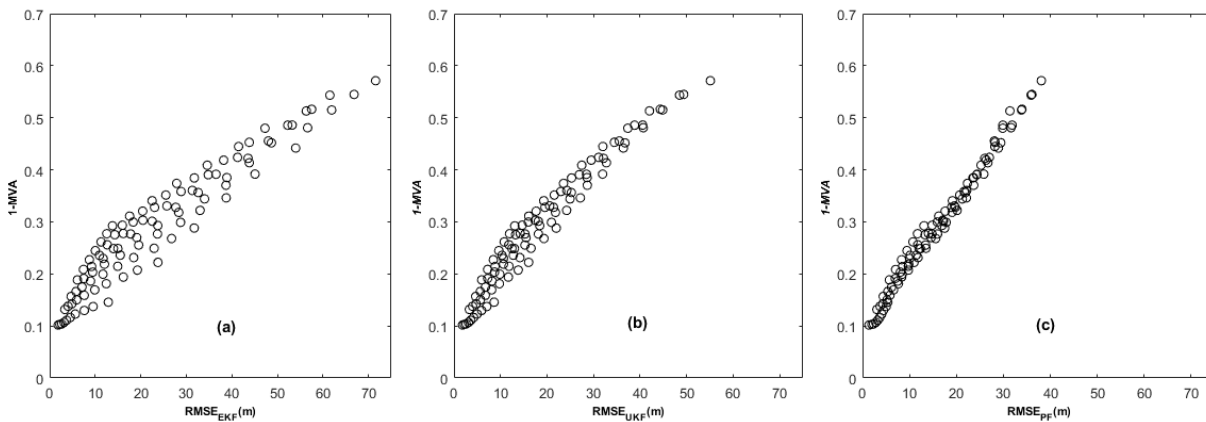


Fig. 5-10. Scatter plots of 100 data about 1-*MVA* and RMSE of EKF, UKF, and PF in (a), (b), and (c), respectively in various measurement uncertainties from 0.2° to 2° and the distances from 0.5 km to 1.4 km.

Fig. 5-10 shows the scatter plots of the relationship between RMSE determined by EKF, UKF, and PF (in the horizontal axis) and 1-MVA (in the vertical axis). In the graphical method, the scatter plots reveal that the data follow a linear pattern. Consequently, it can be better modeled by a linear function. In the numerical method, the intercept and slope coefficients of linear functions in (5-1) are determined, and their GOF values are measured by R^2 (see section 2.2.1). These values are summarized in Table 5-3.

Table 5-3. Determination of coefficients b_0 and b_1 of the linear function and their GOFs in different measurement uncertainties from 0.2° to 2° and the distances from 0.5 km to 1.4 km.

Algorithms	Fitting function	Coefficients		GOF R^2
		b_0	b_1	
EKF	Linear function	0.1325	0.0066	0.9146
UKF	Linear function	0.1156	0.0094	0.9505
PF	Linear function	0.0919	0.0125	0.9857

Table 5-3 indicates that the GOF values of these algorithms are in agreement with the data in Fig. 5-10, in which the GOF obtained by PF is higher than those of UKF and EKF.

Second, measurement uncertainty is altered in the smaller interval while observation geometry is varied in the same interval compared to the first case. The measurement uncertainty is varied in 5 equal steps from 0.2° to 1° , and the observation geometry is changed in 10 equal steps from 0.5 km to 1.4 km. Determination of the best function fitting for the relationship between 1-MVA and RMSE is carried out similarly to the first case.

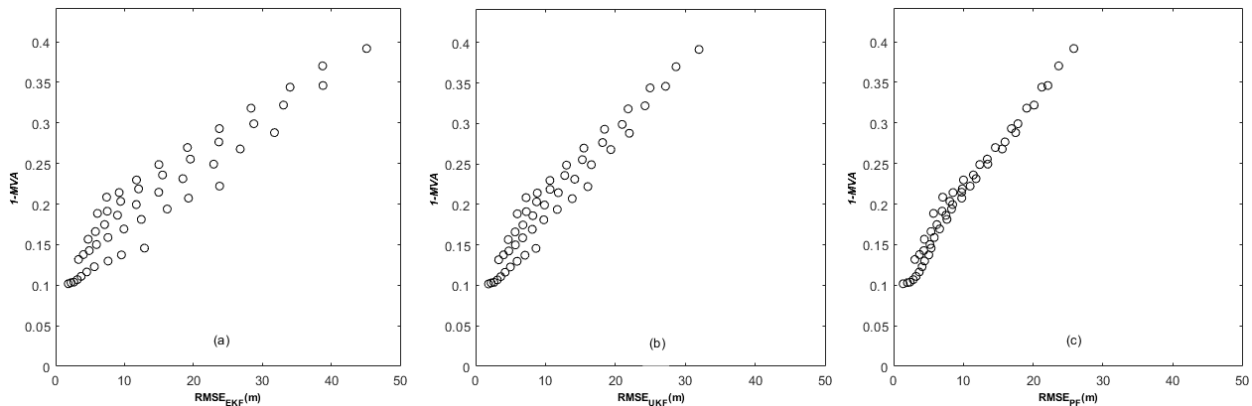


Fig. 5-11. Scatter plots of 50 data about 1-MVA and RMSE of EKF, UKF, and PF in (a), (b), and (c), respectively in various measurement uncertainties from 0.2° to 1° and the distances from 0.5 km to 1.4 km.

From the scatter plots in Fig. 5-11, a linear function should be used for modeling this relationship according to three algorithms, EKF, UKF, and PF. The intercept and slope coefficients of these linear functions are determined, and their GOF values are measured by R^2 depicted in Table 5-4.

Table 5-4. Determination of coefficients b_0 and b_1 of the linear function and their GOFs in different measurement uncertainties from 0.2° to 1° and the distances from 0.5 km to 1.4 km.

Algorithms	Fitting function	Coefficients		GOF R^2
		b_0	b_1	
EKF	Linear function	0.1136	0.0064	0.8901
UKF	Linear function	0.0976	0.0096	0.9366
PF	Linear function	0.0922	0.0119	0.9746

The GOF values of these algorithms in Table 5-4 also match with the data in Fig. 5-11, in which the GOF obtained by PF is also higher than those of UKF and EKF.

Third, both measurement uncertainty and observation geometry are varied in smaller intervals in comparison with the first case in this analysis. The measurement uncertainty is changed in 5 equal steps in the interval $[0.2^\circ, 1^\circ]$ and the observation geometry is changed in 5 equal steps in the distance interval $[0.7 \text{ km}, 1.1 \text{ km}]$. The best function fitting for the relationship between 1-MVA and RMSE is determined by using the graphical method in the first step. The linear function is still proposed as a fitting function for these relationships.

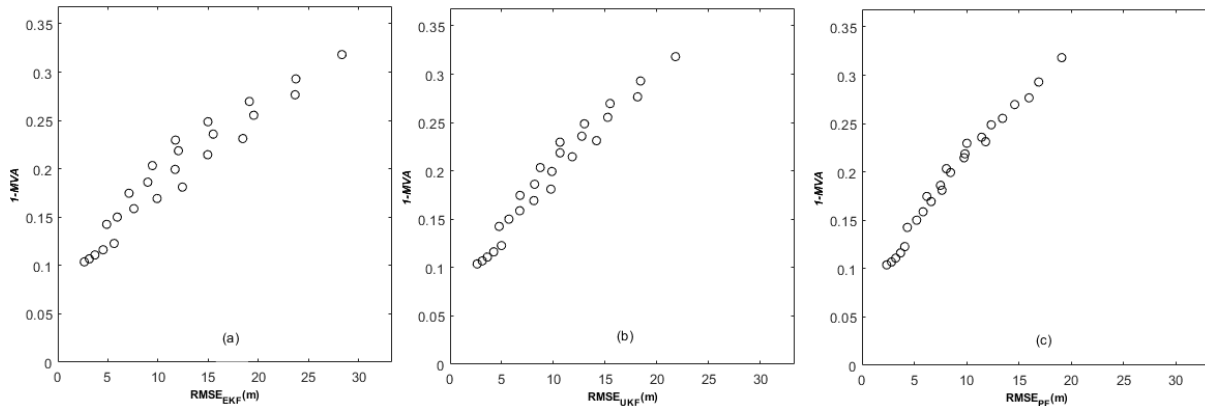


Fig. 5-12. Scatter plots of 25 data about 1-MVA and RMSE of EKF, UKF, and PF in (a), (b), and (c), respectively in various measurement uncertainties from 0.2° to 1° and the distances from 0.7 km to 1.1 km.

In the numerical method, the coefficients of these fitting functions and their GOF values can be calculated and listed in Table 5-5.

Table 5-5. Determination of coefficients b_0 and b_1 of the linear function and their GOFs in different measurement uncertainties from 0.2° to 1° and the distances from 0.7 km to 1.1 km.

Algorithms	Fitting function	Coefficients		GOF
		b_0	b_1	R^2
EKF	Linear function	0.0968	0.0083	0.9217
UKF	Linear function	0.0814	0.0116	0.9585
PF	Linear function	0.0816	0.0130	0.9764

Tables 5-3, 5-4, and 5-5 show the coefficients of fitting functions and their corresponding GOFs for the relationship between 1-MVA and RMSE in case of changing both measurement uncertainty and observation geometry. The linear function is a potential candidate for the establishment of these relationships. The GOF values are larger than 0.89, which indicates that the above functions are still appropriate to model the data since more than 89% of data can be explained by these functions. These results also reveal that the GOF value, according to the PF algorithm, is the highest among the three algorithms, which means that the relationship built for PF is stronger than those of both UKF and EKF. This result is consistent with the accuracy obtained by three algorithms, in which the accuracy of PF is higher than those of both UKF and EKF, as analyzed in Chapter 4.

5.2.4 Summary

In this section, the relationship between 1-*MVA* and RMSE is established in two cases: (1) changing only one influencing factor, and (2) changing both influencing factors simultaneously.

First, the relationship between 1-*MVA* and RMSE is established in case of varying only one influencing factor (measurement uncertainty or observation geometry). The relationship is strong (GOF values > 0.99), and the differences in GOFs among the three algorithms are trivially small. The linear function is the most suitable for the fitting function of this relationship in almost cases. In some special cases of small measurement uncertainty or a short distance between radars and the moving object, the second-order polynomial function is more suitable for describing this relationship.

Second, the relationship between 1-*MVA* and RMSE is built in case of simultaneously varying both measurement uncertainty and observation geometry in their different ranges. These results indicate that the linear function is still the best fitting function, and their GOF values in three corresponding ranges of these factors are quite similar. The GOF values are smaller than the case of varying only one influencing factor, which means these relationships are weaker. Furthermore, the GOF values dramatically change due to algorithms, in which the GOF value of PF is the highest among the three algorithms.

5.3 Evaluation of the non-linear characteristic for the selection of algorithms

The purpose of this section is to evaluate the ability to use non-linearity as a characteristic for the selection of filtering algorithms. The main idea behind this issue is based on the existing relationships between non-linearity and position accuracy in section 5.2. In general, one filtering algorithm can be chosen based on certain parameters. In Chapter 4, performances in terms of position accuracy and computational time can be used as parameters to define the optimal filtering algorithm. In that case, position accuracy can only be determined if the true trajectory is available. However, in real situations, the true trajectory is frequently unknown. In this section, the issue of the selection of filtering algorithms, when the true trajectory is not available, is investigated. Non-linearity is proposed as a characteristic to solve this problem since it can be identified without information about the true trajectory. Therefore, a procedure for determining the optimal algorithm, when the true trajectory is not available, is developed. The non-linear characteristic of the observation model measured by 1-*MVA* is used for these evaluations based on numerical examples.

5.3.1 Procedure of the selection of algorithms

In this study, a procedure is proposed for determining the optimal algorithm based on 1-*MVA* and computational time as the primary and secondary parameters, respectively. The main idea behind this procedure is a direct comparison between the 1-*MVA* of the observation model and the threshold of 1-*MVA* of given algorithms, which are obtained from the corresponding threshold of RMSE. Then, the computational time is used as the second parameter for possible algorithms, which is selected by the 1-*MVA* parameter. This procedure is presented in detail in Fig. 5-13.

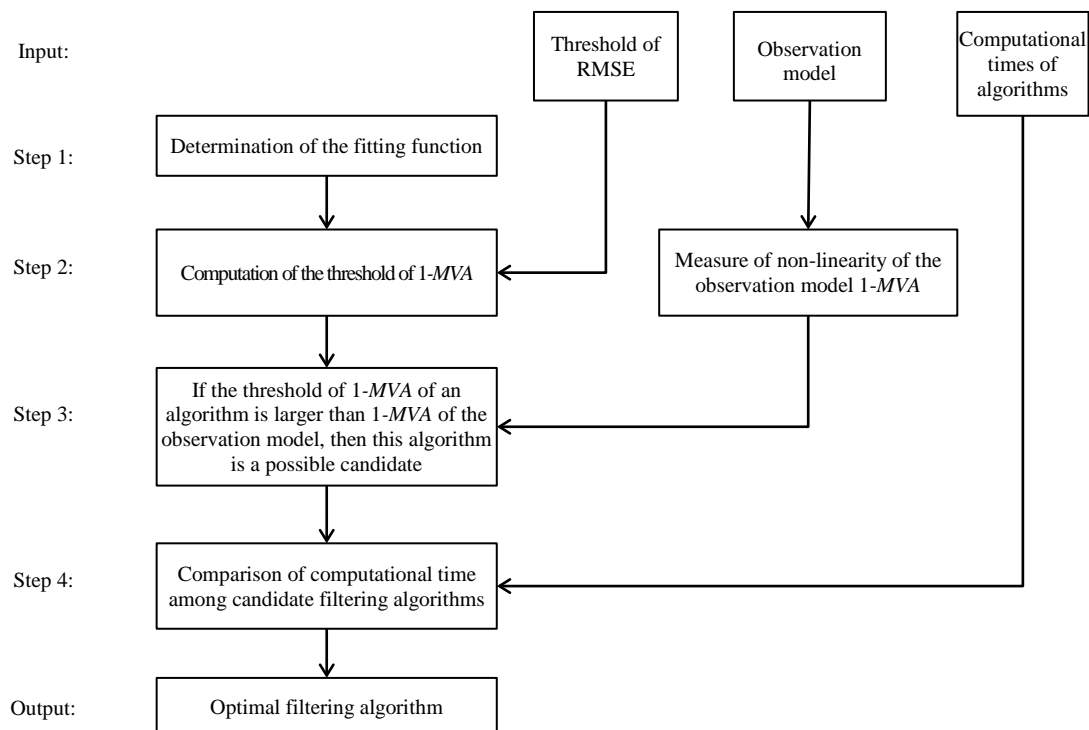


Fig. 5-13. Procedure for the selection of filtering algorithms.

The procedure of finding the optimal algorithm using the 1-*MVA* parameter and the computational time parameter can be summarized into four steps as follows:

Step 1: The coefficients of fitting function modeling the relationship between 1-*MVA* and RMSE of one scenario are computed by the linear interpolation method from corresponding coefficients of two neighborhood scenarios. In this work, the difference in factors of two consecutive scenarios is relatively small (i.e., a step of the interval of measurement uncertainty is 0.2° , and that of the distant interval of observation geometry is 0.1 km). Besides, the fitting function for the above relationship is the same type in two consecutive scenarios (see Appendixes A5 and A6). Hence, for one scenario, the type of fitting function is assumed to be similar to those of two neighborhood scenarios, and its coefficients can be interpolated from their corresponding coefficients of these scenarios.

Step 2: The threshold of 1-*MVA* for a filtering algorithm is identified when the coefficients of fitting function and the requirement of accuracy (threshold of RMSE) are known. In parallel, non-linearity of the observation model is measured by 1-*MVA*.

Step 3: The non-linear characteristic is used by a straightforward comparison between 1-*MVA* and the threshold of 1-*MVA* of an algorithm from step 2. Specifically, a filtering algorithm is chosen if its threshold value of 1-*MVA* is higher than the 1-*MVA* of the observation model.

Step 4: The computational time parameter is applied in the fourth step. From the selected filtering algorithms in step 3, the optimal algorithm is determined to be the fastest one in terms of computational time.

The main limitation of this procedure is that the relationship between 1-*MVA* and RMSE has been built in certain scenarios. Hence, the non-linear characteristic can only be applied for similar scenarios. The following numerical examples will present how this procedure in selecting algorithms may be used.

5.3.2 Numerical examples

In the following numerical examples, the positioning of the kinematic object is considered in marine applications, such as harbor entrances, inland waterways, and coastal operations. A vessel can be tracked by multiple radars that are located at different reference points along the seashore (Swierczynski and Czaplewski 2015). For simplification, two bearing radars fixed at two reference points in the coastline are utilized for observing the vessel in this example (see Fig. 5-14).

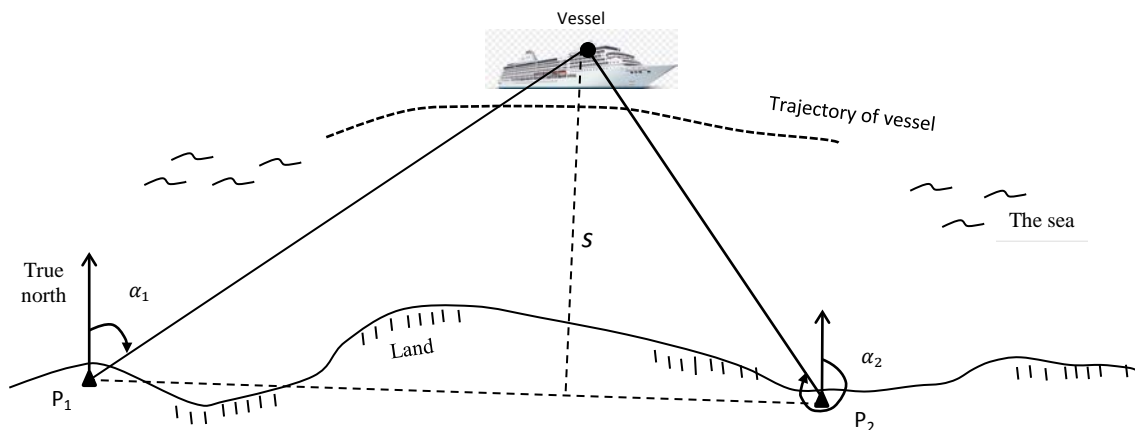


Fig. 5-14. Radars generating bearing angles are able to track the trajectory of a vessel. These radars are located at reference points P_1 and P_2 , and s is used to describe different observation geometries.

Due to the mentioned applications, a short distance between radars and the vessel is given for numerical examples in this section. Besides, to meet the requirement of IMO performance standards (Bole et al. 2005), the uncertainty of the bearing angle is assumed to be smaller than 1° in all six scenarios. These scenarios are examined in order to assess the ability of the non-linear characteristic in the selection of filtering algorithms. These scenarios are similar to the scenario of two bearing angles in section 4.1.1, but the measurement uncertainty and distance between radars and vessel are given in different values and listed in Table 5-6.

Table 5-6. Given bearing angle uncertainty and observation geometry of six scenarios.

Scenarios	Bearing angle uncertainty	Distance between radars and vessel
A	0.5°	$s = 0.85$ km
B	0.5°	$s = 0.95$ km
C	0.5°	$s = 1.05$ km
D	0.7°	$s = 0.85$ km
E	0.7°	$s = 0.95$ km
F	0.7°	$s = 1.05$ km

Note that the given values about measurement uncertainty and observation geometry are in the limited intervals of scenarios that are used for evaluating the relationship between 1-MVA and RMSE in section 5.2. Hence, all six scenarios in Table 5-4 can apply these established relationships. According to the previously mentioned applications, the required position accuracy (RMSE < 10 m) (see the International Maritime Organization (IMO) standards in Table 5-7) is considered.

Table 5-7. General absolute position accuracy requirements.

Navigation Phase	Accuracy according to IMO resolution A.1046(27)	Accuracy according to IMO resolution A.915(22)
Ocean	100 m	10 m
Coastal	10 m	10 m
Harbor approach	10 m	10 m
Harbor entrance	10 m	10 m
Inland waterways	10 m	10 m
Port	NA	1 m

The following examples will be presented the selection of algorithms using non-linear characteristic from the established relationships between 1-MVA and RMSE in two cases of varying only one or both influencing factors.

a. Variation only one influencing factor

In this example, the relationship between 1-MVA and RMSE in the case of changing only one influencing factor is used for selecting algorithms and divided into two following examples:

Example 1: Changing only measurement uncertainty

In this example, the established relationship in the case of varying only measurement uncertainty (see section 5.2.1) is applied. The procedure in section 5.3.1 can be applied here to determine the optimal algorithm. Suppose that the fitting functions of this relationship for six above scenarios are linear functions. The coefficients of these functions can be computed using step 1 of this procedure. For

example, according to scenario A ($s = 0.85$ km), the fitting function of the relationship according to EKF can be derived from scenario 4 and scenario 5, which have $s = 0.8$ km and $s = 0.9$ km, respectively. The coefficients of the fitting function of scenarios A $b_0^{(A)}$ and $b_1^{(A)}$ can be computed as:

$$b_0^{(A)} = b_0^{(4)} + \frac{(0.85 - 0.8) \cdot (b_0^{(5)} - b_0^{(4)})}{(0.9 - 0.8)}, \quad (5-3)$$

$$b_1^{(A)} = b_1^{(4)} + \frac{(0.85 - 0.8) \cdot (b_1^{(5)} - b_1^{(4)})}{(0.9 - 0.8)}, \quad (5-4)$$

where $b_0^{(4)}$, $b_1^{(4)}$, and $b_0^{(5)}$, $b_1^{(5)}$ are the coefficients of the fitting functions of scenario 4, and scenario 5, respectively. These values are listed in Table A5-1 of Appendix A5. For other algorithms and scenarios, the coefficients of the fitting function can be determined similarly, as shown in Table 5-8.

Table 5-8. Coefficients of fitting functions in six scenarios due to varying measurement uncertainties.

Scenarios	s (km)	EKF		UKF		PF	
		b_0	b_1	b_0	b_1	b_0	b_1
A, D	0.85	0.0853	0.0100	0.0753	0.0126	0.0807	0.0131
B, E	0.95	0.0826	0.0092	0.0739	0.0121	0.0799	0.0129
C, F	1.05	0.0774	0.0087	0.0731	0.0115	0.0748	0.0131

The analysis results from step 2 to step 4 are summarized in Table 5-9 below. From the coefficients in Table 5-8, the threshold of 1-MVA of EKF, UKF, and PF corresponding 10 m of the required RMSE is computed and listed in the 2nd, 3rd, and 4th columns in Table 5-9, respectively in step 2. Note that scenarios that have the same observation geometry (i.e., scenarios A and D) have an equal threshold value concerning one algorithm. The non-linearity of the observation model is measured by 1-MVA in the 5th column. Step 3 is to obtain potential algorithms listed in the 6th column by using the 1-MVA parameter, in which one algorithm is selected if its threshold of 1-MVA is higher than 1-MVA of the observation model. Finally, the optimal algorithm is chosen (the 7th column) based on the computational time parameter, in which the computational time of EKF is shortest, followed by UKF and PF, as analyzed in section 4.2.

Table 5-9. Determination of the optimal algorithm using 1-MVA and computational time parameters in the case of varying measurement uncertainties.

Scenarios (1)	Threshold value of 1-MVA			1-MVA (5)	Possible algorithms (6)	Optimal algorithm (7)
	EKF (2)	UKF (3)	PF (4)			
A	0.1853	0.2013	0.2112	0.1739	EKF, UKF, PF	EKF
B	0.1741	0.1944	0.2084	0.1860	UKF, PF	UKF
C	0.1644	0.1876	0.2058	0.1996	PF	PF
D	0.1853	0.2013	0.2112	0.2101	PF	PF
E	0.1741	0.1944	0.2084	0.2266	No*	No*
F	0.1644	0.1876	0.2058	0.2448	No*	No*

Note: no chosen algorithm indicates by asterisk (*).

Example 2: Changing only observation geometry

The relationship between 1-*MVA* and RMSE with varying only observation geometry in section 5.2.2 is used for this example. The coefficients of the fitting function are determined in certain measurement uncertainties of scenarios. According to a given scenario, these coefficients can be linearly interpolated from corresponding coefficients of two neighborhood scenarios. For example, according to scenario A ($\sigma_\alpha = 0.5^\circ$), its coefficients of the fitting function in the relationship between 1-*MVA* and RMSE of EKF can be derived from scenario 2 and scenario 3, which have $\sigma_\alpha = 0.4^\circ$ and $\sigma_\alpha = 0.6^\circ$, respectively, as shown in Table A6-1 of Appendix A6. The fitting function of scenario A is also linear, and its coefficients b_0 and b_1 determined by using (5-3) and (5-4) are 0.1312 and 0.0046, respectively. For other algorithms and scenarios, the fitting functions and their corresponding coefficients can be defined similarly and shown in Table 5-10.

Table 5-10. Coefficients of fitting functions in six scenarios due to varying observation geometries.

Scenarios	σ_α	EKF		UKF		PF	
		b_0	b_1	b_0	b_1	b_0	b_1
A, B, C	0.5°	0.1312	0.0046	0.1167	0.0073	0.1025	0.0109
D, E, F	0.7°	0.1491	0.0049	0.1313	0.0076	0.1189	0.0099

From the coefficients of fitting functions listed in Table 5-8, the corresponding values of the 1-*MVA* threshold of EKF, UKF, and PF for the above six scenarios are identified in step 2 of this procedure. The next steps are solved in the same manner, as shown in examples 1 and listed in Table 5-11.

Table 5-11. Determination of the optimal algorithm using 1-*MVA* and computational time parameters in the case of varying observation geometries.

Scenarios (1)	Threshold value of 1- <i>MVA</i>			1- <i>MVA</i> (5)	Possible algorithms (6)	Optimal algorithm (7)
	EKF (2)	UKF (3)	PF (4)			
A	0.1772	0.1897	0.2115	0.1739	EKF, UKF, PF	EKF
B	0.1772	0.1897	0.2115	0.1860	UKF, PF	UKF
C	0.1772	0.1897	0.2115	0.1996	PF	PF
D	0.1976	0.2068	0.2179	0.2101	PF	PF
E	0.1976	0.2068	0.2179	0.2266	No*	No*
F	0.1976	0.2068	0.2179	0.2448	No*	No*

Note: no chosen algorithm indicates by asterisk (*).

b. Variations of both influencing factors

The algorithm is selected based on the non-linear characteristic using the established relationship between 1-*MVA* and RMSE with changing both measurement uncertainty and observation geometry. The established relationship in the three ranges of these factors (see section 5.3.2) is applied for the three corresponding following examples.

Example 3: $[0.2^\circ, 2^\circ]$ for uncertainties and $[0.5 \text{ km}, 1.4 \text{ km}]$ for ranges

In this example, the established relationship between 1-*MVA* and RMSE with varying measurement uncertainty in the interval $[0.2^\circ, 2^\circ]$ and varying observation geometry in the distance interval $[0.5 \text{ km}, 1.4 \text{ km}]$ is applied. From the coefficients of fitting functions in Table 5-3, the threshold value of 1-*MVA* for three algorithms corresponding 10 m of the required RMSE can be computed and listed in the 2nd, 3rd, and 4th columns, respectively of Table 5-12. Note that the threshold values of 1-*MVA* for six scenarios

according to one algorithm are the same since the coefficients of fitting function are commonly used for these scenarios. Step 1 of the procedure of section 5.3.1 can also be ignored in this case. Then, the non-linearity of the observation model is measured by 1-*MVA* in the 5th column is compared to their corresponding threshold of three algorithms. An algorithm is selected when its 1-*MVA* threshold is larger than 1-*MVA* of the observation model and shown in the 6th column. Finally, the optimal algorithm is derived from chosen algorithms in the 6th column based on the computational time parameter and listed in the 7th column.

Table 5-12. Determination of the optimal algorithm using 1-*MVA* and computational time parameters in the case of changing both measurement uncertainties from 0.2° to 2° and the distances from 0.5 km to 1.4 km.

Scenarios (1)	Threshold value of 1- <i>MVA</i>			1- <i>MVA</i> (5)	Possible algorithms (6)	Optimal algorithm (7)
	EKF (2)	UKF (3)	PF (4)			
A	0.1985	0.2096	0.2169	0.1739	EKF, UKF, PF	EKF
B	0.1985	0.2096	0.2169	0.1860	EKF, UKF, PF	EKF
C	0.1985	0.2096	0.2169	0.1996	UKF, PF	UKF
D	0.1985	0.2096	0.2169	0.2101	PF	PF
E	0.1985	0.2096	0.2169	0.2266	No*	No*
F	0.1985	0.2096	0.2169	0.2448	No*	No*

Note: no chosen algorithm indicates by asterisk (*).

Example 4: [0.2° , 1°] for uncertainties and [0.5 km, 1.4 km] for ranges

The relationship between 1-*MVA* and RMSE established in section 5.2.3 is used for this example. In this relationship, measurement uncertainty is varied in the interval [0.2° , 1°] and observation geometry is altered in the distance interval [0.5 km, 1.4 km]. The optimal algorithms are chosen in the same way, as presented in example 3, and summarized in Table 5-13.

Table 5-13. Determination of the optimal algorithm using 1-*MVA* and computational time parameters in the case of changing both measurement uncertainties from 0.2° to 1° and the distances from 0.5 km to 1.4 km.

Scenarios (1)	Threshold value of 1- <i>MVA</i>			1- <i>MVA</i> (5)	Possible algorithms (6)	Optimal algorithm (7)
	EKF (2)	UKF (3)	PF (4)			
A	0.1777	0.1935	0.2108	0.1739	EKF, UKF, PF	EKF
B	0.1777	0.1935	0.2108	0.1860	UKF, PF	UKF
C	0.1777	0.1935	0.2108	0.1996	PF	PF
D	0.1777	0.1935	0.2108	0.2101	PF	PF
E	0.1777	0.1935	0.2108	0.2266	No*	No*
F	0.1777	0.1935	0.2108	0.2448	No*	No*

Note: no chosen algorithm indicates by asterisk (*).

Example 5: [0.2° , 1°] for uncertainties and [0.7 km, 1.1 km] for ranges

The relationship between 1-*MVA* and RMSE established in section 5.2.3 is used, in which measurement uncertainty is varied in the interval [0.2° , 1°] and observation geometry is altered in the distance interval [0.7 km, 1.1 km]. The optimal algorithms are chosen in the same manner, as example 4, and listed in Table 5-14.

Table 5-14. Determination of the optimal algorithm using 1-*MVA* and computational time parameters in the case of changing both measurement uncertainties from 0.2° to 1° and the distances from 0.7 km to 1.1 km.

Scenarios (1)	Threshold value of 1- <i>MVA</i>			1- <i>MVA</i> (5)	Possible algorithms (6)	Optimal algorithm (7)
	EKF (2)	UKF (3)	PF (4)			
A	0.1802	0.1971	0.2114	0.1739	EKF, UKF, PF	EKF
B	0.1802	0.1971	0.2114	0.1860	UKF, PF	UKF
C	0.1802	0.1971	0.2114	0.1996	PF	PF
D	0.1802	0.1971	0.2114	0.2101	PF	PF
E	0.1802	0.1971	0.2114	0.2266	No*	No*
F	0.1802	0.1971	0.2114	0.2448	No*	No*

Note: no chosen algorithm indicates by asterisk (*).

5.3.3 Assessments of the non-linear characteristic in choice of algorithms

This section aims to assess the ability of the non-linear characteristic in the choice of algorithms. The chosen algorithms using 1-*MVA* parameter in section 5.3.2 are compared to those using RMSE parameter. The RMSE is known as a primary parameter, as discussed in Chapter 4. In order to use RMSE parameter, the true trajectory of vessel in six above scenarios is assumed to be known. The selection of optimal algorithm using the RMSE parameter is described in Table 5-15. The 2nd, 3rd, and 4th columns are RMSEs of the vessel in all six scenarios estimated by EKF, UKF, and PF, respectively. The requirement of RMSE of the vessel is 10 m and written in the 5th column. An algorithm is chosen in the 6th column when its estimated RMSE is smaller than 10 m. Last, the 7th column shows the optimal algorithms in terms of computational time.

Table 5-15. Determination of the optimal algorithm using RMSE and computational time parameters.

Scenarios (1)	RMSE (m)			Required position RMSE (m) (5)	Possible algorithms (6)	Optimal algorithm (7)
	EKF (2)	UKF (3)	PF (4)			
A	8.379	7.593	6.785	10	EKF, UKF, PF	EKF
B	10.795	9.152	7.848	10	UKF, PF	UKF
C	13.833	10.988	8.884	10	PF	PF
D	11.921	10.374	9.326	10	PF	PF
E	15.174	12.475	10.954	10	No*	No*
F	19.045	14.890	12.811	10	No*	No*

Note: no chosen algorithm indicates by asterisk (*).

From the comparison of chosen algorithms between 1-*MVA* parameter and RMSE parameter based on numerical examples, a brief conclusion about the ability of non-linear characteristic for decision algorithms can be summarized as follows:

Regarding the relationship between 1-*MVA* and RMSE in case of varying only one influencing factor, the chosen algorithms in six scenarios using 1-*MVA* parameter, as illustrated in Table 5-8 and 5-10 of examples 1 and 2, and those using the RMSE parameter, as shown in Table 5-15, are exactly the same. Hence, the non-linear characteristic can be used for selecting algorithms in this case. The reason for this ability is that a strong above established relationships in case of varying only one influencing factor is applied.

Regarding the relationship between 1-*MVA* and RMSE in case of varying both influencing factors, the ability of the non-linear characteristic in choosing algorithms mainly depends not only on the interval of

influencing factors and but also on the strength of this relationship. For a relationship established in narrow intervals of these factors (see examples 3 and 4), chosen algorithms by using the 1-*MVA* parameter and RMSE parameter are the same. For a relationship built in large intervals of these factors (see example 5), however, the UKF and EKF, which are chosen in scenarios B and C, respectively, are not correct while PF is still correct in all scenarios. This is because the relationship between 1-*MVA* and RMSE of PF is stronger than those of UKF and EKF.

However, since the above relationship is built according to certain ranges of influencing factors, it leads to a limit on the application of the non-linear characteristic for choosing an optimal algorithm. Besides, the determination of an appropriated interval of factors in the establishment of the relationship between 1-*MVA* and RMSE, so that this relationship can meet the requirement of selecting the algorithms, was not investigated in this study.

5.4 Summary

This chapter presents non-linearity of the system and observation models measured by different indicators. A relationship between non-linearity and position accuracy is also established through a functional relation between $1-MVA$ and RMSE. Moreover, the use of the non-linear characteristic in the selection of filtering algorithms is investigated through numerical examples.

First, regarding the measure of non-linearity, three indicators, $1-R^2$, $1-MVA$, and M , are used to determine the non-linearity of models. Multiple indicators $1-MVA$ and M can provide a joint assessment of the non-linearity of multiple output variables. Conversely, the single indicator $1-R^2$ can measure the non-linearity of a single output variable and distinguish the non-linearity of one output variable compared to other ones. According to given parameters of scenarios, the non-linearity of the system model is small (< 0.05) due to a relatively small amount of process noise, and it is only influenced by velocity, data rate, and orientation change. In contrast, the non-linearity of the observation model is considerably high (i.e., $0.1 < 1-MVA < 0.6$) due to high uncertainty from given measurements of low-cost sensors. This investigation also indicates that the non-linearity of the observation model is importantly influenced by given large ranges of both measurement uncertainty and observation geometry.

Second, regarding the establishment of the relationship between $1-MVA$ and RMSE, this relationship is considered in two cases. In the first case, this relationship is established with varying only one influencing factor (measurement uncertainty or observation geometry). These results show that the $1-MVA$ linearly relates to the RMSE obtained by three algorithms in almost scenarios. This relationship is strong, which is measured by GOF values ($R^2 > 0.99$). In the second case, both influencing factors are varied simultaneously in different ranges in the establishment of this relationship. The linear function is still the best fitting function in modeling this relationship. There is no difference in the GOF values of these relationships between different ranges of factors. The GOF values of these relations are smaller than those in the case of varying only one factor. Besides, the quantity of this relationship mainly depends on the algorithms used, in which the relationship established for the PF is the strongest, followed by UKF and EKF, respectively.

Third, the non-linear characteristic is proposed for use in the case of a lack of information about the true trajectory, since the determination of non-linearity does not depend on this information. The ability to use the non-linear characteristic in the selection of filtering algorithms is assessed through numerical examples. These assessments suggest that the above-established relationship considered with varying one influencing factor of scenarios is adequate to decide for the optimal algorithm by non-linearity. In the case of both influencing factors varied simultaneously, the ability of the non-linear characteristic for the selection of algorithms depends on both the given range of these factors and the filtering algorithm used. Non-linearity is sufficient to choose the optimal algorithm when the above relationship is built in an appropriate range of these factors. According to the relationship established in a large range of these above factors, non-linearity can be utilized for this purpose if only this above relationship is adequately strong (i.e., the PF is correct in all cases). Indeed, non-linearity can replace accuracy as a characteristic for choosing algorithms in the case of lack of the true trajectory. Inversely, the non-linear characteristic cannot solve this issue when the relation between $1-MVA$ and RMSE is established in a relatively large range of the factor and this relationship is not sufficiently strong (i.e., the UKF and EKF are an incorrect choice in some cases). However, the determination of an appropriate range for influencing factors so that the relationship between $1-MVA$ and RMSE is sufficient for selecting algorithms was not investigated in this thesis. Moreover, since this relationship is identified for certain scenarios, the non-linear characteristic can only be applied for the limited scenarios. As a result, the non-linearity characteristic cannot become the global criterion for the selection of algorithms.

6. Conclusions

The main goal of the present study is to determine a potential parameter for selecting the optimal filtering algorithm when the true trajectory is not available. This issue is one of the most frequent occurring situations in reality. The study proposes the non-linearity as an alternative characteristic which is measured by the *1-MVA* parameter for solving this issue. This is because the non-linearity can be measured with known factors of scenarios but does not use any information about the true trajectory. The idea behind this approach is based on the hypothesis that if a relationship exists between the accuracy and non-linearity, the non-linearity can be used to replace for accuracy in the selection of algorithms. From analyses of the achieved algorithm's RMSE and *1-MVA* of the observation model, the relationship between these parameters is investigated. The contributions of this study can be summarized in three main respects: (1) Comparison of the performance among filtering algorithms; (2) measures of non-linearity of system and observation models; and (3) assessment of the ability to use the non-linear characteristic in the decision of filtering algorithms. These three aspects are discussed in the following.

First, regarding the comparison of performance among filtering algorithms in terms of both accuracy and computational time, the PF can cope well with high non-linear problems. In addition, the PF can reduce the negative impact of poor observation geometry or a small number of measurements. However, the budget of computational time of the PF presents a challenge in real-time applications. For this reason, the PF should only be used in cases of severe non-linearity. Inversely, the EKF is efficient for the requirement of accuracy according to low uncertainty (or weak non-linearity) with a short computational time. This algorithm is effective for data processing with a huge number of observations collected from multiple radars. Moreover, although the UKF can achieve a considerable improvement in performance over EKF, this algorithm does only require a little more computational time. This indicates that UKF is a promising algorithm in practical applications. Both EKF and UKF become less effective when the scenarios become more non-linear (i.e., in the case of high measurement uncertainty).

Second, an investigation of the non-linearity of both the system and observation models is performed. For the system model, the non-linearity of this model is small (< 0.05) and slightly affected by three factors: data rate, velocity of the moving object, and orientation change. This characteristic of the system model is due to the small amount of standard deviation of disturbance quantities in the assumption. In contrast, the non-linearity of the observation model is considerably high (approximately from 0.1 to 0.6), according to the given parameters of the scenario in the case of using low-cost sensors. This value is also remarkably influenced by the two factors of measurement uncertainty and observation geometry. The results indicate that the non-linearity of the observation model is approximately from two to ten times larger than that of the system model in the case of high measurement uncertainty or poor observation geometry.

Third, the main finding of this study is the relationship between position accuracy and the non-linearity of the observation model. The establishment of this relationship is conducted in two cases: changing only one influencing factor and changing both influencing factors together. When only one factor (measurement uncertainty or observation geometry) is changed, the GOF values of the three algorithms are larger than 0.99, which means that the relationships between *1-MVA* and RMSE are strong. The GOF values are smaller when both measurement uncertainty and observation geometry are varied simultaneously in their different ranges. In this case, the GOF values, calculated by the PF algorithm, are the biggest followed by UKF and EKF, respectively. As a result, if only one influencing factor is varied, the non-linearity, determined by the *1-MVA* parameter, can be used as a characteristic to choose algorithms. In the case of changing both influencing factors, the ability of this characteristic depends not only on the range of their factors but also on the quantity of the relationship measured by the GOF value. For a suitable range of these factors, non-linearity is sufficient to choose algorithms. Conversely, for a relatively large range of these factors, this characteristic can only be applied when the above-mentioned

relationship is sufficiently strong. However, it can lead to incorrect results in the choice of algorithms when this relationship is not adequately strong.

Several potential limitations of this study should be noted. First, the alternative characteristic developed for choosing algorithms is the non-linearity of the observation model. This characteristic, however, is only suitable according to scenarios, in which the non-linearity of the observation model is considerably higher than that of the system model. Therefore, the non-linearity of the observation model cannot be used as a characteristic for any scenario. Second, this relationship is established for certain ranges of scenarios' factors. Consequently, use of the *1-MVA* parameter replacing the RMSE parameter is limited in these ranges of the established relationship. Third, GOF values and the limitation in ranges of both measurement uncertainty and observation geometry were not investigated in this thesis. Fourth, other factors of scenarios that could affect this relationship are not considered in this study. Last, the non-linearity parameter examined in this study is *I-MVA*. Although this indicator can deal with multiple outputs of both system and observation models, it can only work properly with the Gaussian distribution of both process noise and measurement noise.

In future work, first, for determination of the relationship between *1-MVA* and RMSE, a suitable GOF values and the limited range of scenario's factors should be considered such that this relationship is a guarantee to select an algorithm. Besides, other potential characteristics for the selection algorithm should be examined in subsequent research. The geometry is considered a promising characteristic for this purpose since it has a direct effect on the accuracy.

References

- Alkhatib, H. and Kutterer, H. (2013). Estimation of Measurement Uncertainty of kinematic TLS Observation Process by means of Monte-Carlo Method. *Applied Geodesy* 7: 125-133.
- Alkhatib, H.; Neumann, I.; Neuner, H. and Kutterer, H. (2008). Comparison of Sequential Monte Carlo Filtering with Kalman Filtering for Nonlinear State Estimation. 1st International Conference on Machine Control and Guidance. Zurich, Switzerland.
- Allgöwer, F. (1995). Definition and Computation of a Nonlinearity Measure. IFAC Symposium on Nonlinear Control Systems Design. Taheo City, California, USA.
- Anderson, T. W. (2003). An Introduction to Multivariate Statistical Analysis. John Wiley & Sons, Inc. Hoboken, New Jersey, USA.
- Atkinson, K. (1989). An Introduction to Numerical Analysis. John Wiley & Sons, Inc, Québec, Canada.
- Aussems, T. (1999). Positionsschätzung von Landfahrzeugen mittels Kalman-Filterung aus Satelliten- und Koppelnavigationsbeobachtungen. Veröffentlichung des Geodätischen Instituts der Rheinisch-Westfälischen Technischen Hochschule Aachen Nr. 55.
- Bar-Shalom, Y. (1990). Multitarget-Multisensor Tracking: Advanced Applications. Artech House, Norwood, Mass., Boston.
- Bar-Shalom, Y.; Li, X. R. and Kirubarajan, T. (2001). Estimation with Application to Tracking and Navigation. John Wiley & Sons, Inc., New York.
- Bates, D. M. and Watts, D. G. (1980). Relative Curvature Measures of Nonlinearity. *Journal of the Royal Statistical Society. Series B (Methodological)* 42(1): 1-25.
- Beale, E. M. L. (1960). Confidence Regions in Non-linear Estimation. *Journal of the Royal Statistical Society. Series B (Methodological)* 22(1): 41-88.
- Beddar-Wiesing, S. and Bieshaar, M. (2020). Multi-Sensor Data and Knowledge Fusion: A Proposal for a Terminology Definition. arXiv preprint arXiv:2001.04171, 2020.
- Berg, J. C. and Miller, K. (2010). Force Estimation via Kalman Filtering for Wind Turbine Blade Control. Proceeding of the IMAX-XXVIII, Jacksonville, Florida, USA.
- Bole, A.; Dineley, B. and Wall, A. (2005). RADAR and ARPA manual. Elsevier Butterworth-Heinemann, Linacre House, Jordan Hill, Oxford OX2 8DP.
- Borga, M. (1998). Learning Multidimensional Signal Processing, Linköping University, Sweden, SE-581 83 Linköping, Sweden. Ph.D. thesis.
- Buslenko, N. P.; Golenko, D. I.; Sobol, I. M. and Sragovich, V. G. (1966). The Monte Carlo Method. Pergamon Press, Oxford/London/Edinburgh/New York/Paris/Frankfurt.
- Choudhury, M. A. A. S.; Shah, S. L. and Thornhill, N. F. (2008). Diagnosis of Process Nonlinearities and Valve Stiction. Springer, Springer-Verlag Berlin Heidelberg.
- Cramer, E. M. (1974). A Generalization of Vector Correlation and its Relation to Canonical Correlation. *Multivariate Behavioral Research* 9: 347-352.
- Cramer, E. M. and Nicewander, W. A. (1979). Some Symmetric, Invariant Measures of Multivariate Association. *Psychometrika* 44: 43-54.
- Cramer, H. (1946). *Mathematical Method of Statistics*. Princeton University Press, Princeton, New Jersey.
- Curry, G. R. (2005). Radar System Performance Modeling. Artech house, Boston, London.
- Desoer, C. A. and Wang, Y. T. (1980). Foundations of Feedback Theory for Nonlinear Dynamical Systems. *IEEE Trans. Circuits Syst.*, 27(2): 104-123.
- Doucet, A.; Freitas, N. d. and Gordon, N. (2001). *Sequential Monte Carlo Methods in Practice*. Springer-Verlag, New York.
- Dunik, J.; Straka, O. and Garcia-Fernandez, A. F. (2017). Performance Evaluation of Nonlinearity and Non-Gaussianity Measures in State Estimation. 20th International Conference on Information Fusion. Xi'an, China.
- Dunik, J.; Straka, O. and Simandl, M. (2013). Nonlinearity and Non-Gaussianity Measures for Stochastic Dynamic Systems. Proceedings of the 16th Inter. Conference on Information Fusion, Istanbul.

- Efron, B. (1979). Bootstrap Method: Another look at the Jackknife. *The annals of Statistics* 7(1): 1-26.
- Eichhorn, A. (2005). Ein Beitrag zur Identifikation von dynamischen Strukturmodellen mit Methoden der adaptiven KALMAN-Filterung. Institut für Anwendungen der Geodäsie im Bauwesen, Universität Stuttgart. Ph.D. thesis, Deutsche Geodätische Kommission (DGK), München, Reihe C, Heft-Nr. 585.
- Elvira, V.; Miguez, J. and Djuric, P. M. (2017). Adapting the Number of Particles in Sequential Monte Carlo Methods through an Online Scheme for Convergence Assessment. *IEEE Transactions on Signal Processing* 65(7): 1781-1794.
- Fredrik, G. (2010). Particle Filter Theory and Practice with Positioning Applications. *IEEE A & E Systems magazine* 25(7): 53-81.
- Garcia, J.; Guerrero, J. L.; Luis, A. and Molina, J. M. (2010). Robust Sensor Fusion in Real Maritime Surveillance Scenarios. 13th International Conference on Information Fusion. Edinburgh, UK, IEEE.
- Gelb, A. (1979). Applied Optimal Estimation. The M.I.T press, Massachusetts, USA.
- Gordon, N. J.; Salmond, D. J. and Smith, A. F. M. (1993). Novel Approach to Nonlinear/non-Gaussian Bayesian State Estimation. *IEEE Proceedings F, Radar and Signal Processing*.
- Hammersley, J. M. and Morton, K. W. (1954). Poor man's Monte Carlo. *Journal of the Royal Statistical Society, Series B (Statistical Methodology)* 16: 23-38.
- Heidger, R.; Klenner, T. and Mallwitz, R. (2004). The PHOENIX Multi-radar Tracker System for Air Traffic Control Applications. *Air traffic control Quarterly* 12(3): 193-222.
- Helbig, A.; Marquardt, W. and Allgöwer, F. (2000). Nonlinearity Measures: Definition, Computation and Applications. *Journal of Process Control* 10: 113-123.
- Helton, J. C. and Davis, F. J. (2000). Sensitivity analysis. Sampling-based Methods: In: Saltelli, A.; Chan, K.; Scott, E.M. 4th. John Wiley and Sons, Chichester.
- Helton, J. C. and Davis, F. J. (2003). Latin Hypercube Sampling and the Propagation of Uncertainty in Analyses of Complex Systems. *Reliability Engineering and System Safety* 81: 23-69
- Heunecke, O. (1995). Zur Identifikation und Verifikation von Deformationsprozessen mittels adaptiver Kalman-Filterung (Hannoversches Filter). *Wissenschaftliche Arbeiten der Fachrichtung Vermessungswesen der Universität Hannover* (208).
- Hol, J. D.; Schön, T. B. and Gustafsson, F. (2006). On Resampling Algorithms for Particle Filters. 2006 IEEE Nonlinear Statistical Signal Processing Workshop. Cambridge: 79-82.
- Hosseini, S. M.; Johansen, T. A. and Fatehi, A. (2011). Comparison of Nonlinearity Measures based on Time Series Analysis for Nonlinearity Detection. *Modeling, Identification and Control* 32(4): 123-140.
- Hotelling, H. (1936). Relations between Two Sets of Variates. *Biometrika* 28: 321-377.
- Isard, M. and Blake, A. (1998). Condensation-conditional Density Propagation for Visual Tracking. *International Journal of Computer Vision* 29(1): 5-28.
- Julier, S. J. and Uhlmann, J. K. (1997). A New Extension of the Kalman Filter to Nonlinear Systems. *Signal Processing, Sensor Fusion, and Target Recognition VI, AeroSense '97, 1997, Orlando, FL, United States*.
- Julier, S. J. and Uhlmann, J. K. (1997). A New Extension of the Kalman Filter to Nonlinear Systems. *Proceedings Volume 3068, Signal Processing, Sensor Fusion, and Target Recognition VI, AeroSense '97, 1997, Orlando, FL, United States*.
- Julier, S. J. and Uhlmann, J. K. (2004). Unscented Filtering and Nonlinear Estimation. *Proceedings of the IEEE, IEEE*.
- Julier, S. J.; Uhlmann, J. K. and Durrant-Whyte, H. F. (1995). A New Approach for Filtering Nonlinear Systems. *Proceedings of the American Control Conference, Seattle, Washington, USA*.
- Kalman, R. E. (1960). A New Approach to Linear Filtering and Prediction Problems. *Basic Engineering* 82(1): 35-45.
- Karlsson, R.; Schön, T. and Gustafsson, F. (2005). Complexity Analysis of the Marginalized Particle Filter. *IEEE Transactions on Signal Processing* 53(11): 4408-4411.
- Khameneh, M. A. A. (2015). On Optimisation and Design of Geodetic networks. Department of Urban Planning and Environment. Stockholm, Sweden, Royal Institute of Technology. Doctor.

- Konatowski, S.; Kaniewski, P. and Matuszewski, J. (2016). Comparison of Estimation Accuracy of EKF, UKF and PF filters. *Annual of navigation* 23(1): 69-87.
- Kroll, M. H. and Emancipator, K. (1993). A Theoretical Evaluation of Linearity. *Clinical Chemistry* 39(3): 405-413.
- Li, G.; Yi, W.; Jiang, M. and Kong, L. (2017). Distributed Fusion with PHD Filter for Multi-Target Tracking in Asynchronous Radar System. *IEEE Radar Conference*. May, 2017.
- Li, X. R. (2012). Measure of Nonlinearity for Stochastic Systems. *Proceedings of the 15th International Conference on Information fusion*, Singapore.
- Li, X. R. and Jilkov, V. P. (2005). Survey of Maneuvering Target Tracking. part V: Multiple Model Methods. *IEEE Transactions On Aerospace and Electronics Systems* 41(4).
- Liu, Y. and Li, X. R. (2015). Measure of Nonlinearity for Estimation. *IEEE Transactions on Signal Processing* 63(9): 2377-2388.
- Madrigal, J. A. F. and Claraco, J. L. B. (2013). Simultaneous Localization and Mapping for Mobile Robots: Introduction and Methods. *Information Science Reference* (an imprint of IGI Global), USA.
- Mallick, M. (2004). Differential Geometry Measures of Nonlinearity with Applications to Ground Target Tracking. In *Proceedings of the 7th International Conference on Information Fusion*, Stockholm, Sweden.
- Mallick, M.; Bar-Shalom, Y.; Kirubarajan, T. and Morelan, M. (2015). An Improved Single-Point Track Initiation using GMTI Measurements. *IEEE Transactions on Aerospace and Electronic Systems* 51(4): 2697-2714.
- Mallick, M. and Ristic, b. (2017). Comparison of Measures of Nonlinearity for Bearing-only and GMTI Filtering. *20th International Conference on Information Fusion*. Xi'an, China July 10-13, 2017.
- Mallick, M.; Scala, B. F. L. and Arulampalam, M. S. (2005). Differential Geometry Measures of Nonlinearity for the Bearing-only Tracking Problem. In *Proceeding of SPIE Signal Processing, Sensor Fusion, and Target Recognition XIV*, Bellingham, WA, USA.
- Mendel, J. M. (1971). Computational Requirements for a Discrete Kalman Filter. *IEEE Transactions on Automatic control* ac-16(6): 748-758.
- Niu, R.; Varshney, P. K.; Alford, M.; Bubalo, A.; Jones, E. and Scalzo, M. (2008). Curvature Nonlinearity Measure and Filter Divergence Detector for Nonlinear Tracking Problems. *11th International Conference on Information Fusion*, Cologne, Germany, IEEE.
- O'Brien, T.; Jamroenpinyo, S. and Bumrungrsup, C. (2010). Curvature Measures for Nonlinear Regression Models Using Continuous Designs with Applications to Optimal Experimental Design. *A Journal of mathematics* 3(3): 317-333.
- Pham, D. and Schwieger, V. (2016). Comparison of Filtering Algorithms in Vehicle Positioning by Using Low-Cost Sensors. *5th International Conference on Machine Control & Guidance*. Vichy, France.
- Pitt, M. K. and Shephard, N. (1999). Filtering via Simulation: Auxiliary Particle Filters. *Journal of American Statistical Association* 94(446): 590-599.
- Ramm, K. (2008). Evaluation von Filter-Ansätzen für die Positionsschätzung von Fahrzeugen mit den Werkzeugen der Sensitivitätsanalyse. Institut für Anwendungen der Geodäsie im Bauwesen, Stuttgart. Ph. D. thesis, Deutsche Geodätische Kommission (DGK), München, Reihe C, Heft-Nr. 619.
- Ristic, B.; Arulampalam, S. and Gordon, N. (2004). *Beyond the Kalman Filter*. Artech House, Boston, London.
- Robert, C. P. and Casella, G. (2004). *Monte Carlo Statistical Methods*. Springer-Verlag, Berlin, Heidelberg.
- Robert, P. and Escoufier, Y. (1976). A Unifying Tool for Linear Multivariate Statistical Methods: The RV-Coefficient. *Application Statist* 25(3): 257.
- Rozeboom, W. W. (1965). Linear Correlations between Sets of Variables. *Psychometrika* 30(1): 57-71.
- Samsuri, S. B.; Zamzuri, H.; Rahman, M. A. A.; Mazlan, S. A. and Rahman, A. H. A. (2015). Computational Cost Analysis of Extended Kalman Filter in Simultaneous Localization and Mapping (EKF-SLAM) Problem for Autoumous Vehicle. *ARPN Journal of Engineering and Applied Sciences* 10(17): 7764-7768.

- Särkkä, S. (2013). *Bayesian Filtering and Smoothing*. Cambridge University Press.
- Scala, B. F. L.; Mallick, M. and Arulampalam, S. (2007). Differential Geometry Measures of Nonlinearity for Filtering with Nonlinear Dynamic and Linear Measurement Models. In *Proceedings of SPIE Signal and Data Processing of Small Targets*, San Diego, CA, USA.
- Schweitzer, J. (2012). Modular Positioning using Different Motion Models. 3rd International Conference on Machine Control & Guidance. Stuttgart, Germany.
- Schwieger, V. (2005). Nicht-lineare Sensitivitätsanalyse gezeigt an Beispielen zu bewegten Objekten. Habilitation, Deutsche Geodätische Kommission (DGK), München, Reihe C, Heft-Nr. 581.
- Serlin, R. C. (1982). A Multivariate Measure of Association Based on the Pillai-Bartlett Procedure. *Psychological Bulletin* 91(2): 413-417.
- Swierczynski, S. and Czaplewski, K. (2015). Determining the Accuracy of Ship Position as a Function of Radar Bearing. International Association of Institutes of Navigation World Congress (IAIN 2015), Prague, Czech Republic.
- Teunissen and Montenbruck (2017). *Springer Handbook of Global Navigation Satellite Systems*. Springer Nature, Cham, Switzerland.
- Vaispacher, T.; Andoga, R.; Bréda, R. and Jr, F. A. (2015). Application of Linearized Kalman Filter in Integration of Navigation Systems. 16th IEEE International Symposium on Computational Intelligence and Informatics. Budapest, Hungary.
- Vanicek, P. and Krakiwsky, E. J. (1986). *Geodesy: The concepts*. Elsevier science publishers.
- Verlaan, M. and Heemink, A. W. (2000). Nonlinearity in Data Assimilation Applications: A Practical Method for Analysis. *Monthly Weather Review* 129: 1578–1589.
- Veth, M. J. (2013). Nonlinear Estimation Techniques for Navigation. *Navigation Sensors and Systems in GNSS Degraded and Denied Environments*, NATO STO lecture series SET-197.
- Wan, E. A. and van der Merwe, R. (2000). The Unscented Kalman Filter for Nonlinear Estimation. *Proceedings of the IEEE 2000 Adaptive Systems for Signal Processing, Communications, and Control Symposium*, Lake Louise, Alberta, Canada, IEEE.
- Wang, P.; Blasch, E.; Li, X. R.; Jones, E.; Hanak, R.; Yin, W.; Beach, A. and Brewer, P. (2016). Degree of Nonlinearity (DoN) Measure for Target Tracking in Videos. 19th International Conference on Information Fusion. Heidelberg, Germany.
- Wang, X.; Li, T.; Sun, S. and Corchado, J. M. (2017). A Survey of Recent Advances in Particle Filters and Remaining Challenges for Multitarget Tracking. *sensors* 17(12): 21.
- Weintrit, A. and Neumann, T. (2019). *Advances in Marine Navigation and Safety of Sea Transportation*. CRC Press, Netherlands.
- Weisberg, S. (2005). *Applied Linear Regression*. John Wiley & Sons, New Jersey.
- Wen, H.; Xiao, Z.; Markham, A. and Trigoni, N. (2014). Accuracy Estimation for Sensor Systems. *IEEE Transactions on Mobile Computing* 14(7): 1330 - 1343.
- Wolff, C. (1998). "Radar basics." from <http://www.radartutorial.eu/index.en.html>, Last access: 18.06.2019.
- Yanai, H. (1974). Unification of Various Techniques of Multivariate Analysis by Means of Generalized Coefficient of Determination. *Japanese Journal of Behaviormetrics I*: 46-54.

Appendix A1: Accuracy of measurements of bearing and range radars

Table A1. Accuracy of bearing angle and distance measurements of radars (Wolff 1998) and (Weintrit and Neumann 2019).

Radar unit	Accuracy in bearing	Accuracy in range
BOR-A 500	$< \pm 0.3^\circ$	< 20 m
Lanza	$< \pm 0.14^\circ$	< 50 m
GM 400	$< \pm 0.3^\circ$	< 50 m
RRP-117	$< \pm 0.18^\circ$	< 463 m
MSSR-2000	$< \pm 0.049^\circ$	< 44.4 m
STAR-2000	$< \pm 0.16^\circ$	< 60 m
Variant	$< \pm 0.25^\circ$	< 25 m
Radio direction finder	$\pm 3^\circ$ to $\pm 10^\circ$	93 m -310 m
Radar bearing	$\pm 1^\circ$	32 m
Radar distance measurement		30 m
LORAN-C/CHAYKA		
eLORAN		8-10 m

Appendix A2: Influence of the number of measurements on position accuracy

The scenario of two bearing angles in section 4.1.1 is also used for this evaluation, but the location of the second bearing and range radars is changed in Fig. A2-1. The shortest range between radars and the object is approximately 0.8 km, and the intersection angle is approximately 60° .

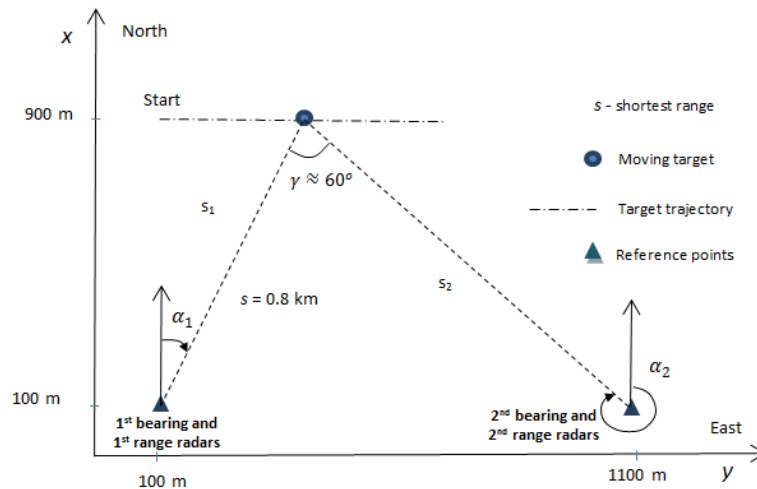


Fig. A2-1. The geometric configuration of radar measurements in the case of 60° intersection angle.

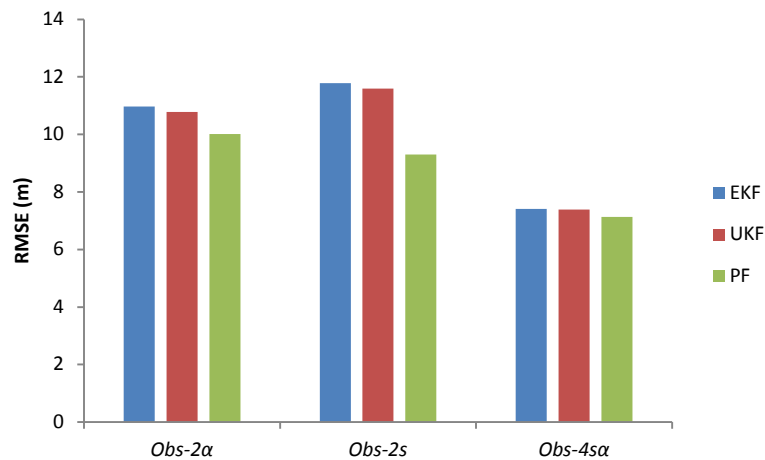


Fig. A2-2. RMSEs of EKF, UKF, and PF in three cases of radar measurements. In *Obs-4s α* , the RMSEs of these algorithms decrease approximately 1.5 times compared to *Obs-2 α* and *Obs-2s*.

Appendix A3: Optimal number of MC runs for determining non-linearity

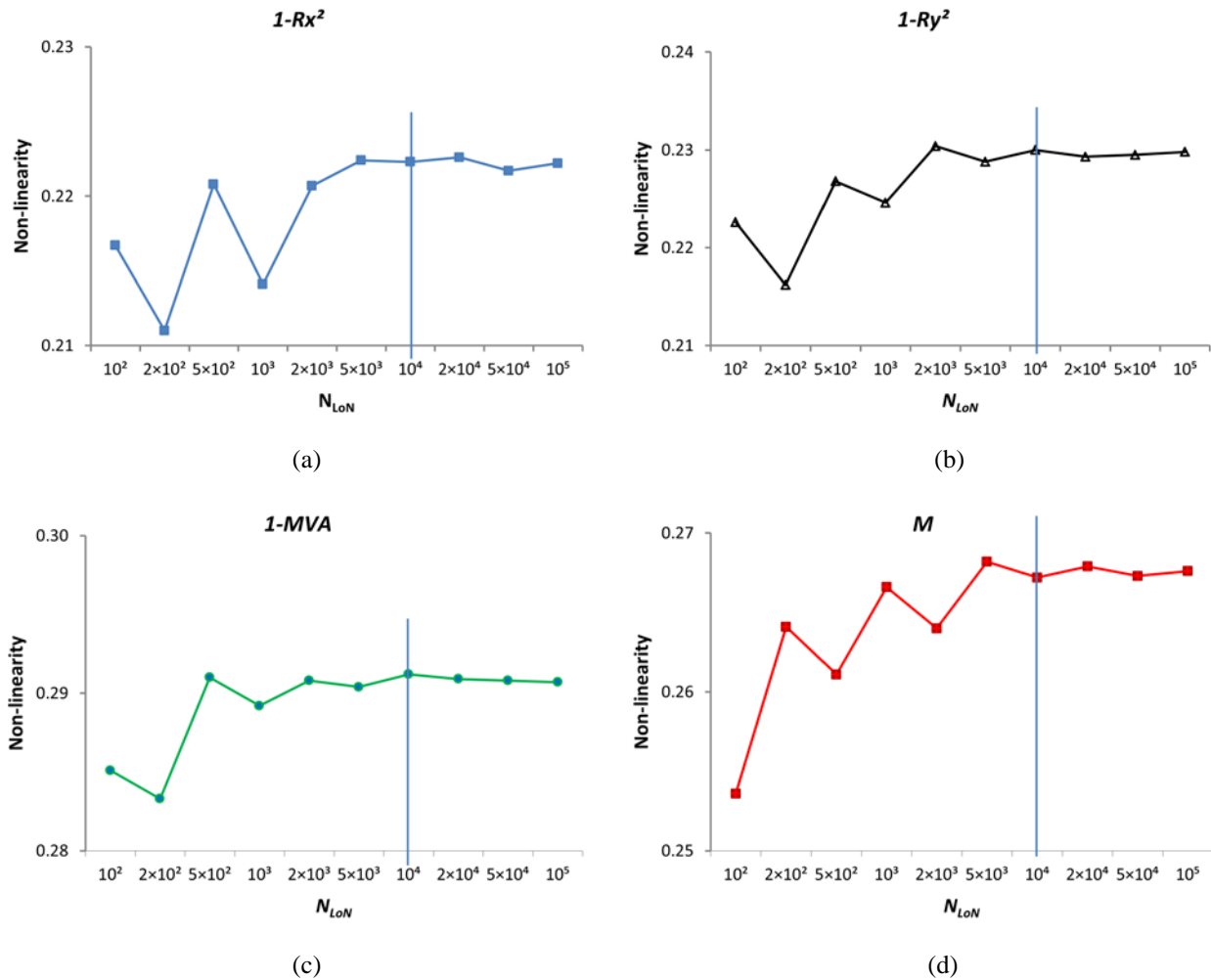


Fig. A3-1. Measures of non-linearity of observation model with varying number of MC runs, N_{LoN} by three indicators $1-R^2$ (a and b), $1-MVA$ (c), and M (d).

The purpose of this part is to determine the optimal number of MC runs in the quantification of non-linearity. Non-linearity is evaluated with varying the number of MC runs in the interval $[10^2, 10^5]$. The scenario of two bearing angles in section 4.1.1 is also used for this evaluation. The non-linearity of the observation model determined by $1-R^2$, $1-MVA$, and M changes dramatically with an inadequate number of MC runs ($N_{LoN} < 10^4$) and stable with a sufficiently large number of MC runs ($N_{LoN} \geq 10^4$). Therefore, $N_{LoN} = 10^4$ is considered as an optimal value of MC runs in the determination of non-linearity in this evaluation.

Appendix A4: Non-linearity of the system model with varying the data rate, velocity, and orientation change

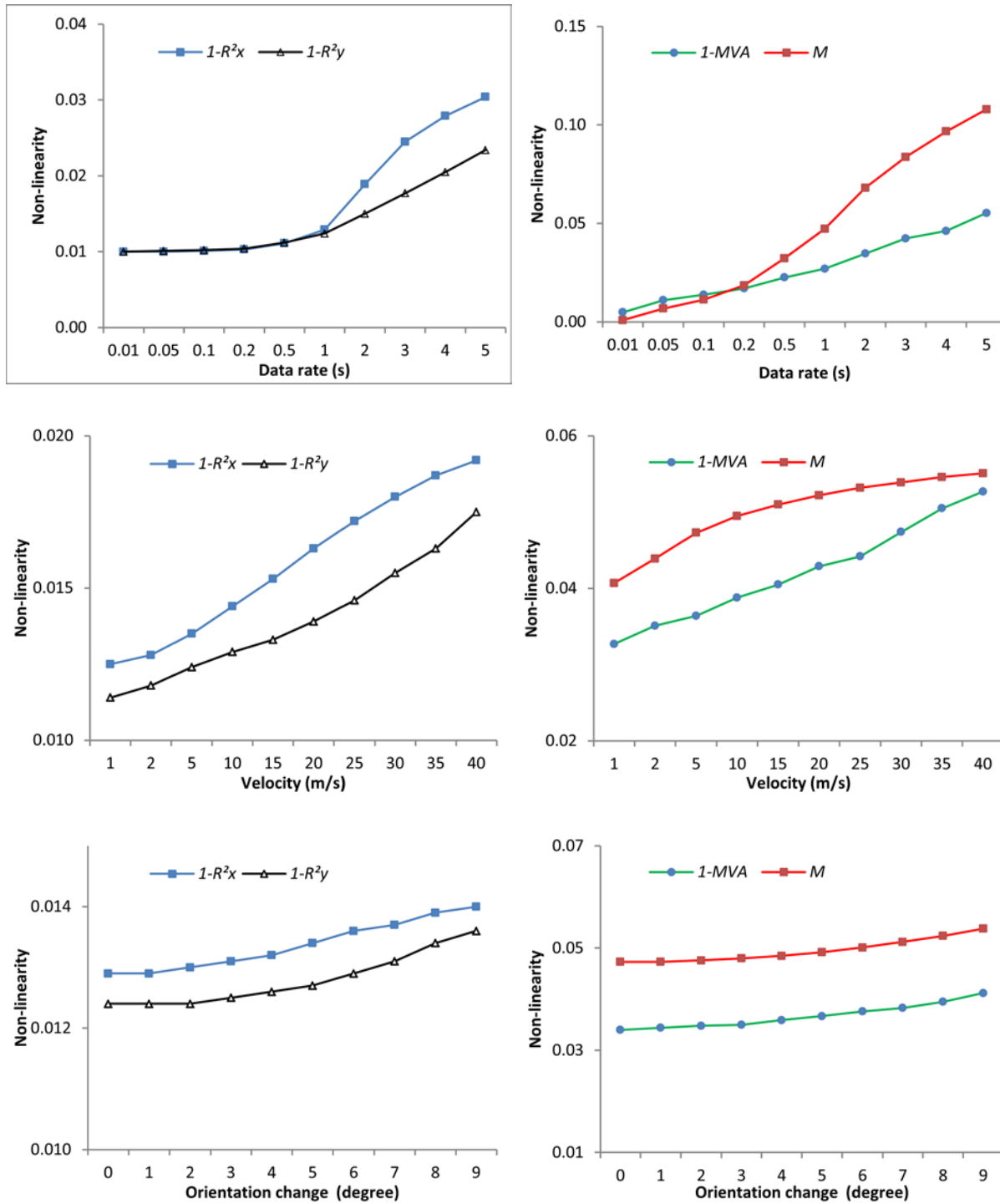


Fig. A4-1. Non-linearity of the system model determined by the change of factors, including data rate, velocity, and orientation change when STDs of acceleration and rotational rate are given at 0.04 m/s^2 and 0.04 rad/s^2 , respectively. Note that the non-linearity values in the vertical axis of these graphs are at a different scale.

Appendix A5: Determination of the coefficients of fitting function and their GOFs for different measurement uncertainties

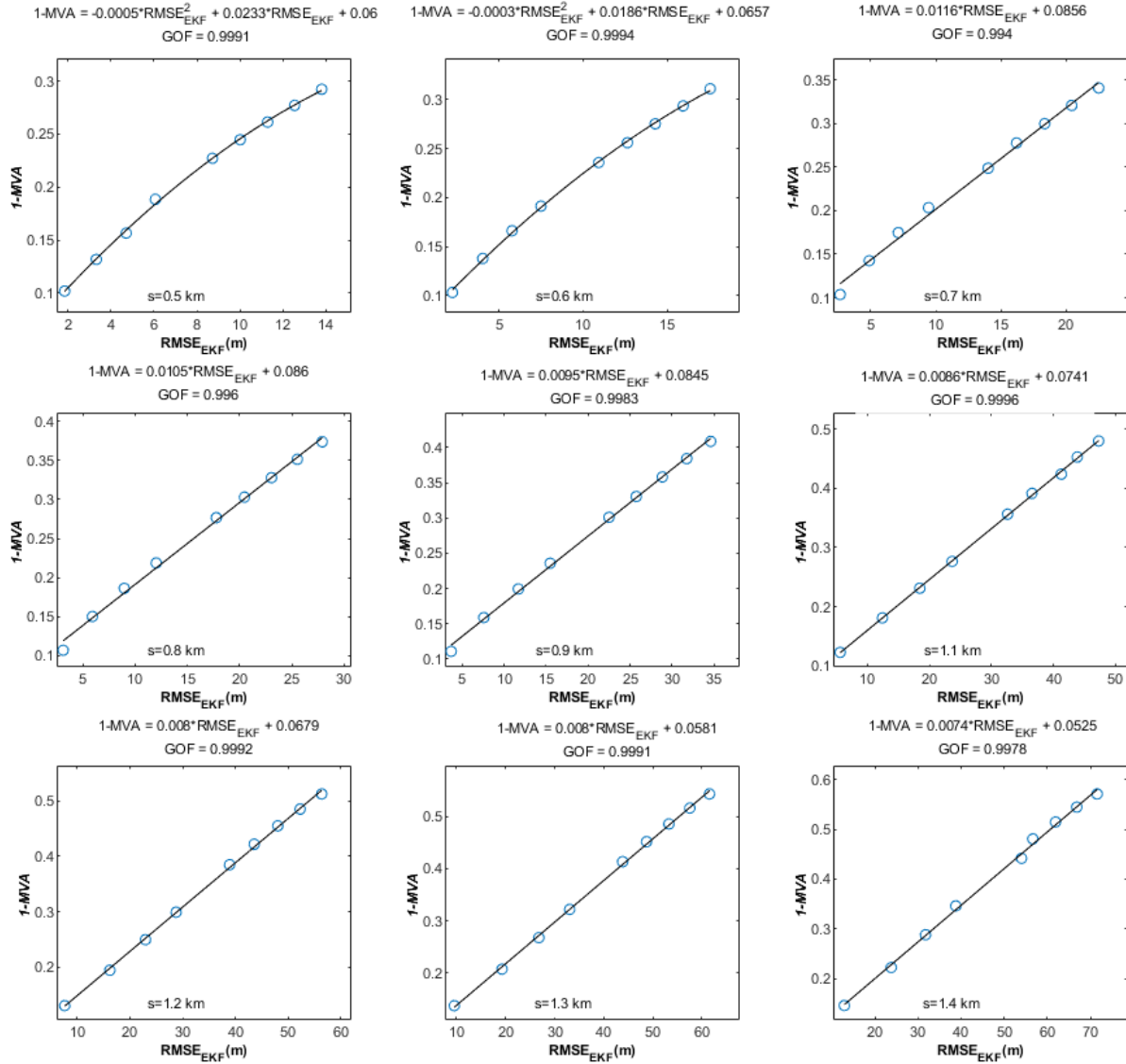


Fig. A5-1. Scatterplot of the relationship between 1-MVA and RMSE of EKF in different measurement uncertainties.

Table A5-1. Coefficients of the fitting function and their GOFs in different measurement uncertainties according to EKF.

Scenarios	s (km)	Fitting function			GOF	Scenarios	s (km)	Fitting function			GOF
		b_0	b_1	b_2				b_0	b_1	b_2	
1	0.5	0.0600	0.0233	-0.0005	0.9991	6	1.0	0.0807	0.0088	0.9995	
2	0.6	0.0657	0.0186	-0.0003	0.9994	7	1.1	0.0741	0.0086	0.9996	
3	0.7	0.0856	0.0116		0.9940	8	1.2	0.0679	0.0080	0.9992	
4	0.8	0.0860	0.0105		0.9960	9	1.3	0.0581	0.0080	0.9991	
5	0.9	0.0845	0.0095		0.9983	10	1.4	0.0525	0.0074	0.9978	

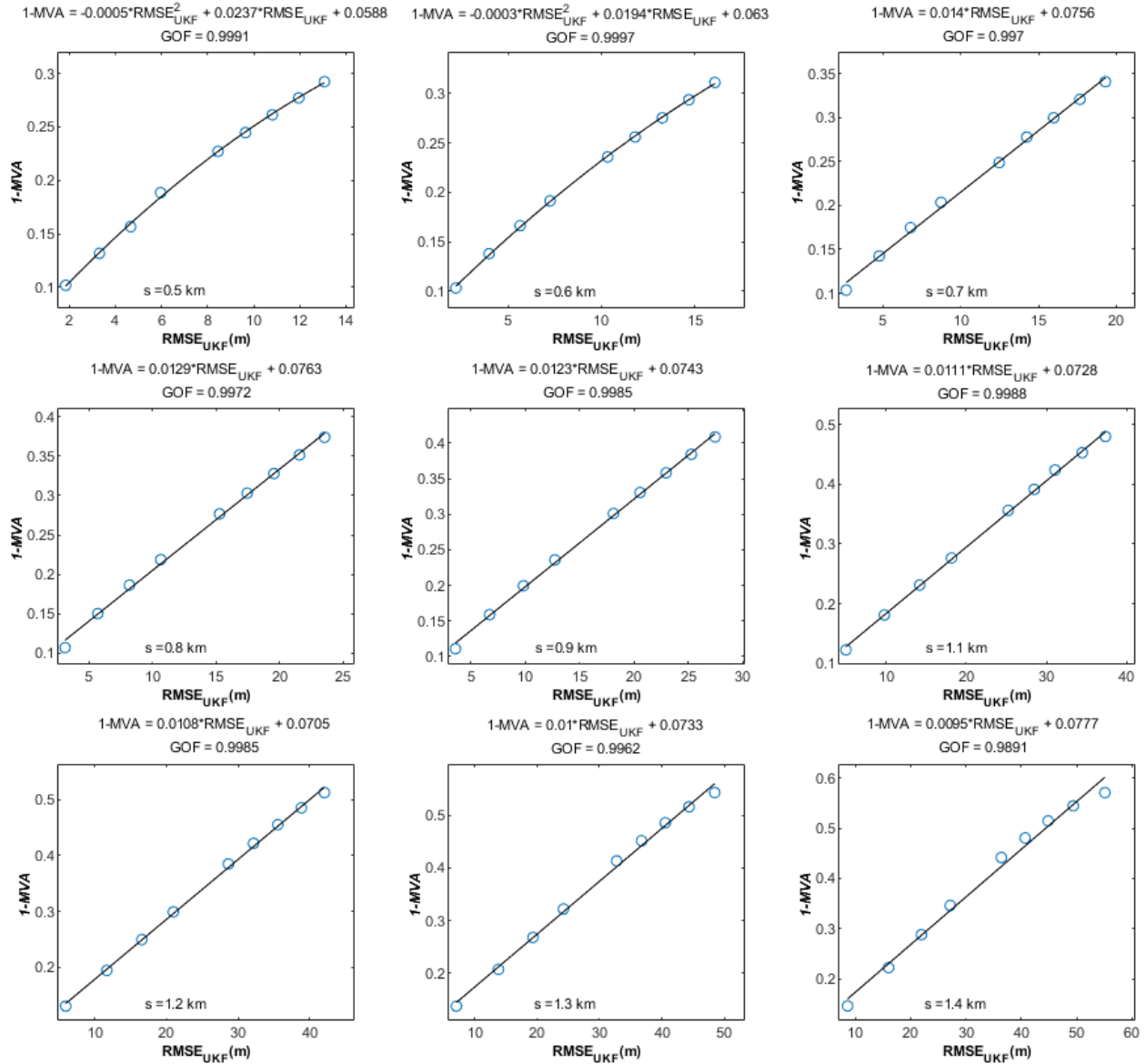


Fig. A5-2. Scatterplot of the relationship between 1-MVA and RMSE of UKF in different measurement uncertainties.

Table A5-2. Coefficients of the fitting function and their GOFs in different measurement uncertainties according to UKF.

Scenarios	s (km)	Fitting function			GOF	Scenarios	s (km)	Fitting function			GOF
		b_0	b_1	b_2				b_0	b_1	b_2	
1	0.5	0.0588	0.0237	-0.0005	0.9991	6	1.0	0.0734	0.0118	0.9990	
2	0.6	0.0630	0.0194	-0.0003	0.9997	7	1.1	0.0728	0.0111	0.9988	
3	0.7	0.0756	0.0140		0.9970	8	1.2	0.0705	0.0108	0.9985	
4	0.8	0.0763	0.0129		0.9972	9	1.3	0.0733	0.0100	0.9962	
5	0.9	0.0743	0.0123		0.9985	10	1.4	0.0777	0.0095	0.9891	

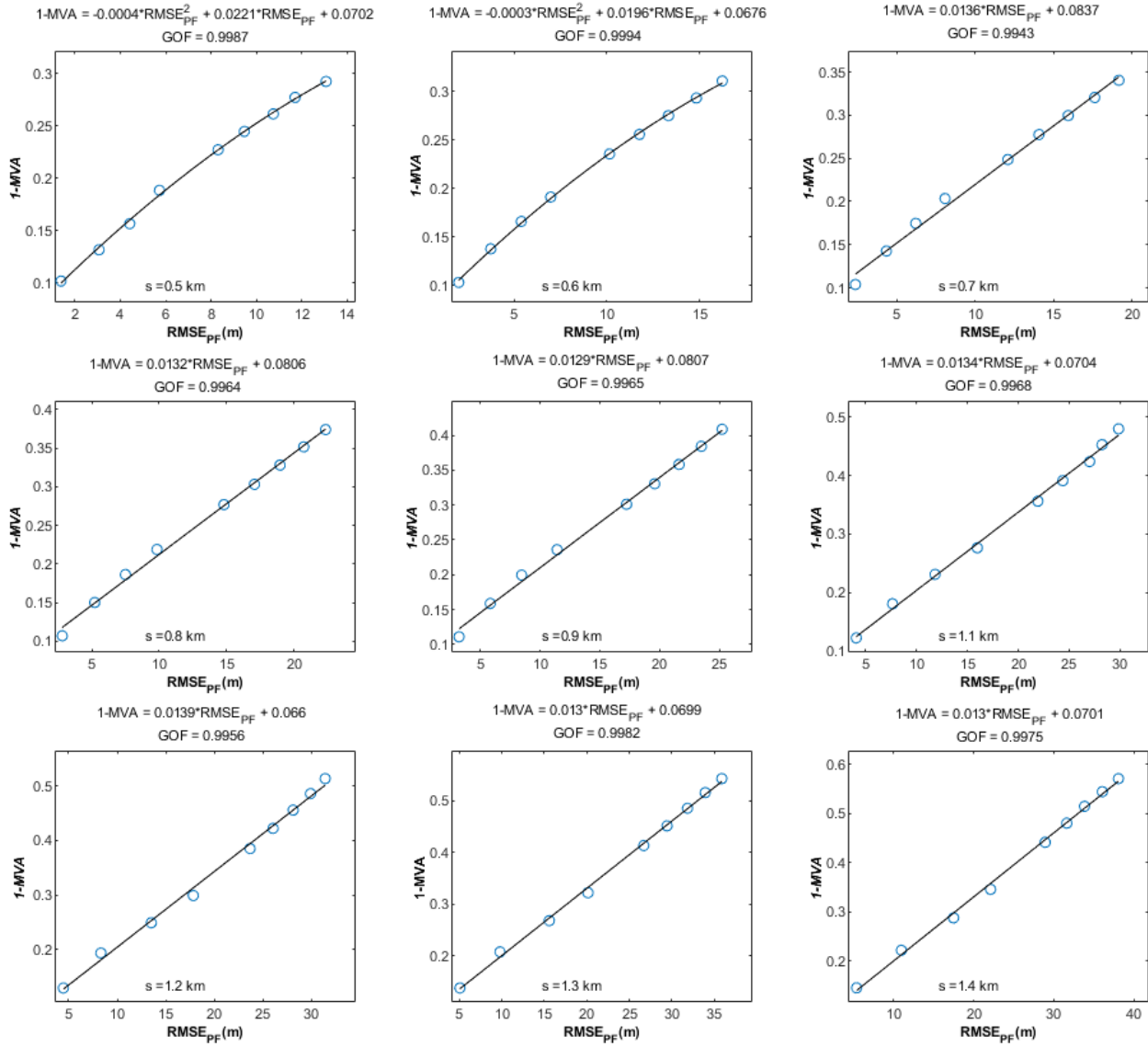


Fig. A5-3. Scatterplot of the relationship between 1-MVA and RMSE of PF in different measurement uncertainties.

Table A5-3. Coefficients of the fitting function and their GOFs in different measurement uncertainties according to PF.

Scenarios	s (km)	Fitting function			GOF	Scenarios	s (km)	Fitting function			GOF
		b_0	b_1	b_2				b_0	b_1	b_2	
1	0.5	0.0702	0.0221	-0.0004	0.9987	6	1.0	0.0791	0.0128		0.9967
2	0.6	0.0676	0.0196	-0.0003	0.9994	7	1.1	0.0704	0.0134		0.9968
3	0.7	0.0837	0.0136		0.9943	8	1.2	0.0660	0.0139		0.9956
4	0.8	0.0806	0.0132		0.9964	9	1.3	0.0699	0.0130		0.9982
5	0.9	0.0807	0.0129		0.9965	10	1.4	0.0701	0.0130		0.9975

Appendix A6: Determination of the coefficients of fitting function and their GOFs for different observation geometries

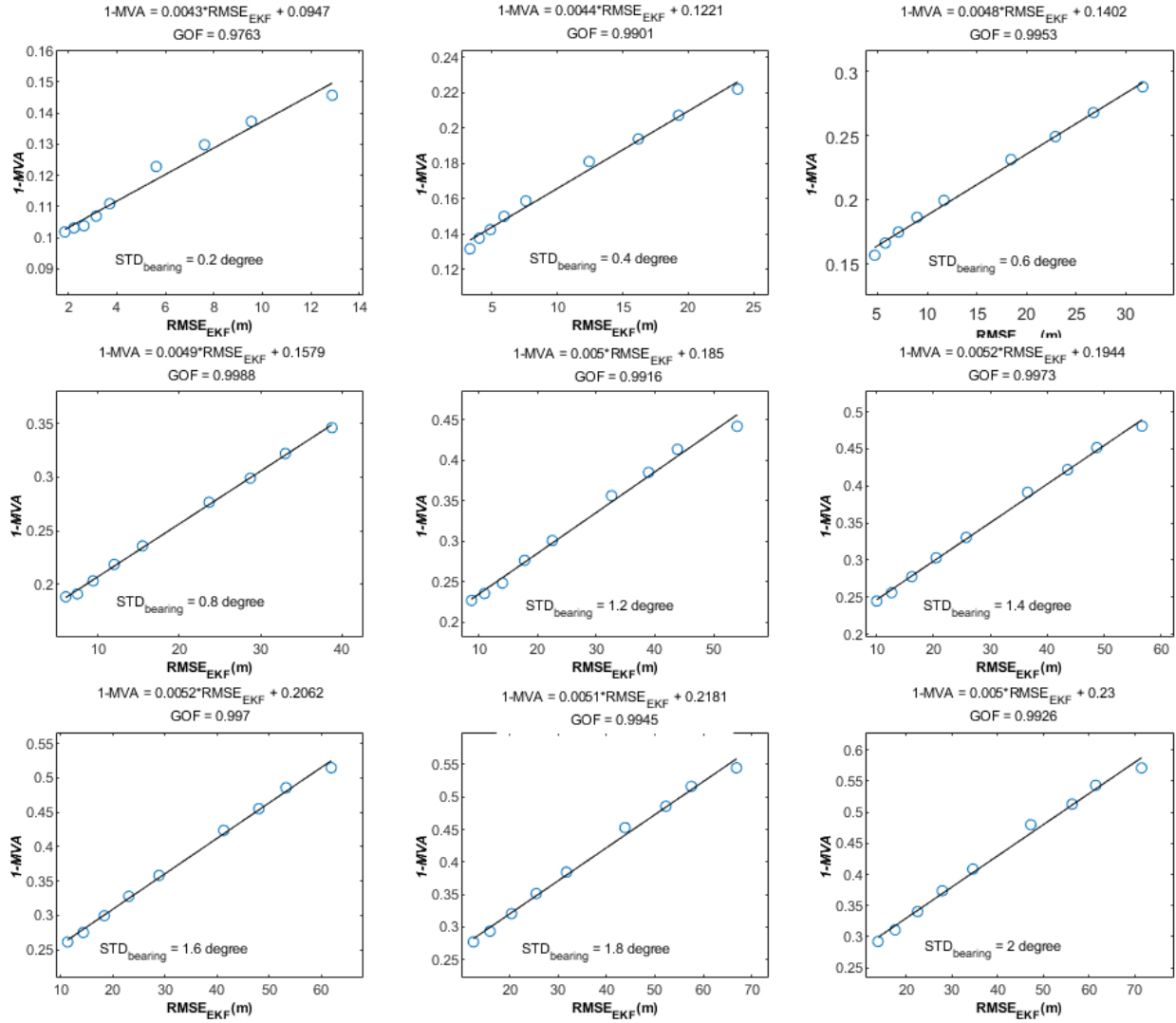


Fig. A6-1. Scatterplot of the relationship between 1-MVA and RMSE of EKF in different observation geometries.

Table A6-1. Coefficients of the fitting function and their GOFs in different observation geometries according to EKF.

Scenarios	σ_α	Fitting function			GOF	Scenarios	σ_α	Fitting function			GOF
		b_0	b_1	b_2				b_0	b_1	b_2	
1	0.2°	0.0947	0.0043		0.9763	6	1.2°	0.1850	0.0050		0.9967
2	0.4°	0.1221	0.0044		0.9901	7	1.4°	0.1944	0.0052		0.9973
3	0.6°	0.1402	0.0048		0.9953	8	1.6°	0.2062	0.0052		0.9970
4	0.8°	0.1579	0.0049		0.9988	9	1.8°	0.2181	0.0051		0.9945
5	1.0°	0.1720	0.0050		0.9973	10	2.0°	0.2300	0.0050		0.9926

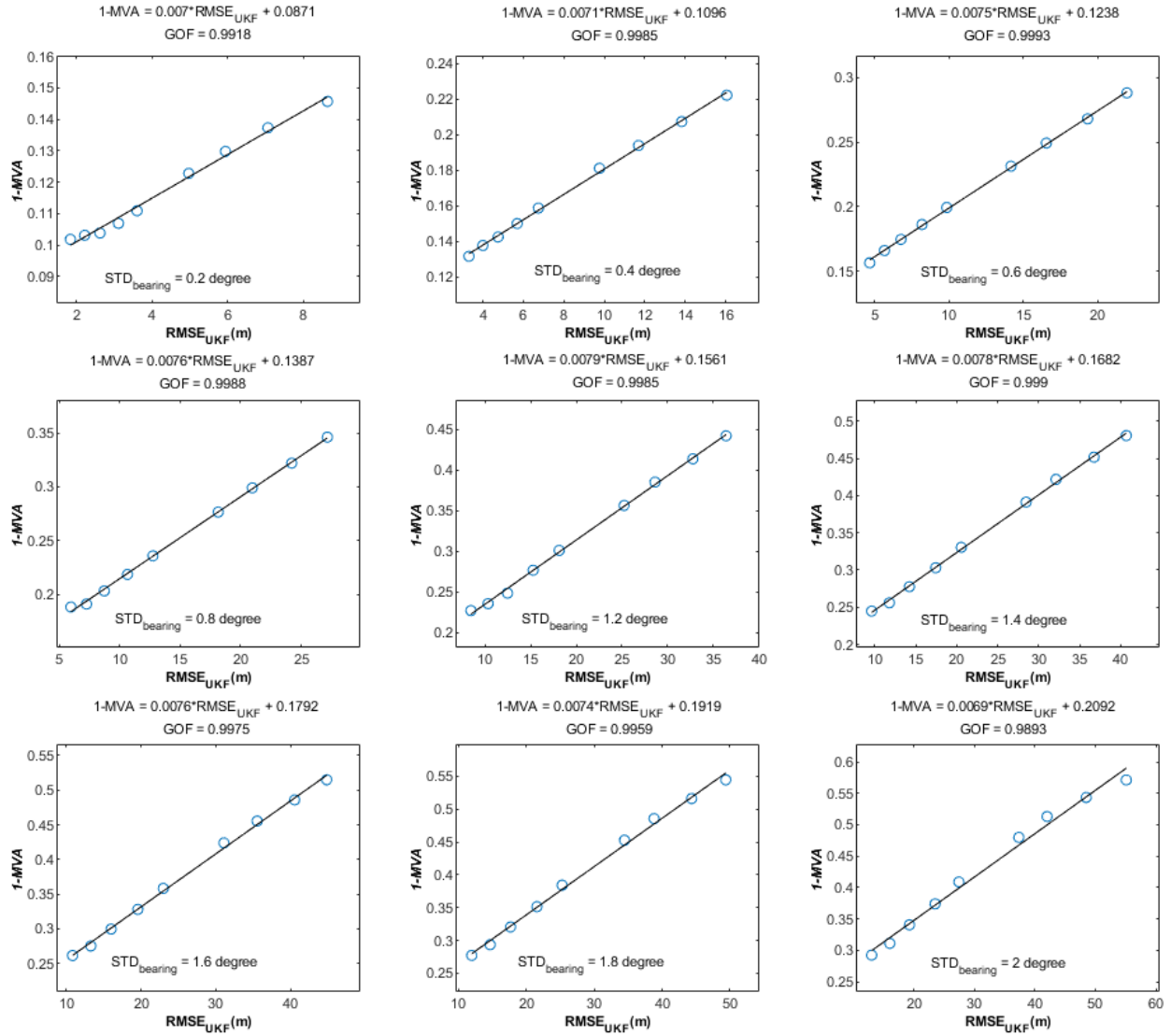


Fig. A6-2. Scatterplot of the relationship between 1-MVA and RMSE of UKF in different observation geometries.

Table A6-2. Coefficients of the fitting function and their GOFs in different observation geometries according to UKF.

Scenarios	σ_α	Fitting function			GOF	Scenarios	σ_α	Fitting function			GOF
		b_0	b_1	b_2				b_0	b_1	b_2	
1	0.2°	0.0871	0.0070		0.9918	6	1.2°	0.1561	0.0079		0.9985
2	0.4°	0.1096	0.0071		0.9985	7	1.4°	0.1682	0.0078		0.9990
3	0.6°	0.1238	0.0075		0.9993	8	1.6°	0.1792	0.0076		0.9975
4	0.8°	0.1387	0.0076		0.9988	9	1.8°	0.1919	0.0074		0.9959
5	1.0°	0.1501	0.0077		0.9987	10	2.0°	0.2092	0.0069		0.9893

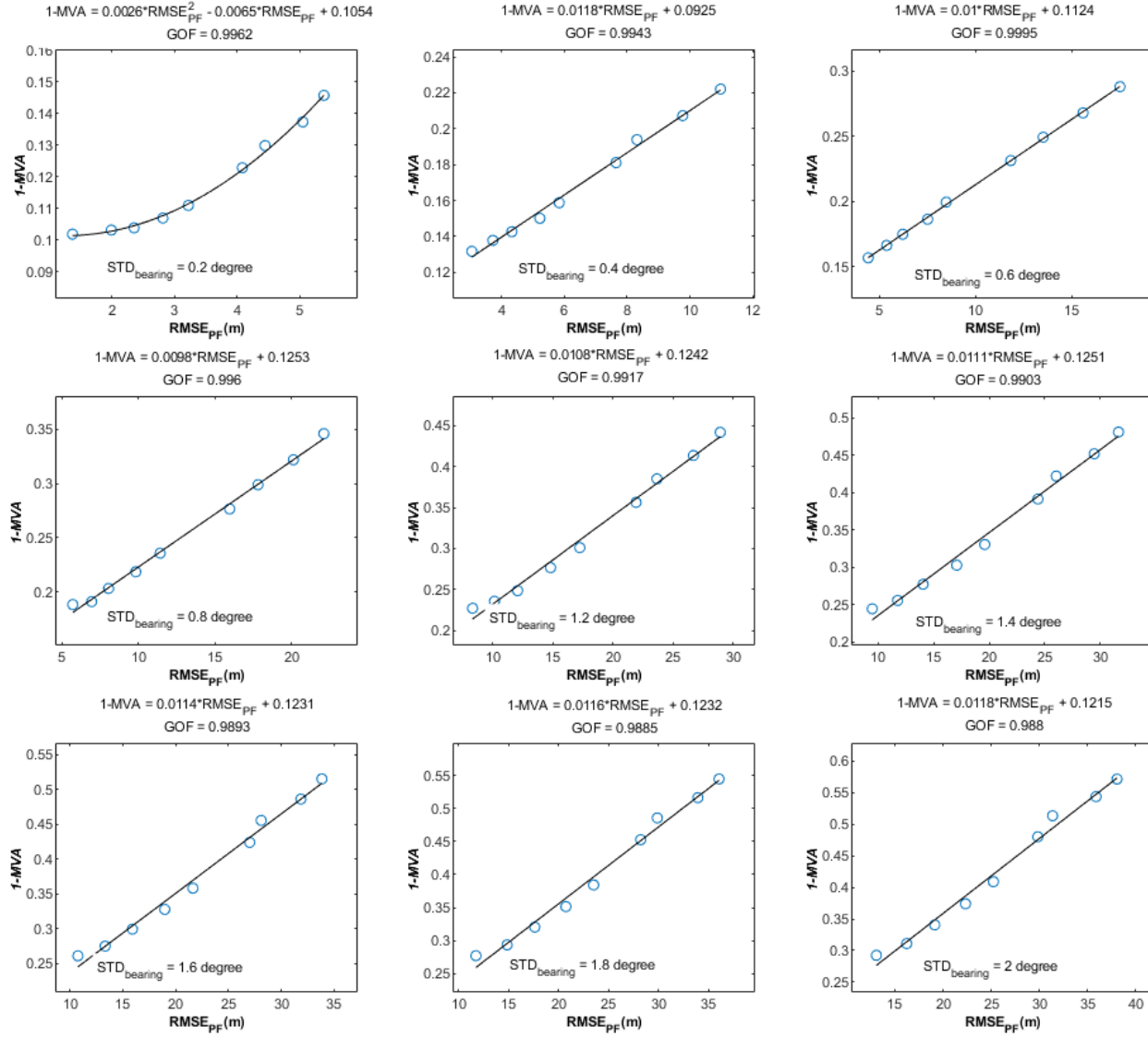


Fig. A6-3. Scatterplot of the relationship between 1-MVA and RMSE of PF in different observation geometries.

Table A6-3. Coefficients of the fitting function and their GOFs in different observation geometries according to PF.

Scenarios	σ_α	Fitting function			GOF	Scenarios	σ_α	Fitting function			GOF
		b_0	b_1	b_2				b_0	b_1	b_2	
1	0.2°	0.1054	-0.0065	0.0026	0.9962	6	1.2°	0.1242	0.0108	0.9917	
2	0.4°	0.0925	0.0118		0.9943	7	1.4°	0.1251	0.0111	0.9903	
3	0.6°	0.1124	0.0100		0.9995	8	1.6°	0.1231	0.0114	0.9893	
4	0.8°	0.1253	0.0098		0.9960	9	1.8°	0.1232	0.0116	0.9985	
5	1.0°	0.1286	0.0101		0.9954	10	2.0°	0.1215	0.0118	0.9880	

Appendix A7: Hypothesis test for the quadratic coefficient b_2

This part is to test whether the quadratic coefficient b_2 of a quadratic function modeling the relationship between 1-MVA and RMSE can be neglected or not. For this purpose, a statistical hypothesis test will be applied. The null hypothesis and alternative hypothesis are denoted by H_0 and H_A , then:

$$\text{Null hypothesis } H_0: E(b_2) = 0$$

$$\text{Alternative hypothesis } H_A: E(b_2) \neq 0$$

with $E(b_2)$ is expected value of quadratic coefficient b_2 .

An approximate confidence interval for b_2 with a confidence coefficient $1 - \alpha$ is given by:

$$P\left(b_2 - y_{1-\frac{\alpha}{2}} \cdot \sigma \leq E(b_2) \leq b_2 + y_{1-\frac{\alpha}{2}} \cdot \sigma\right) = 1 - \alpha$$

where α is the size of the test; $y_{1-\frac{\alpha}{2}}$ is the quantile of the standard normal distribution; and σ is the standard deviation.

The value of the quadratic coefficient b_2 and its confidence interval with 95% derived from the Curve Fitting Toolbox in Matlab are listed in Table A8. The standard deviation is calculated in the 4th row, and the quantile value is 1.96 in the 5th row, which is obtained from the standard normal distribution given $\alpha = 0.05$.

Table A8: Hypothesis test of the coefficient b_2 equals 0

Size of the test $\alpha = 0.05$	Algorithms	
	UKF	PF
Lower bound $b_2 - y_{1-\frac{\alpha}{2}} \cdot \sigma$	-10.11×10^{-5}	-4.054×10^{-5}
Quadratic coefficient b_2	-4.771×10^{-5}	6.688×10^{-5}
Higher bound $b_2 + y_{1-\frac{\alpha}{2}} \cdot \sigma$	0.5704×10^{-5}	17.430×10^{-5}
Standard deviation σ	2.724×10^{-5}	5.481×10^{-5}
$d = b_2 - 0$	-4.771×10^{-5}	6.688×10^{-5}
$ y = \left \frac{d}{\sigma}\right $	1.75	1.22
$y_{1-\frac{\alpha}{2}}$	1.96	1.96
Comparison between $ y $ and $y_{1-\frac{\alpha}{2}}$	$ y < y_{1-\frac{\alpha}{2}}$	$ y < y_{1-\frac{\alpha}{2}}$
Decision	Accept H_0	Accept H_0

Table A8 shows that the coefficient b_2 of the quadratic function modeling the relationship between 1-MVA and RMSE according to both UKF and EKF does not differ significantly from 0.

Acknowledgements

First, I would never have been able to complete my thesis without the unwavering guidance of my colleagues, assistance from my friends, and support from my family and wife.

I would like to express my deep gratitude to my supervisor, Prof. Dr. -Ing. habil. Volker Schwieger, for his exemplary guidance, and providing me with a conducive atmosphere for performing research. I would also like to acknowledge my colleagues and members of the Institute of Engineering Geodesy (IIGS) for their important assistance.

My deepest gratitude is given to my dear beloved members of my family, my wife, and my daughters, for their patience, dedication, and direction in this and all of my life adventures, as well as to my teachers, co-workers, and friends who gave me invaluable advice and guidance.

I would also like to thank my colleagues at Hanoi University of Mining and Geology, who always provide me with motivation through their wholehearted work.

Last, but not least, I express my sincere gratitude to the Ministry of Education and Training and the Government of Vietnam.

Curriculum Vita

Personal Information:

Name:	Pham Trung Dung
Date of birth:	January 17, 1983
Place of birth:	Quang Ninh, Vietnam
Nationality:	Vietnamese
Marital status:	Married, 2 children

Education and work information:

Since 10/2014	Doctoral candidate and research associate at the Institute of Engineering Geodesy (IGS), University of Stuttgart, Germany.
10/2007 - 10/2010	M. Sc. in Surveying Engineering
7/2007 - 10/2014	Research Associate at Hanoi University of Mining and Geology, Vietnam.
10/2001 - 6/2006	Bachelor at Hanoi University of Mining and Geology, Vietnam.
9/1998 - 5/2001	High school education at Uong Bi school, Quang Ninh, Vietnam.

Publications:

Pham, D.; and Schwieger, V. (2016): Comparison of Filtering Algorithm in Vehicle Positioning by Using Low-Cost sensors. 5th International Conference on Machine Control and Guidance, October 5-6th Vichy, France.